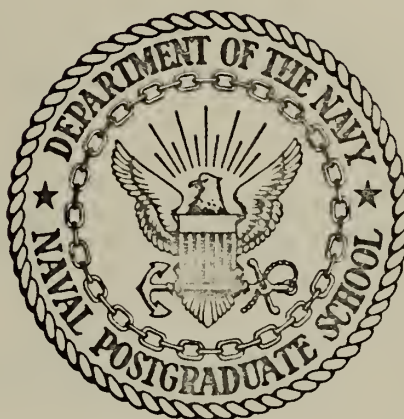


AN INVESTIGATION OF INITIAL YIELD SURFACES
FOR UNIDIRECTIONAL REINFORCED COMPOSITES

Walter Alfred Ericson

NAVAL POSTGRADUATE SCHOOL

Monterey, California



THESIS

AN INVESTIGATION OF INITIAL YIELD SURFACES
FOR UNIDIRECTIONAL REINFORCED COMPOSITES

by

Walter Alfred Ericson

Thesis Advisor:

D. Salinas

March 1972

Approved for public release; distribution unlimited.

An Investigation of Initial Yield Surfaces
for Unidirectional Reinforced Composites

by

Walter Alfred Ericson
Lieutenant, United States Navy
B.S., United States Naval Academy, 1964

Submitted in partial fulfillment of the
requirements for the degree of

MECHANICAL ENGINEER

from the

NAVAL POSTGRADUATE SCHOOL
March 1972

ABSTRACT

Initial yield surfaces of unidirectional fiber reinforced composites subjected to combined longitudinal, transverse normal, and longitudinal shear loads are calculated. The composite is composed of filaments arranged in a periodic square array embedded in a matrix material. The constituent materials are assumed to be homogeneous and isotropic, while the composite is assumed to be macroscopically homogeneous and transversely isotropic. The finite element method, using linear strain triangles, is employed to calculate the stresses throughout the composite. Von Mises yield criterion is used to calculate the elastic limit of the local microscopic combined stresses in the composite. A parametric evaluation is carried out by changing individual constituent properties and evaluating the effect of this variation on the composite properties. Yield surfaces for several functional composites are included, as well as a computer program, in FORTRAN IV language, for the calculation of a yield surface.

TABLE OF CONTENTS

I.	INTRODUCTION -----	12
A.	COMPOSITE MATERIALS -----	12
B.	DEFINITIONS -----	13
C.	BACKGROUND -----	20
D.	SCOPE AND OBJECTIVES -----	21
II.	METHOD OF ANALYSIS -----	23
III.	EVALUATION OF NUMERICAL RESULTS -----	30
A.	INITIAL YIELD SURFACE CHARACTERISTICS -----	30
B.	EVALUATION OF COMPOSITE MECHANICAL PROPERTIES -	36
C.	COMPARISON OF NUMERICAL RESULTS -----	40
IV.	PARAMETRIC ANALYSIS OF COMPOSITES -----	62
A.	EFFECT OF FILAMENT VOLUME -----	63
B.	EFFECT OF FILAMENT YOUNG'S MODULUS -----	68
C.	EFFECT OF MATRIX YOUNG'S MODULUS -----	72
D.	NON-DIMENSIONAL PARAMETER CONSIDERATIONS -----	75
E.	EFFECT OF POISSON'S RATIO -----	86
F.	EFFECT OF MATRIX YIELD STRENGTH -----	87
G.	EFFECT OF FILAMENT CROSS SECTION -----	90
V.	COMPARISON OF MATERIAL COMBINATIONS -----	99
VI.	CONCLUSIONS AND RECOMMENDATIONS -----	111
APPENDIX A:	YIELD LOCUS CALCULATIONS -----	115
APPENDIX B:	CONSTITUTIVE EQUATIONS FOR A HOOKEAN FIBROUS COMPOSITE -----	120
APPENDIX C:	YIELD LOCI -----	131
APPENDIX D:	PROGRAM OVERLAY STRUCTURE -----	161

APPENDIX E: COMPUTER PROGRAM -----	163
LIST OF REFERENCES -----	198
INITIAL DISTRIBUTION LIST -----	201
FORM DD 1473 -----	202

LIST OF TABLES

I.	Initial Yield for $S_{xz}=0$ -----	32
II.	Material Properties -----	41
III.	Comparison of Transverse Normal Loading Solutions -----	42
IV.	Shear Modulus Comparison for THORNEL/Epoxy -----	43
V.	Longitudinal Stiffness Comparison for THORNEL/Epoxy -----	45
VI.	Effect of Matrix Yield Strength on Composite Properties -----	46
VII.	Transverse Poisson's Ratio Study -----	54
VIII.	SCF for Transverse Normal Loading -----	60
IX.	SCF for Longitudinal Shear Loading -----	61
X.	Filament Young's Modulus Variation -----	68
XI.	Matrix Young's Modulus Variation -----	72
XII.	Matrix Yield Strength Variation -----	87
XIII.	Effect of Filament Cross Section on Longitudinal Strength and Stiffness -----	91
XIV.	Effect of Filament Cross Section on Transverse Strength and Stiffness -----	92
XV.	Effect of Cross Section Variation on Composite Shear Modulus -----	97
XVI.	Specific Ultimate Strength and Specific Modulus for Common Structural Materials -----	100
XVII.	Comparative Strength per Unit Cost -----	110
XVIII.	Effect of Constituent Properties on Composite Properties -----	112

LIST OF FIGURES

1.	Relationship of Microstresses and Macro stresses -----	15
2.	Rectangular Array of Filaments and a Basic Block -----	24
3.	A Quadrant of the Basic Block -----	24
4.	Deformation States -----	26
5.	Finite Element Model for Circular Filament Cross Section -----	27
6.	Boron/6061 Aluminum Yield Surface, ($v_f=.5$) -----	31
7.	Symmetric Nature of a Yield Locus -----	34
8.	MODMOR I/NARMCO Epoxy Yield Locus ($v_f=.5$) -----	35
9.	Shear Modulus, G, vs. Fiber Volume Fraction, v_f -----	44
10.	Strength Comparison of Different Alloy Matrix Materials -----	47
11.	Stress-Strain Diagram for Failure Occurring in the Filament -----	49
12.	Stress-Strain Diagram for Failure Occurring in the Matrix -----	50
13.	Longitudinal Poisson's Ratio vs. Filament Volume -----	52
14.	Effect of Constituent Stiffness Ratio on Transverse Poisson's Ratio -----	55
15.	Simulated Tension Test of a Composite -----	56
16.	Transverse Poisson's Ratio -----	57
17.	Composite Elastic Properties vs. Filament Volume -----	65
18.	Stress Concentration Factor vs. Filament Volume -----	69
19.	Composite Elastic Properties vs. Filament Modulus of Elasticity -----	71
20.	Composite Elastic Properties vs. Matrix Modulus of Elasticity -----	73
21.	Effect of Matrix Stiffness on Longitudinal Yield Strength -----	74

22.	Effect of Constituent Stiffness on Longitudinal Stiffness ($v_f=.5$) -----	77
23.	Non-dimensional Longitudinal Stiffness -----	78
24.	Effect of Constituent Stiffness on Transverse Stiffness -----	81
25.	Effect of Constituent Shear Modulus on Composite Shear Modulus -----	85
26.	Effect of Matrix Yield Strength Variation -----	88
27.	Effect of Matrix Yield Strength on Composite Yield Strength -----	89
28.	Elliptical Cross Sections -----	90
29.	Stress and Strain Distribution on the Boundary of a Transversely Loaded Elliptical Filament -----	93
30.	Approximate Optimum Cross Section for Particular Properties -----	95
31.	Transverse Strength Relation to Filament Cross Section -----	96
32.	Transverse Stiffness Comparison -----	102
33.	Transverse Strength Comparison -----	103
34.	Longitudinal Stiffness Comparison -----	105
35.	Longitudinal Strength Comparison -----	106
36.	Combined Effect of Matrix Modulus and Matrix Yield Strength Changes for MODMOR II/Epoxy -----	107
B-1.	Reflection of a Plane of Symmetry (x_1, x_2) -----	122
B-2.	Reflection of a Plane of Symmetry (x_2, x_3) -----	125
B-3.	45 Degree Rotation of Plane (x_1, x_2) -----	127
C-1.	Matrix Yield Strength Variation, $Y_{om} = 3 \times 10^3$ psi -----	132
C-2.	Matrix Yield Strength Variation, $Y_{om} = 2.3 \times 10^4$ psi ---	133
C-3.	Filament Stiffness Variation, $E_f = 30 \times 10^6$ psi -----	134
C-4.	Filament Stiffness Variation, $E_f = 40 \times 10^6$ psi -----	135
C-5.	Filament Stiffness Variation, $E_f = 75 \times 10^6$ psi -----	136

C-6.	Boron/6061 Aluminum, $v_f=0.4$ -----	137
C-7.	Boron/6061 Aluminum, $v_f=0.5$ -----	138
C-8.	Boron/6061 Aluminum, $v_f=0.6$ -----	139
C-9.	Boron/6061 Aluminum, Elliptical -----	140
C-10.	Boron/6061 Aluminum, Elliptical -----	141
C-11.	Boron/NARMCO Epoxy, $v_f=0.5$ -----	142
C-12.	E-glass/Epoxy, $v_f=0.3$ -----	143
C-13.	E-glass/Epoxy, $v_f=0.4$ -----	144
C-14.	E-glass/Epoxy, $v_f=0.5$ -----	145
C-15.	E-glass/Epoxy, $v_f=0.6$ -----	146
C-16.	E-glass/Epoxy, $v_f=0.7$ -----	147
C-17.	MODMOR I (graphite)/NARMCO Epoxy, $v_f=0.3$ -----	148
C-18.	MODMOR I (graphite)/NARMCO Epoxy, $v_f=0.4$ -----	149
C-19.	MODMOR I (graphite)/NARMCO Epoxy, $v_f=0.5$ -----	150
C-20.	MODMOR I (graphite)/NARMCO Epoxy, $v_f=0.6$ -----	151
C-21.	MODMOR I (graphite)/NARMCO Epoxy, $v_f=0.7$ -----	152
C-22.	MODMOR II (graphite)/NARMCO Epoxy, $v_f=0.4$ -----	153
C-23.	MODMOR II (graphite)/NARMCO Epoxy, $v_f=0.5$ -----	154
C-24.	MODMOR II (graphite)/NARMCO Epoxy, $v_f=0.6$ -----	155
C-25.	MODMOR II (graphite)/4617 Epoxy, $v_f=0.4$ -----	156
C-26.	MODMOR II (graphite)/4617 Epoxy, $v_f=0.5$ -----	157
C-27.	MODMOR II (graphite)/4617 Epoxy, $v_f=0.6$ -----	158
C-28.	THORNEL 25 (graphite)/4617 Epoxy, $v_f=0.5$ -----	159
C-29.	THORNEL 40 (graphite)/4617 Epoxy, $v_f=0.6$ -----	160
D-1.	Overlay Root-Segment Structure -----	162

LIST OF SYMBOLS

E	Modulus of Elasticity, psi
E_L	Composite Longitudinal Stiffness, psi
E_T	Composite Transverse Stiffness, psi
G	Shear Modulus, psi
S	Macrostress, psi
S_L	Composite Longitudinal Yield Strength, psi
S_T	Composite Transverse Yield Strength, psi
SCF	Stress Concentration Factor
u_i	Displacement in the i direction ($i = x, y, z$)
v_f	Filament Volume Fraction
v_m	Matrix Volume Fraction
x, y, z	Co-ordinate axes
$< >$	Row Matrix
$\{ \}$	Column Matrix
ϵ	Strain
σ	Microstress, psi
ν	Poisson's Ratio

Subscripts

c	Composite
f	Filament
m	Matrix
x, y, z	Co-ordinate axes directions
ult	Ultimate
T	Transverse

L Longitudinal

Superscripts

I, II, III, IV Load Cases

ACKNOWLEDGEMENT

The author is grateful to Professor David Salinas for his aid and encouragement throughout this investigation. Gratitude is also due Professor Gilles Cantin for his assistance in computer programming and in reading the manuscript.

I. INTRODUCTION

A. COMPOSITE MATERIALS

The requirements of modern technology, especially that of the aerospace industry, have necessitated the development of materials possessing much higher strength to weight ratios than common structural materials. This result has been achieved through the introduction of composite materials, that is two or more constituent materials combined in such a way that the gross properties of the composite are favorable combinations of those of the constituents. This indicates that the desirable properties such as strength/weight and stiffness/weight ratios are increased while less desirable properties such as low ductility are minimized.

A specific type of a two constituent composite is a unidirectional fiber reinforced composite. This consists of continuous lengths of a stiff reinforcing fiber imbedded in a ductile matrix material. All the reinforcing fibers are oriented in the same direction within a single layer of material. Generally several layers, or laminae, are bonded one on top of another to form a high strength laminated composite.

Each of the lamina may be considered as an anisotropic, homogeneous material. The transverse properties, i.e., those in a direction perpendicular to the filament orientation, are weaker than those in the longitudinal (fiber)

direction for a single lamina. To counteract this weakness in a laminated composite, adjacent lamina are arranged such that they have different filament orientation. The fundamental unit is therefore the single layer of unidirectionally reinforced materials. It is this type of basic layer that is analyzed in this investigation.

The physical dimensions of such a lamina can vary considerably, although the largest is generally but a fraction of an inch thick. The fibers vary in diameter from .0001" for glass and .0003" for graphite to .004" for boron. Lamina thickness depends on the materials used and the intended purpose. An individual lamina can be produced in nearly any desired thickness. However standard laminae are becoming popular. For example, most graphite comes in a standard .01" thickness. Allowing for the presence of the matrix material such a lamina may contain in excess of 25 fibers across its thickness.

B. DEFINITIONS

The terminology of composite materials is often confusing due to a lack of precision in defining specific terms. For example, at times it is unclear whether a term such as tensile strength refers to the ultimate strength of a material, i.e., its failure point, or to the point of initial yield. In composite materials it is necessary to be especially clear by noting whether a term refers to a composite property or to a property of a constituent material. In order to avoid such difficulties the definitions of this section will be adhered to in this study.

1. Macroscopic Quantities

These are quantities of the composite material. They are calculated by assuming that the composite consists of anisotropic, homogeneous layers.

2. Microscopic Quantities

These quantities are determined on a point by point basis throughout the composite. The different mechanical properties of the matrix and filament materials are considered in the calculation of these quantities. To see the relationship between macroscopic and microscopic quantities consider Fig. (1). Figure (1a) represents a body with microstress, σ_x . In Fig. (1b) the macrostress S_x in the x-direction obtained from the microstress field of Fig. (1a) is

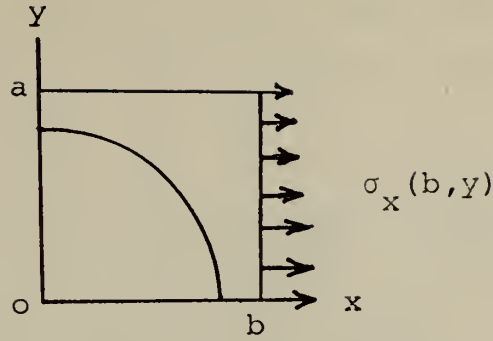
$$S_x = \frac{1}{a} \int_0^a \sigma_x(y) dy \quad (I-1)$$

S_x is the macrostress for the face $x = b$, and represents the average value of the microstresses.

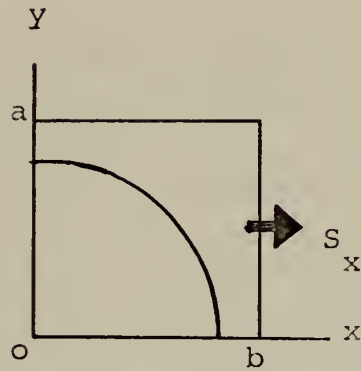
3. Initial Yield Strength

That combination of macroscopic stresses at which a point in the composite first reaches its elastic limit, i.e., no plastic strain has occurred in the composite.

This study is restricted to plane macrostress fields with components S_x , S_z , and S_{xz} , where the z axis is along the length of the fiber. Specific cases of initial yield strength associated with this investigation are



a) Microstress Field $\sigma_x(b, y)$



b) Macrostress S_x

Figure (1). Relationship of Microstresses and Macrostresses

a) Longitudinal Yield Strength, when the only macroscopic stress is in the axial direction, i.e.,

$$S_z \neq 0, S_x = S_{xz} = 0.$$

b) Transverse Yield Strength, when the only macroscopic stress is in the transverse normal direction, i.e.,

$$S_x \neq 0, S_z = S_{xz} = 0.$$

c) Longitudinal Shear Yield Strength, when the only macroscopic stress is in the longitudinal shear direction, i.e., $S_{xz} \neq 0, S_x = S_z = 0$.

4. Second Deviated Stress Invariant, \bar{J}_2

The second deviated stress invariant at a point is defined as [1]

$$\bar{J}_2 = \frac{1}{2} (\sigma_{xy}^2 + \sigma_{yz}^2 + \sigma_{zx}^2) + \frac{1}{6} \left[(\sigma_x - \sigma_y)^2 + (\sigma_y - \sigma_z)^2 + (\sigma_z - \sigma_x)^2 \right] \quad (I-2)$$

This quantity can be related to the yield strength of a material.

5. Effective Microstress, $\bar{\sigma}$

The effective microstress, $\bar{\sigma}$, is proportional to the square root of the second deviated stress invariant, [1]

$$\bar{\sigma} = \frac{1}{\sqrt{2}} \left[(\sigma_x - \sigma_y)^2 + (\sigma_y - \sigma_z)^2 + (\sigma_z - \sigma_x)^2 + 6 (\sigma_{xy}^2 + \sigma_{yz}^2 + \sigma_{zx}^2) \right]^{\frac{1}{2}} \quad (I-3)$$

6. Specific Strength

The ratio of a particular initial strength term, as defined above, to the specific density of the composite. The strength considered must be specified, for example, specific longitudinal strength. This may be applied to composite materials as well as single phase materials.

7. Specific Modulus

The ratio of the Young's modulus of a material to the specific density of the material. In the case of anisotropic materials it must be specified which modulus is being considered, such as the specific transverse modulus.

8. Ultimate Strength

That point in macroscopic stress space at which either a matrix element or a filament element actually fails, i.e., breaks, cracks, or separates. Due to the brittle nature of filament materials the initial yield strength and ultimate strength usually coincide for filament materials.

9. Initial Yield Surface

In a general three-dimensional system the stress state is defined by six stress components, three normal stresses, S_x , S_y , and S_z , and three shearing stresses, S_{xy} , S_{xz} , and S_{yz} . Thus an initial yield surface may be represented in macrostress space. Any macroscopic stress state within the surface means that the effective microstress at every point in the composite is less than that required for yield. Any stress state lying on the surface means that some point in the material has an effective microstress equal to the elastic limit. For brittle materials without a plastic region loading states outside this surface are not possible. For ductile materials stress states outside the initial yield surface (within the limits of the ultimate strength of the material) will result in plastic deformation.

The three-dimensional yield surface considered in this study is a specific case of the general initial yield surface described above. Macroscopic stresses, S_y , S_{xy} , and S_{yz} are set equal to zero in the calculation of the yield surface. The resultant surface represents the yield surface due to plane macrostress loading conditions.

10. Stress Concentration Factor

A stress concentration factor, denoted as SCF, is generally defined as the maximum microstress in the composite to the applied macrostress. In this study three particular cases of stress concentration factors are investigated.

a) SCFX. Transverse loading stress concentration factor, associated with macrostress state $(S_x, S_z, S_{xz}) = (S_x, 0, 0)$.

$$SCFX = \frac{(\sigma_x)_{\max}}{S_x} \quad (I-4)$$

b) SCFZ. Longitudinal loading stress concentration factor, associated with macrostress state $(S_x, S_z, S_{xz}) = (0, S_z, 0)$.

$$SCFZ = \frac{(\sigma_z)_{\max}}{S_z} \quad (I-5)$$

c) SCFXZ. Longitudinal shear loading stress concentration factor, associated with macrostress state $(S_x, S_z, S_{xz}) = (0, 0, S_{xz})$.

$$SCFXZ = \frac{(\sigma_{xz})_{\max}}{S_{xz}} \quad (I-6)$$

11. Transverse Stiffness, E_T

The transverse stiffness of a composite is the macroscopic modulus of elasticity in a direction perpendicular to the fiber direction.

12. Longitudinal Stiffness, E_L

The longitudinal stiffness of a composite is the macroscopic modulus of elasticity in the fiber direction.

13. Longitudinal Poisson's Ratio, ν_L

The longitudinal Poisson's ratio is the measure of the contraction in the transverse direction due to tension in the longitudinal direction, i.e., $\nu_L = \frac{\epsilon_x}{\epsilon_z}$, for the case $(S_x, S_y, S_z) = (0, 0, S_z)$.

14. Transverse Poisson's Ratio, ν_T

The transverse Poisson's ratio is the measure of the contraction in the transverse direction due to tension in the same plane, that is $\nu_T = \epsilon_y/\epsilon_x$, for the case $(S_x, S_y, S_z) = (S_x, 0, 0)$.

15. Shear Modulus, G

The composite shear modulus is the modulus of elasticity in shear due to longitudinal shear loading. As the transverse composite shear modulus is a dependent quantity any reference to composite shear modulus in this study will mean the longitudinal shear modulus unless specifically stated to the contrary.

16. Filament Volume Fraction, ν_f

The filament volume fraction is the ratio of filament material volume to total material volume,

$$\nu_f = \frac{\text{Filament Volume}}{\text{Total Volume}} \quad (\text{I-7})$$

Note that $0 \leq \nu_f \leq 1.0$.

17. Matrix Volume Fraction, v_m

The matrix volume fraction is the ratio of the matrix material volume to the total material volume,

$$v_m = \frac{\text{Matrix Volume}}{\text{Total Volume}} \quad (\text{I-8})$$

Again, $0 \leq v_m \leq 1.0$. For a material without voids the sum of the matrix and filament volume fractions must equal unity,

$$v_f + v_m = 1.0. \quad (\text{I-9})$$

C. BACKGROUND

When a tensile test is performed on a composite material specimen to determine an ultimate tensile strength the value obtained is a macroscopic property. When design specifications require certain properties these also are macroscopic properties. To accurately determine the behavior of a composite and to bridge the gap between design requirements and design practice, macroscopic behavior must be related to microscopic behavior within the composite.

Numerous analytical approaches for the determination of composite properties have been utilized. These include strength-of-materials, stress function, finite difference, and finite element techniques, among others. Chamis and Sendekyj [2] present a comprehensive review of the various analytical methods.

Specific examples of micro-stress analysis include the longitudinal shear loading solutions of Adams and Doner, [3]

and Tsai, Adams and Doner [4]. The longitudinal load case was considered by Bloom and Wilson [5] using a series solution technique. Transverse normal loading was investigated by Tsai, Adams and Doner [4] , and Adams and Doner [6] using finite difference analyses, and by Foye [7] using a finite element method. Lin, Salinas and Ito [8] employed finite element techniques to consider the problem of combined loading, by superposing the effects of longitudinal, transverse, and longitudinal shear loading. Lin et al calculated an initial yield surface based on this combined loading analysis and later extended their work into the plastic region, [9],[10]. Adams [11] also considered inelastic loading but restricted his study to transverse normal loading.

The combined loading problem has received the least attention though it is the most practical from a design standpoint. It is of great importance to the designer to know what combination of macrostresses will result in a micro-stress distribution sufficient to cause yield. The initial yield surface provides this information.

D. SCOPE AND OBJECTIVES

The analytical approach used in this investigation was originally developed and programmed by Lin, Salinas, and Ito. [8] The author's objectives have been

- i) Modify the program to allow use of an overlay system structure in order to reduce the required computer storage.

- ii) Substitute the use of random access disk unit for the original tape storage methods.

iii) Perform a parametric study of the effects of constituent properties on the properties of the composite.

iv) Compare several realistic material combinations to evaluate their structural efficiency.

v) Provide selected initial yield surface plots for design assistance.

vi) Make some general observations relating composite behavior to constituent materials.

II. METHOD OF ANALYSIS

The analytical method described in this section was developed by Lin, Salinas, and Ito [8]. The present discussion is a general presentation of the basic principles of that analysis. Appendix A is a detailed description of the method.

The basic assumptions necessary to the analysis are,

i) The filament and matrix materials are isotropic and homogeneous.

ii) The filament and matrix materials are perfectly bonded.

It should also be noted that the macroscopic stress state is one of plane stress, with components S_x , S_z , and S_{xz} .

The microscopic stress distribution within a unidirectionally reinforced composite depends upon the arrangement of the filament material within the matrix. In order to facilitate this analysis the filament array is assumed to be a doubly periodic rectangular array. In such an array the two-dimensional (x-y) surface may be divided into identical segments called basic blocks, of width $2a$ and height $2b$ as shown in Fig. (2). Away from the edges of the composite the microscopic stress distribution should be identical within each block. Due to symmetry within a basic block only one quadrant need be analyzed, as shown in Fig. (3).

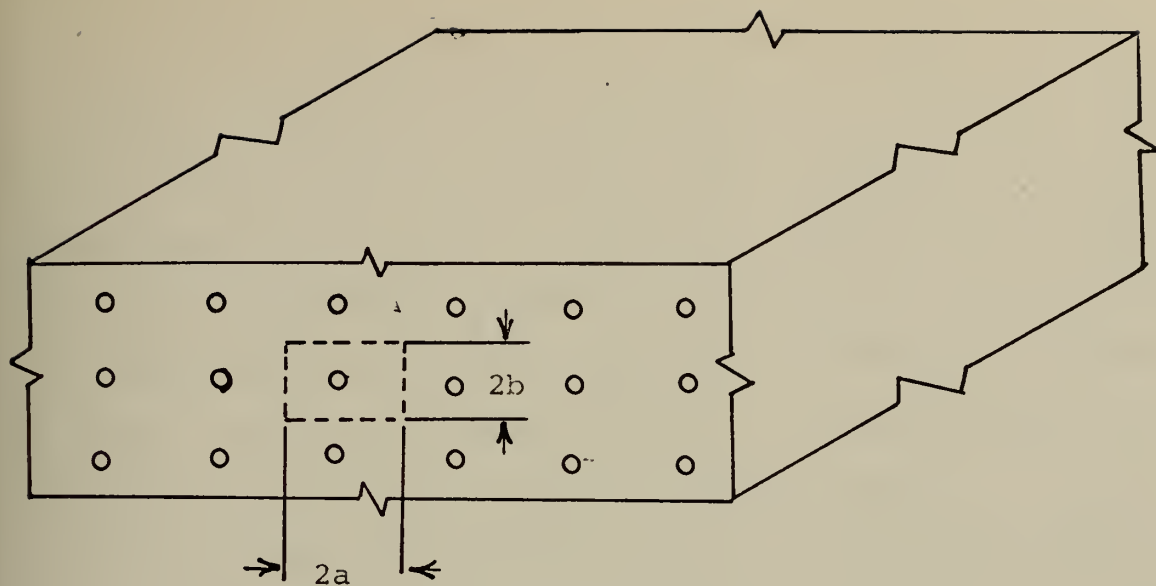


Figure (2). Rectangular Array of Filaments and a Basic Block [8]

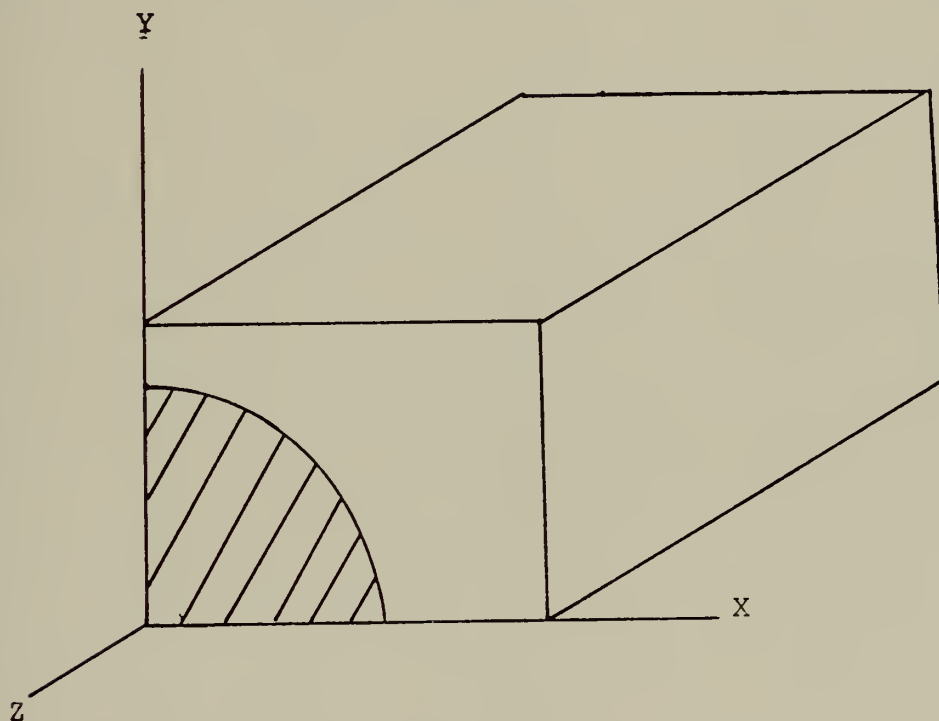


Figure (3). A Quadrant of the Basic Block [8]

In order that no voids be formed and that adjacent blocks neither separate or overlap it is necessary that the rectangular basic blocks remain rectangular during deformation. In order to produce a combined macroscopic plane stress state, as well as maintaining the rectangular form of the blocks, four specific load cases are defined. These four cases, shown in Fig. (4), are superposed to give plane stress and boundary compatibility.

Load cases I and II are plane strain states with $\epsilon_z = 0$. Load case III is a generalized plane strain case with unit strain. Load cases I, II, and III are superposed to give $S_y = 0$. Load case IV is a state of longitudinal shear. All four load cases have $S_{xy} = S_{yz} = 0$. The boundary conditions for each problem are shown in Fig. (4).

These four load cases are solved by the finite element method using linear strain triangles. Felippa [12] presents a detailed discussion of finite element theory and a derivation of the linear strain triangle. The finite element model utilized for the circular filament cross section problems is shown in Fig. (5). This model was adapted from that of Lin et al [9]. In this work convergence tests were conducted to establish the validity of the model.

Each load case yields a microstress distribution and associated macrostresses. The microstresses are designated by σ_{ij}^α , with subscripts determining the stress component and superscripts denoting the load case. For example σ_{ij}^I is the microstress σ_{ij} at a specific point associated with

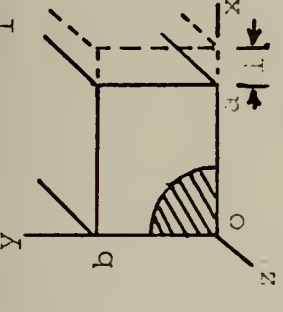
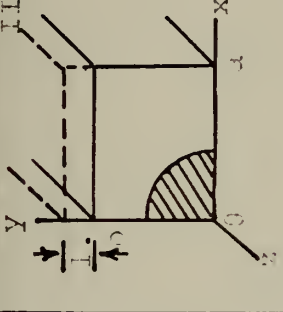
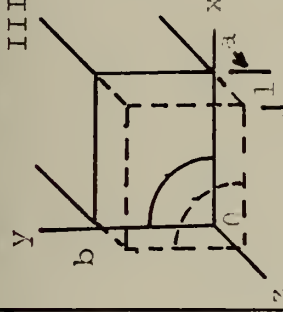
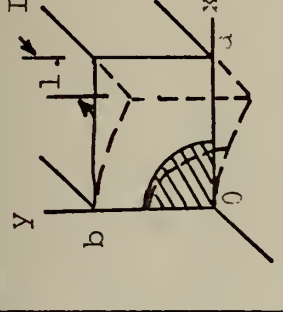
Deformation States and Boundary Conditions	I	II	III	IV
	 <p> $u_x = l$ on $x=a$ $u_y = 0$ on $y=0, b$ $u_z = 0$ on $x=0$ </p>	 <p> $u_y = l$ on $y=b$ $u_x = 0$ on $x=0, a$ $u_z = 0$ on $y=0$ </p>	 <p> $u_x = 0$ on $x=0, a$ $u_y = 0$ on $y=0, b$ $\epsilon_z = l$ </p>	 <p> $u_x = 0$ on $x=0, a$ $u_y = 0$ on $y=0, b$ $u_z = 0$ on $x=a$ $u_z = 0$ on $x=0$ </p>
Macro Results	S_x^I, S_y^I, S_z^I	$S_x^{II}, S_y^{II}, S_z^{II}$	$S_x^{III}, S_y^{III}, S_z^{III}$	S_{xz}^{IV}
Micro Results	$\sigma_x^I, \sigma_y^I, \sigma_z^I, \sigma_{xy}^I$ u_x^I u_y^I	$\sigma_x^{II}, \sigma_y^{II}, \sigma_z^{II}, \sigma_{xy}^{II}$ u_x^{II} u_y^{II}	$\sigma_x^{III}, \sigma_y^{III}, \sigma_z^{III}, \sigma_{xy}^{III}$ u_x^{III} u_y^{III}	$\sigma_{xz}^{IV}, \sigma_{yz}^{IV}$ u_z^{IV}

Figure (4). Deformation States [8]

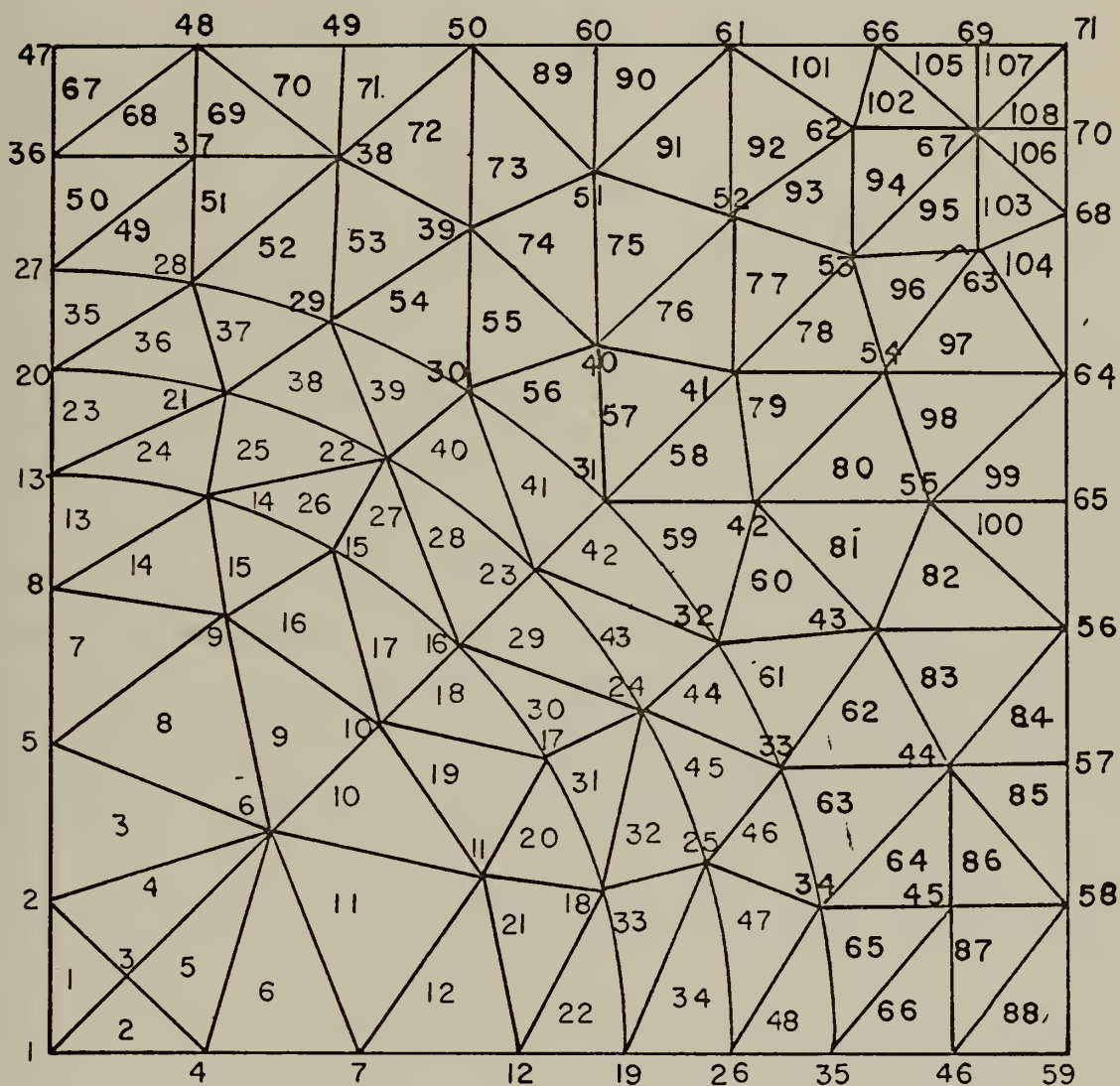


Figure (5). Finite Element Model for Circular Filament Cross Section.

problem I. Macroscopic stresses are represented by S_{ij}^α with subscripts and superscripts similar to microstresses.

Appendix A treats the solution of the individual problems and demonstrates how the results may be combined to relate the combined loading microstresses at a point to macrostresses as

$$[\sigma] = [A] [S] \quad (II-1)$$

See Appendix A, Eq. (A-13), for the explicit form of these matrices.

As noted, the microstresses vary from point to point. Therefore the A matrix, evaluated as

$$[A] = [\sigma] [S]^{-1} \quad (II-2)$$

is also point dependent.

In this thesis the Von Mises yield criteria was taken to govern initial yield of the composite. In terms of microscopic stresses, yielding occurs when [1]

$$\begin{aligned} \bar{J}_2 &= \sigma_{xz}^2 + \sigma_{yz}^2 + \sigma_{xy}^2 + \frac{1}{3} \left[\sigma_x^2 + \sigma_y^2 + \sigma_z^2 - \sigma_x \sigma_y - \sigma_y \sigma_z - \sigma_z \sigma_x \right] \\ &= \frac{1}{3} Y_0^2 \end{aligned} \quad (II-3)$$

where Y_0 is the elastic limit of the material for the tensile stress state.

Using Eq. (II-2) to relate microscopic and macroscopic stresses Appendix A shows that the yield equation, Eq. (II-3), may be written as

$$C_1 S_z^2 + C_2 S_x S_z + C_3 S_x^2 + C_4 S_{xz}^2 = \frac{1}{3} Y_o^2 \quad (\text{II-4})$$

The terms C_1 , C_2 , C_3 , and C_4 are second order polynomials of the components of the A matrix and are functions of position. For given values of S_x and S_{xz} , Eq. (II-4) may be solved for the value of S_z necessary to cause yield. Each point within the fundamental block will yield a different value of S_z . Each combination of S_x and S_{xz} yields two values of S_z at each point, a maximum and a minimum. The minimum of the maximum values and the maximum of the minimum values determine two yield points for the given values of S_x and S_{xz} . Continuing in this manner the initial yield surface for a composite subjected to a macroscopic plane stress state is calculated.

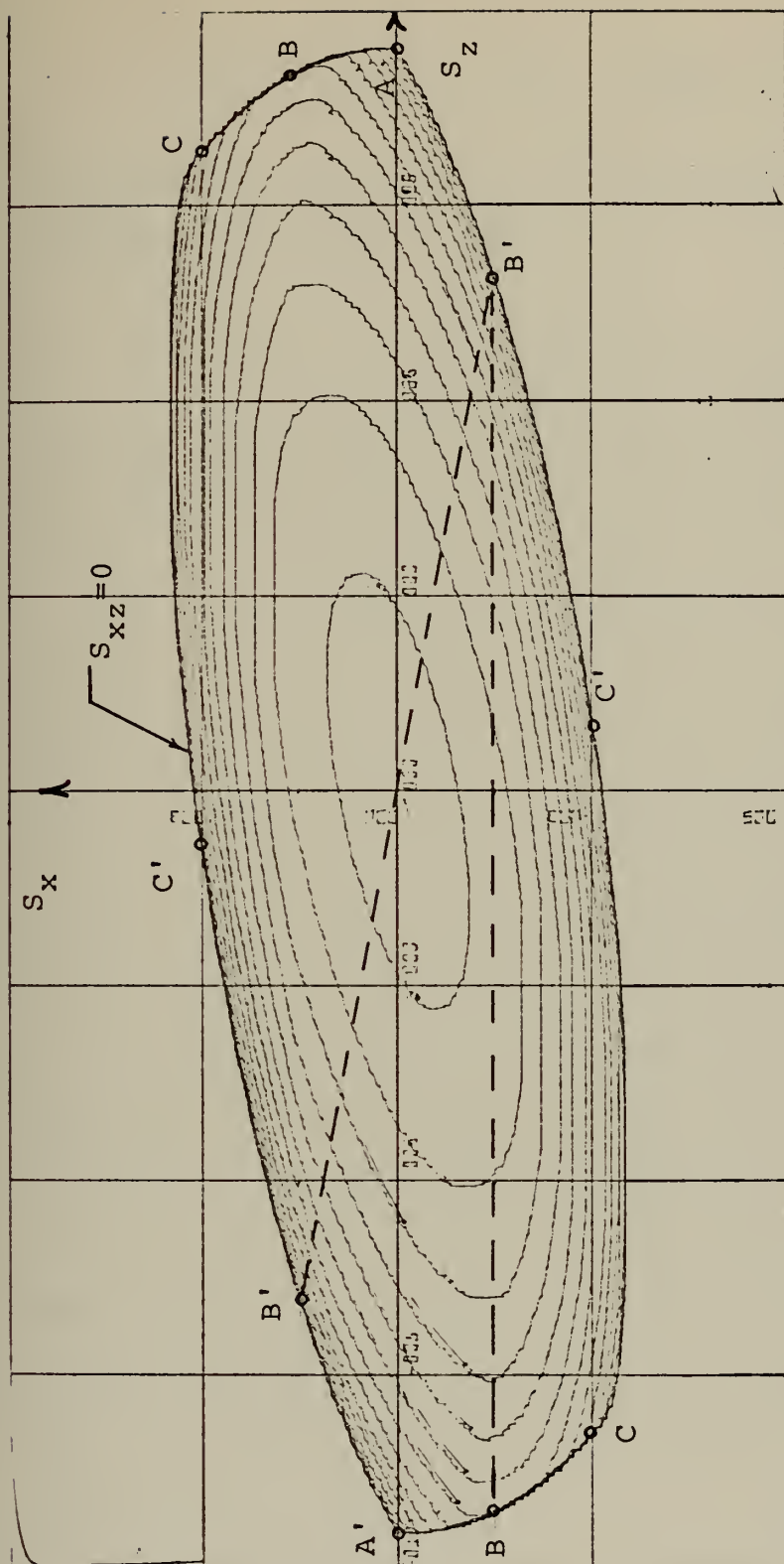
III. EVALUATION OF NUMERICAL RESULTS

A. INITIAL YIELD SURFACE CHARACTERISTICS

The two-dimensional plots of the yield loci of this investigation have the general form of Fig. (6). Each locus represents a specific value of longitudinal shear stress, S_{xz} , with the outermost locus corresponding to $S_{xz} = 0$, as seen in Fig. (6).

Each point on a yield locus indicates that some point within the material would yield under the given macrostress state. The analysis used in this investigation provides the location of the area of yield associated with each point of a yield locus. These area locations refer to the triangular elements of the finite element grid, Fig. (5). Figure (6) is the yield surface for a 50% Boron/6061 Aluminum composite. The elemental areas that first reach yield under specific loading conditions are listed in Table I. The corresponding macrostress states are noted on Fig. (6). Proceeding in this manner a particular triangular element could be associated with every point on each yield locus. This information could be useful to a designer in determining if failure is associated with a particular region.

On initial consideration it seems somewhat unusual that a yield locus is not symmetric about the S_x and S_z axes. To explain this behavior first recall the yield equation of the previous section, Eq. (II-4).



S_x scale = 3×10^4 psi/in S_{xz} increment = 1000 psi
 S_z scale = 3×10^4 psi/in

Figure (6). Boron/6061 Aluminum Yield Surface ($v_f = .5$).

$$C_1 S_z^2 + C_2 S_z S_x + C_3 S_x^2 + C_4 S_{xz}^2 = \frac{1}{3} Y_0^2 \quad (\text{III-1})$$

The exact definition of the terms C_1 , C_2 , C_3 , and C_4 can be ascertained from Eq. (A-22).

TABLE I. INITIAL YIELD FOR $S_{xz} = 0$

Point	S_x (ksi)	S_z (ksi)	Yield Location (Element)
A	0	114	66
A'	0	-114	66
B	± 15	± 112	67
B'	± 15	∓ 75	88
C	± 30	± 100	67
C'	± 30	$\mp .45$	88

As stated, the points of the initial yield surface are calculated by setting S_{xz} and S_x to specified values and calculating the value of S_z resulting in a microscopic stress sufficient to cause yield. Assume that the macrostress combination (S_{xz}, S_x, S_{z1}) is known to be such a yield point. It will be shown that for different combinations of S_x and S_{z1} , i.e., $(S_x, -S_{z1})$ etc., a specific type of symmetry exists.

For (S_x, S_{z1}) Eq. (III-1) becomes

$$C_1 S_{z1}^2 + C_2 S_{z1} S_x + C_3 S_x^2 + C_4 S_{xz}^2 = \frac{1}{3} Y_0^2 \quad (\text{III-2})$$

For $(-S_x, -S_{z1})$ Eq. (III-1) is

$$C_1 S_{z1}^2 + C_2 S_{z1} S_x + C_3 S_x^2 + C_4 S_{xz}^2 = \frac{1}{3} Y_0^2 \quad (\text{III-3})$$

Equations (III-2) and (III-3) are identical and show that yield occurs at the same point and for the same absolute values of macrostresses in quadrants I and III of the yield locus, as shown in Fig. (7). This indicates symmetry about the S_{xz} axis, perpendicular to the (S_x, S_z) plane.

For combinations of (S_x, S_{z1}) such that their product is negative, $(S_x, -S_{z1})$ or $(-S_x, S_{z1})$, Eq. (III-1) becomes

$$C_1 S_{z1}^2 - C_2 S_{z1} S_x + C_3 S_x^2 + C_4 S_{xz}^2 = \frac{1}{3} Y_0^2 \quad (\text{III-4})$$

Comparing Eqs. (III-2) and (III-4) it is seen that if (S_{xz}, S_x, S_{z1}) is a valid solution of Eq. (III-1) as was assumed, then $(S_{xz}, S_x, -S_{z1})$ and $(S_{xz}, -S_x, S_{z1})$ cannot be a solution. For a positive S_x and negative S_z , solution of Eq. (III-1) will yield a different minimum S_z , say S_{z2} . This corresponds to a different point in the basic block than does the solution for quadrants I and III. The combinations $(S_x, -S_{z2}, S_{xz})$ and $(-S_x, S_{z2}, S_{xz})$ identically satisfy Eq. (III-1) establishing the equality of yield points in quadrants II and IV of Fig. (7). The symmetry of the yield locus about the S_{xz} axis is thus established.

Another interesting phenomenon apparent in some yield surfaces is the occurrence of square ends on the yield loci corresponding to small values of S_{xz} . This is shown in Fig.

(8). Generally this indicates that yield is occurring in the filament material rather than the matrix. Note that the S_z scale is considerably larger than the S_x scale. The longitudinal stress values, S_z , in the vicinity of the square ends are many times larger than the transverse, S_x , values. The S_z values are so dominant that increasing the transverse stress from point A to point B of Fig. (8) has little effect on the yield surface. Once the macrostress state B is reached yield occurs in the matrix material.

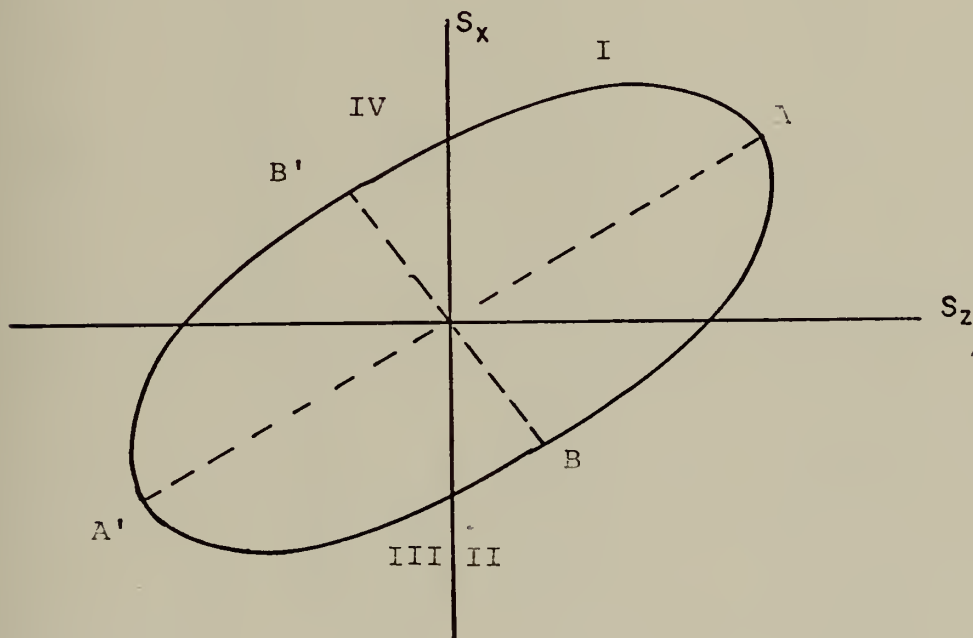
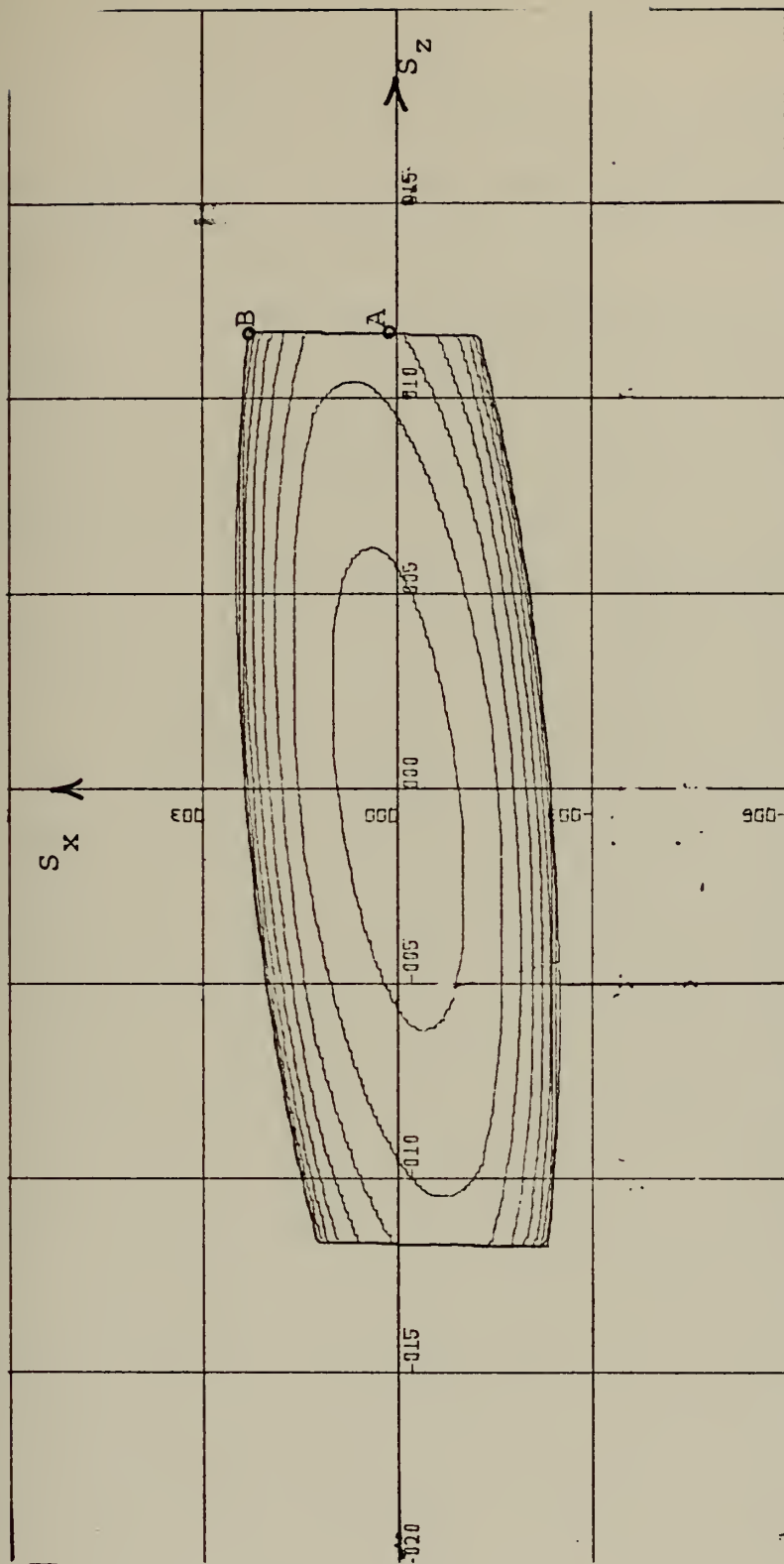


Figure (7). Symmetric Nature of a Yield Locus

As stated the yield locus plot is a two-dimensional representation of a three-dimensional surface. Thus the separation between successive yield loci is an indication of how steep the slope of the yield surface is in that area. The dark areas of the plots indicate an extremely steep slope, such that adjacent loci actually plot very close to one another.



S_x scale = 3×10^3 psi/in S_{xz} increment = 50 psi

S_z scale = 5×10^4 psi/in

Figure (8). MODMOR I/NARMCO Epoxy ($v_f = .5$).

B. EVALUATION OF COMPOSITE MECHANICAL PROPERTIES

1. Composite Strength

Composite strength properties were determined directly from the yield surface associated with each particular composite.

i) Longitudinal yield strength was taken as points S_z on the initial yield surface when $S_{xz} = S_x = 0$.

ii) Transverse yield strength was taken as points on the initial yield surface when $S_z = S_{xz} = 0$.

iii) Longitudinal shear yield strength was taken as the point S_{xz} , on the initial yield surface when $S_x = S_z = 0$.

2. Composite Elastic Constants

Composite elastic constants were calculated from the results of the individual longitudinal, transverse, and longitudinal shear loading problems. The macroscopic stresses associated with each loading case were used in evaluating the transversely isotropic stress-strain relations developed in Appendix B. As discussed in this appendix a transversely isotropic material is an orthotropic material with a single plane of isotropy. It should be noted that the assumption of transverse isotropy limits the applicability of this method of determining the elastic constants of a composite. Composites are not generally transversely isotropic. The particular case treated in this investigation is that of a square array of filaments. For this particular fiber distribution the composite properties approximate those of a transversely isotropic material. For more general

filament arrangements, such as a rectangular array, further consideration must be given to the applicability of these stress-strain relations. The analytical method employed to calculate the displacements, stresses and strains is not effected by this restriction however. The calculation of these quantities is applicable to a general rectangular filament array.

For convenience the transversely isotropic stress-strain relations are repeated here.

$$\begin{aligned}
 \text{a) } \epsilon_x &= \frac{1}{E_T} (S_x - \nu_T S_y) - \frac{\nu_L}{E_L} S_z \\
 \text{b) } \epsilon_y &= \frac{1}{E_T} (S_y - \nu_T S_x) - \frac{\nu_L}{E_L} S_z \\
 \text{c) } \epsilon_z &= -\frac{\nu_L}{E_L} (S_x + S_y) + \frac{1}{E_L} S_z \\
 \text{d) } \epsilon_{xy} &= \frac{1}{G_T} S_{xy} \\
 \text{e) } \epsilon_{yz} &= \frac{1}{G_L} S_{yz} \\
 \text{f) } \epsilon_{xz} &= \frac{1}{G_L} S_{xz}
 \end{aligned} \tag{III-5}$$

In the transverse loading case, problem I, the macroscopic strain, ϵ_x , corresponding to the unit displacement imposed, was calculated. The macroscopic strains ϵ_y and ϵ_z are equal to zero.

In the longitudinal loading case, problem III, the macroscopic strain ϵ_z is equal to unity. In this problem $\epsilon_x = \epsilon_y = 0$.

Equations (III-5), evaluated for these two loading conditions, were solved for longitudinal and transverse composite stiffness and Poisson's ratios, E_L , E_T , ν_L , ν_T .

The longitudinal Poisson's ratio was evaluated directly from Eq. (III-5c) in terms of load case I as

$$\nu_L = \frac{S_z^I}{S_x^I + S_y^I} \quad (III-6)$$

Longitudinal stiffness was evaluated from Eq. (III-5c) in terms of load case III as

$$E_L = S_z^{III} - \nu_L (S_x^{III} + S_y^{III}) \quad (III-7)$$

Equation (III-5b) may be evaluated in terms of load cases I and III and the resulting equations solved simultaneously give

$$E_T = \frac{E_L}{\nu_L} \left[\frac{S_x^{III} S_y^I - S_y^{III} S_x^I}{S_z^I S_x^{III} - S_z^{III} S_x^I} \right] \quad (III-8)$$

$$\nu_T = \nu_L \frac{E_T}{E_L} \left[\frac{S_z^I S_y^{III} - S_y^I S_z^{III}}{S_x^{III} S_y^I - S_x^I S_y^{III}} \right] \quad (III-9)$$

The longitudinal composite shear modulus, G , was obtained from the results of the longitudinal shear loading case, problem IV. The shear strain corresponding to the imposed unit displacement was calculated and used in conjunction with the longitudinal shear strain Eq. (III-5f).

3. Specific Strength and Specific Stiffness

Specific strength and specific stiffness were calculated by dividing the respective properties of the composite by the composite density. Densities of the various material combinations were calculated from the specific weight data of Table II, which lists properties for all materials used in this study.

4. Stress Concentration Factor

Three specific values of the stress concentration factor are calculated in this investigation, corresponding to three specific loading cases. All comply with the general definition of the ratio of the maximum microscopic stress to the macroscopic stress.

i) SCFX refers to the transverse loading problem, problem I. It is defined as the maximum microscopic stress, σ_x , divided by the average surface traction, S_x . From Eq. (I-4),

$$SCFX = \frac{(\sigma_x)_{\max}}{S_x} \quad (III-10)$$

ii) SCFZ refers to the longitudinal loading problem, problem III. It is defined as the maximum microscopic stress, σ_z , divided by the average surface traction. From Eq. (I-5),

$$SCFZ = \frac{(\sigma_z)_{\max}}{S_z} \quad (III-11)$$

iii) SCFXZ refers to the longitudinal shear loading problem, problem IV. It is defined as the maximum microscopic shear stress σ_{xz} , divided by S_{xz} , the average shear stress of this problem.

$$SCFXZ = \frac{(\sigma_{xz})_{\max}}{S_{xz}} \quad (III-12)$$

C. COMPARISON OF NUMERICAL RESULTS

In order to establish the validity of the analysis used in this investigation comparisons were made with available theoretical and experimental results. It is not the intention here to establish the superiority of one method of analysis over another but rather to ensure that the solutions are compatible.

1. Transverse Stiffness, E_T

Using a finite difference approach Tsai et al [4] determined the transverse stiffness of a 40% fiber volume Boron/6061 Aluminum composite as $E_T = 20 \times 10^6$ psi. The present analysis gives $E_T = 20.97 \times 10^6$ psi.

Adams and Doner, [6] also using a finite difference analysis, calculated a theoretical value of transverse stiffness for a 47% E-glass/Epoxy model as 1.55×10^6 psi, and reported an experimental value of 1.30×10^6 psi. This analysis gives 1.42×10^6 psi. Adams and Doner also list a comparison between their results for Glass/Epoxy and several other analyses, including finite element, complex variables, and other solution techniques. These results are compared to the present analyses in Table III.

Transverse stiffness for Boron/Epoxy and Glass/Epoxy also fell within the variation bounds calculated by Dow et al [15]. Further comparisons were made with results of

TABLE II. MATERIAL PROPERTIES

Material ¹	E(psi)	ν	Y_0 (psi) ²	Specific Wt. (lb/in ³)
1. Boron	60×10^6	0.2	4.8×10^5	.085
2. S-glass	12×10^6	0.2	5.0×10^5	.090
3. E-glass	10.6×10^6	0.22	4.0×10^5	.090
4. MODMOR I (graphite)	60×10^6	0.25	2.5×10^5	.072
5. MODMOR II (graphite)	40×10^6	0.25	4.0×10^5	.063
6. THORNEL 25 (graphite)	25×10^6	0.25	1.8×10^5	.052
7. THORNEL 40 (graphite)	40×10^6	0.25	2.5×10^5	.052
8. 6061 Aluminum	10×10^6	0.3	$.346 \times 10^5$.100
9. 2024 Aluminum	8.1×10^6	0.34	$.130 \times 10^5$.100
10. NARMCO 2387 (epoxy)	$.5 \times 10^6$	0.3	$.300 \times 10^5$.045
11. 4617 Epoxy	$.78 \times 10^6$	0.34	$.800 \times 10^5$.045

1. Materials 1 through 7 are filament materials.

Materials 8 through 11 are matrix materials.

2. Y_0 is the elastic limit of the material for the tensile stress state.

Ekvall [16], Whitney [17] and others. The majority of these results are in the form of plotted curves which makes direct numerical comparisons difficult but does provide a general comparison of results.

TABLE III. COMPARISON OF TRANSVERSE NORMAL LOADING SOLUTIONS

$E_f/E_m=20$	$\nu_f=.2$	$\nu_m=.34$	$\nu_f=.55$
Analysis	Transverse Stiffness, E_T		
Adams and Doner [6]			1.86×10^6 psi
Wilson [13]			1.86×10^6 psi
Pickett [14]			1.85×10^6 psi
Foye [7]			1.83×10^6 psi
Present analysis (47%)			1.42×10^6 psi
Present analysis (60%)			2.05×10^6 psi
Present analysis (50% estimate)			1.81×10^6 psi

2. Composite Shear Modulus

Adams and Doner [3], using a finite difference method, have calculated numerous theoretical values of composite shear moduli for specific material combinations. For Glass/Epoxy they obtained a shear modulus of $.417 \times 10^6$ psi and $.589 \times 10^6$ psi for 40% and 55% models respectively. The present analysis yields $.447 \times 10^6$ psi for a 47% model of the same material.

For Boron/Epoxy Adams and Doner obtained $.441 \times 10^6$ psi and $.658 \times 10^6$ psi for 40% and 50% models, compared to the present values of $.476 \times 10^6$ psi for a 47% model.

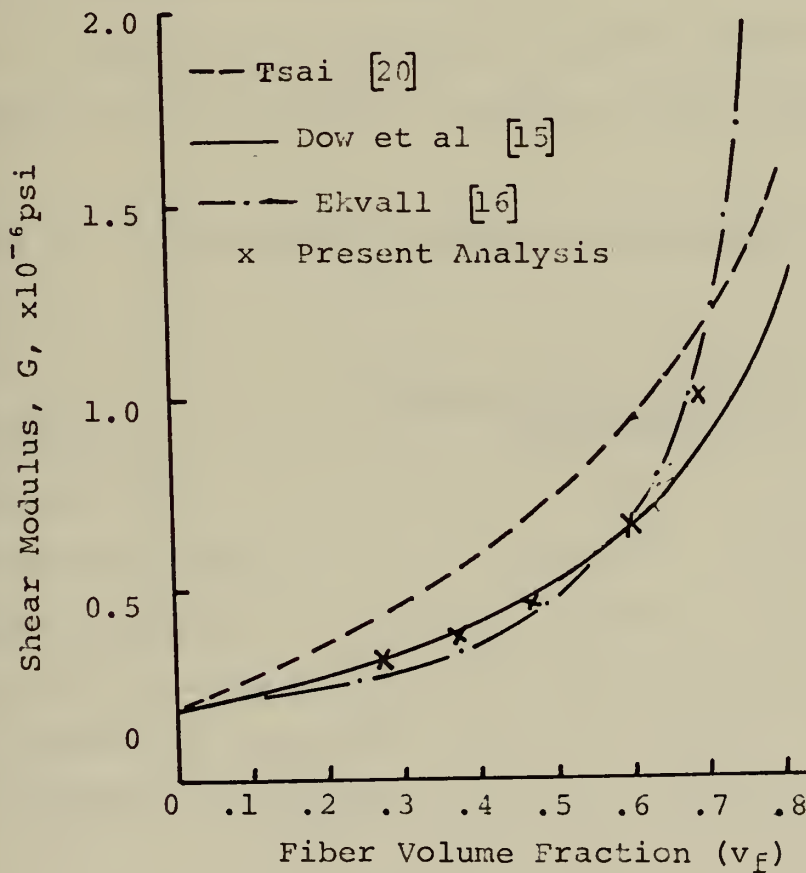
Direct numerical comparisons were available from Blakslee et al [18] who utilized Whitney's micromechanics model [17] based on an Airy stress function. The particular graphite investigated was "Thornel" (a commercial graphite produced by Union Carbide). For Thornel 25 in a 50% model Blakslee reported a theoretical value of the composite shear modulus of $.518 \times 10^6$ psi and an experimental value of $.60 \times 10^6$ psi. This compares to a present value of $.531 \times 10^6$ psi. Similar values for a 60% model of Thornel 40 are $.931 \times 10^6$ psi theoretical and $.740 \times 10^6$ psi experimental, compared to a present value of $.768 \times 10^6$ psi. These comparative values for Thornel are summarized in Table IV.

Graphical comparisons were available with Ekvall [16], Tsai et al, [4] and Whitney [17].

TABLE IV. SHEAR MODULUS COMPARISON FOR THORNEL/EPOXY

	Shear Modulus, G(psi x 10 ⁻⁶)			
Analysis	THORNEL 25*		THORNEL 40**	
Blakslee [18]	.518		.931	
Experimental [18]	.600		.740	
Present Analysis	.531		.768	
* THORNEL 25	E _f /E _m = 32	v _f = .25	v _m = .34	v _f = .5
** THORNEL 40	E _f /E _m = 51	v _f = .25	v _m = .34	v _f = .65

The graphical results of Fig. (9) were compiled by Reidinger et al [19]. This compares the values derived by Tsai [20], Dow et al [21], and Ekvall [16] for Glass/Epoxy. The results of this analysis are marked by X. Both Tsai and Dow et al obtained their results from consideration of variational bounds. Tsai however employs a "contiguity" factor dependent on the amount of contact between filaments. The present analysis and that of Dow et al assume that the filament is completely surrounded by matrix material. This accounts for the closer correspondence of the present results to that of Dow et al.



$$E_f = 10.6 \times 10^6 \text{ psi} \quad E_m = 0.5 \times 10^6 \text{ psi} \quad v_f = .22 \quad v_m = .35$$

Figure (9). Shear Modulus, G , vs. Fiber Volume Fraction, v_f

3. Longitudinal Stiffness, E_L

Longitudinal loading has not been considered as frequently as transverse or shear loading, resulting in fewer numerical comparisons. Blakslee [18] again gives theoretical and experimental values for Thornel/Epoxy composites. For the 50% volume Thornel 25, he reports a theoretical value of 12.78×10^6 psi, and an experimental value of 11.07×10^6 psi. This compares to a value of 11.96×10^6 psi in this study. For 65% Thornel 40 similar results are theoretical 26.20×10^6 psi, experimental 24.6×10^6 psi and a present value of 24.35×10^6 psi. This data is summarized in Table V.

Reasonable correlation was also obtained in comparison with graphical results of Tsai [20] and Ekvall [16].

TABLE V. LONGITUDINAL STIFFNESS COMPARISON FOR THORNEL/EPOXY

Analysis	Longitudinal Stiffness, E_L (psi $\times 10^{-6}$)	
	THORNEL 25*	THORNEL 40**
Blakslee [18]	12.78	26.20
Experimental [18]	11.07	24.60
Present Analysis	12.44	24.35

* THORNEL 25 $E_f/E_m=32$ $v_f=.25$ $v_m=.34$ $v_f=.5$

** THORNEL 40 $E_f/E_m=51$ $v_f=.25$ $v_m=.34$ $v_f=.65$

4. Composite Yield Strength

Strength comparisons were more difficult to obtain. In some cases strength quantities described by identical terminology and applied to seemingly similar materials differed by several hundred per cent. One reason for such discrepancies is the lack of consistent definition of strength terms. Valid comparisons only have meaning if the quantities investigated are precisely defined.

Another important point is the effect of the matrix yield strength on composite yield strength. Matrix materials of the same class, such as different brands of epoxy, normally have elastic constants that show little variation from one another. The difference in yield strength however can be considerable. The result of this difference is shown in Table VI, comparing a 40% filament model of Boron/2024 Aluminum with a matrix yield of 1.30×10^4 psi and Boron/6061 Aluminum with a matrix yield of 3.46×10^4 psi.

TABLE VI. EFFECT OF MATRIX YIELD STRENGTH
ON COMPOSITE PROPERTIES

$$v_f = .5$$

	Boron/6061 Aluminum	Boron/2024 Aluminum	% Difference
E_L (psi)	20.53×10^6	18.86×10^6	8.
E_T (psi)	31.07×10^6	28.71×10^6	8.
G (psi)	6.33×10^6	5.28×10^6	19.
S_L (psi)	94.53×10^3	38.9×10^3	143.
S_T (psi)	28.50×10^3	11.20×10^3	154.

As seen in Table VI the change in elastic properties is insignificant in comparison to the change in strength. The change that does occur in the elastic properties is due to minor differences in the elastic properties of the two matrix materials. The reason for the very large increase in strength may be seen from Fig. (10).

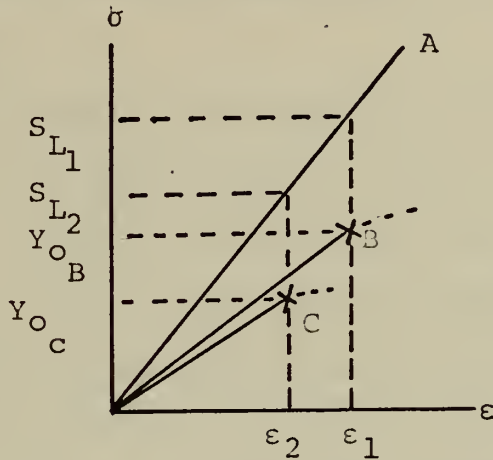


Figure (10). Strength Comparison of Different Alloy Matrix Materials.

The slope of curve A represents the composite longitudinal stiffness, E_L , assumed to be identical for two composites, each having the same filament material but with different alloys of the same matrix material. As seen in Table VI the values of E_L in such a case are quite similar. Curve B represents the stress-strain curve of one matrix material, curve C that of the other matrix material. They are assumed to have approximately the same elastic modulus (as, for instance, two different aluminum alloys) but with different yield stress. For the case of matrix B the yield stress will be reached at a composite strain ϵ_1 . The resultant composite stress is S_{L_1} .

If the matrix material is that corresponding to curve C, matrix yield will occur at composite strain ϵ_2 , resulting in composite stress S_{L_2} . Thus a variation in matrix strength alone may markedly affect the composite strength.

No comparison of strength terms should be attempted unless the complete properties of both constituents are specified.

The example of Boron/2024 Aluminum of Table VI is directly comparable with the results of Adams [11]. For identical material properties using a finite element analysis with constant strain triangles Adams reported a theoretical transverse yield strength of 11,200 psi, identical with the results of this analysis.

Longitudinal strength may be readily analyzed by strength-of-materials methods. Holister and Thomas [22] developed a relationship for determining the ultimate tensile strength of a composite undergoing axial tension by considering the relation

$$S_L = \sigma_f v_f + \sigma_m v_m \quad (\text{III-13})$$

where v_f and v_m are the filament and matrix volume fractions, respectively.

For the case of axial load for continuous fibers, as in this study, the strain will be constant. Holister and Thomas considered the particular case where the strain is such that the ultimate stress of the filament is attained while the matrix material is still in the elastic range.

This is equivalent to assuming a stress-strain relation corresponding to Fig. (11). Curve A represents the composite stress-strain relation and curve B that of the matrix.

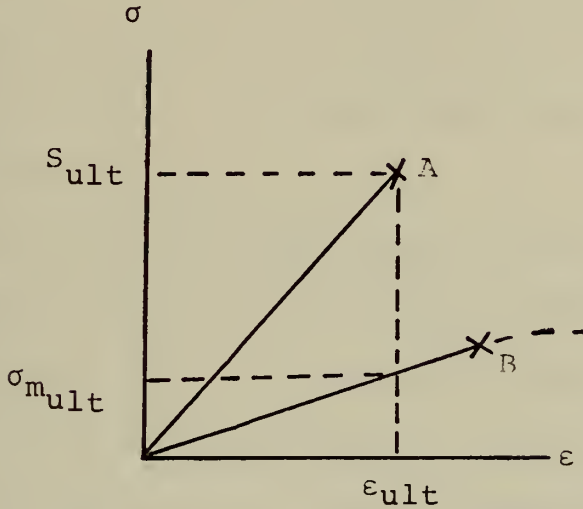


Figure (11). Stress-Strain Diagram for Failure Occurring in the Filament.

If the matrix remains in the elastic region, the strain ϵ_{ult} , for ultimate strength, S_{ult} , must be less than that necessary to cause initial yield in the matrix. Under these conditions

$$\epsilon_{ult} = Y_{of}/E_f = \sigma_m/E_m \quad (III-14)$$

Equations (III-13) and (III-14) along with the relation

$$v_f + v_m = 1. \quad (III-15)$$

give

$$S_{ult} = \epsilon_{ult} v_f E_f (1 - E_m/E_f) + \epsilon_{ult} E_m \quad (III-16)$$

Reidinger et al reported an equivalent form of this equation as

$$S_{ult} = v_f Y_{of} + v_m \sigma_{m_{ult}} \quad (III-17)$$

where $\sigma_{m_{ult}}$ is defined as the stress in the matrix at the ultimate strain of the filament. This is shown in Fig. (11). The yield strength of the filament is Y_{of} .

It must be repeated that these relations are for a composite that fails while the matrix is still elastic. It should be pointed out however that Holister pursues the matter further to consider the case of the matrix being in the plastic range.

For the more common case of the matrix material yielding prior to the filament reaching yield, relations similar to (III-13) and (III-14) may be utilized to find the initial yield strength. In the case of Fig. (12) the strain sufficient to cause initial yield for longitudinal load, S_L , is marked by ϵ_L .

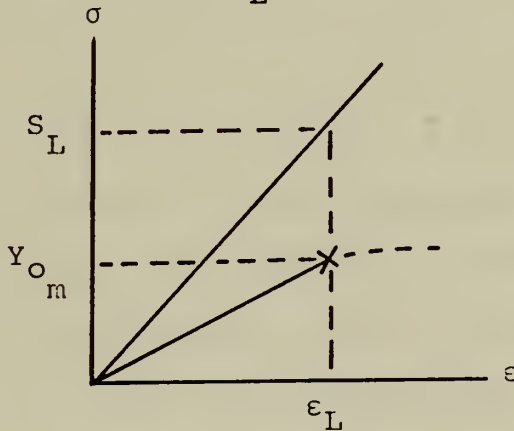


Figure (12). Stress-Strain Diagram for Failure Occurring in the Matrix.

For this case

$$\epsilon_L = \frac{Y_{om}}{E_m} = \frac{\sigma_m}{E_m} = \frac{\sigma_f}{E_f} \quad (\text{III-18})$$

where Y_{om} is the axial yield of the matrix. Using Eqs.

(III-13) and (III-18) yields

$$S_L = v_f \sigma_f^* + v_m Y_{om} \quad (\text{III-19})$$

The stress in the filament at the yield strain of the matrix is σ_f^* , where

$$\sigma_f^* = Y_{O_m} \frac{E_f}{E_m} \quad (\text{III-20})$$

The results for longitudinal strength calculated in this study differed by approximately 2% from those found by Eq. (III-20).

5. Composite Poisson's Ratio

a. Longitudinal Poisson's Ratio. The longitudinal Poisson's ratio, ν_L , as calculated from the transversely isotropic stress-strain relations, Eq. (III-5), exhibits a linear behavior with respect to filament volume fraction. The results of Fig. (13) for E-glass/Epoxy correspond to those of a law of mixtures relation.

$$\nu_L = \nu_f \nu_f + \nu_m \nu_m \quad (\text{III-21})$$

This is in accord with the theoretical results of Rosen et al, [23] Whitney and Riley, [17] and Tsai [20].

Specific experimental results were available from Blakslee et al [18] for THORNEL/Epoxy. This data also showed adherence to a rule of mixtures.

b. Transverse Poisson's Ratio. The comparison of the transverse Poisson's ratio, ν_T , with other theoretical studies raised several interesting points. Values found in the literature ranged from 0.7 [29] to considerably less than 0.1. [18] Thus the literature indicates a range of the composite transverse Poisson's ratio that far exceeds that

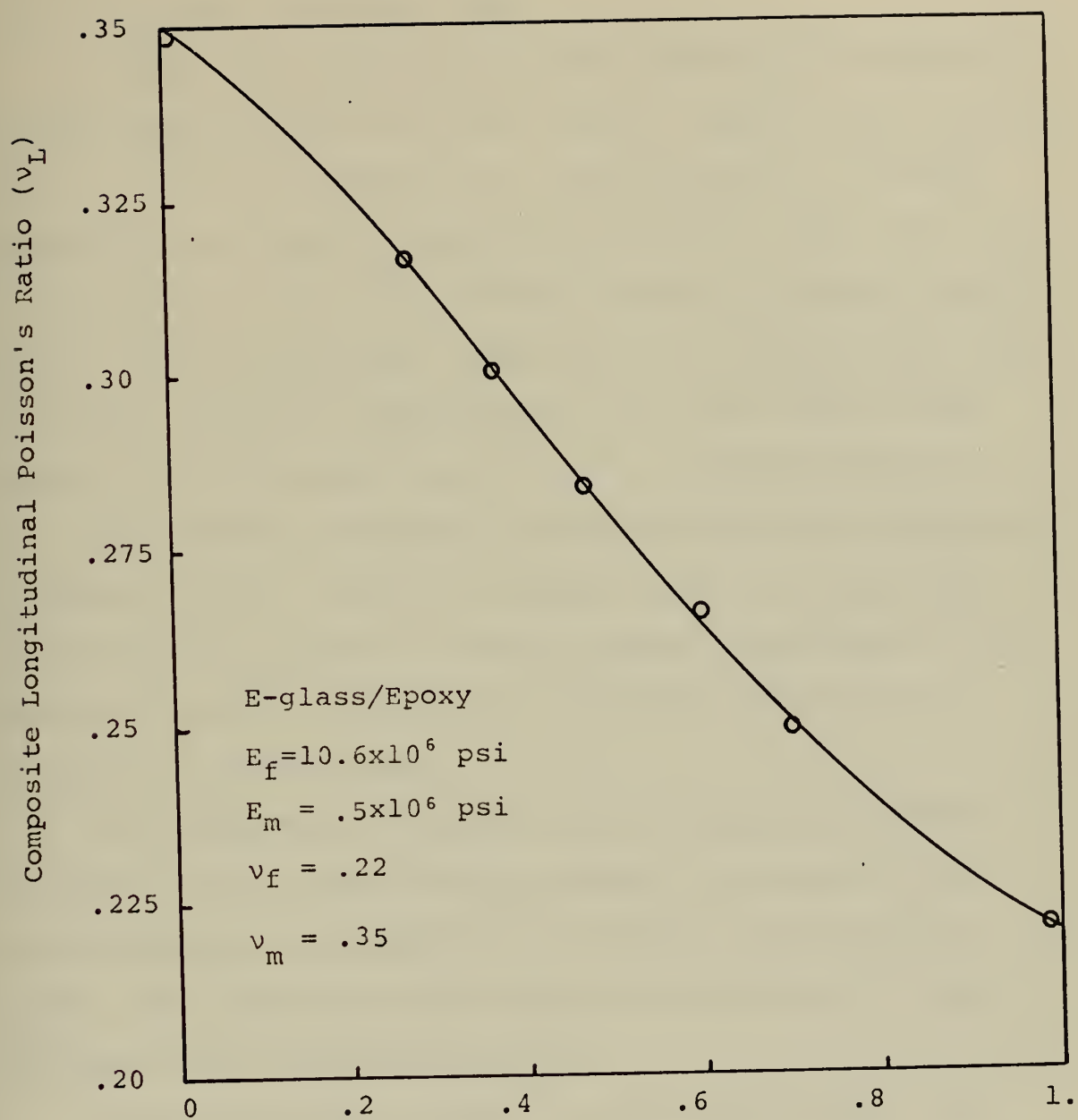


Figure (13). Longitudinal Poisson's Ratio vs. Filament Volume

of the Poisson's ratios of the constituents. The higher values exceed the theoretical maximum of 0.5 associated with isotropic materials. [24]

In this investigation using the transversely isotropic stress-strain relations, Eqs. (III-5), results were obtained for ν_T . With the addition of a small amount of filament material the composite transverse Poisson's ratio takes on a value greater than the Poisson's ratio of either constituent. For the materials considered the increase for a 30% filament volume was approximately 22% above that of the matrix. In all cases the value of ν_T remained below 0.5.

The transverse Poisson's ratio decreased with increasing filament volume. At high filament volume ν_T values were less than the Poisson's ratio of either constituent. The maximum decrease noted in this study was 47% below the filament Poisson's ratio.

To investigate the cause of the transverse composite Poisson's ratio having values outside the range of its constituents several additional computer analyses were made. The constituent and composite properties of these analyses are listed in Table VII.

If the transverse Poisson's ratio was dependent only on the Poisson's ratios of the constituents and the filament volume, the results of analyses 1, 2, and 3 below would be identical. As noted in the previous section, the longitudinal Poisson's ratio, ν_L , is dependent only on these quantities. This fact is borne out by the data of Table VII.

TABLE VII. TRANSVERSE POISSON'S RATIO STUDY

Analysis	E_f/E_m	v_f	v_f	v_m	v_L	v_T
1	1	.7	.25	.25	.25	.250
2	6	.7	.25	.25	.25	.219
3	120	.7	.25	.25	.25	.109
4	120	.7	.25	.30	.26	.134

The results of this study indicate that the Poisson's ratio in the transverse direction is also greatly dependent on the ratio of constituent moduli of elasticity. The greater the ratio E_f/E_m , the greater the variance from the Poisson's ratio of the constituent materials.

At small filament volume fractions the transverse Poisson's ratio exceeds that of either constituent. At large values of filament volume content v_T is considerably less than either constituent. At 50% filament volume the transverse Poisson's ratio is approximately equal to the average of the constituent Poisson's ratios, irrespective of the value of E_f/E_m . This is shown in Fig. (14).

Comparison of analyses 3 and 4 of Table VII shows that an increase in constituent Poisson's ratio does effect v_T but not as significantly as does the ratio E_f/E_m . A 20% increase in v_m resulted in approximately a 20% increase in v_T . The effect of changing constituents Poisson's ratio is limited however by the range of values for available materials.

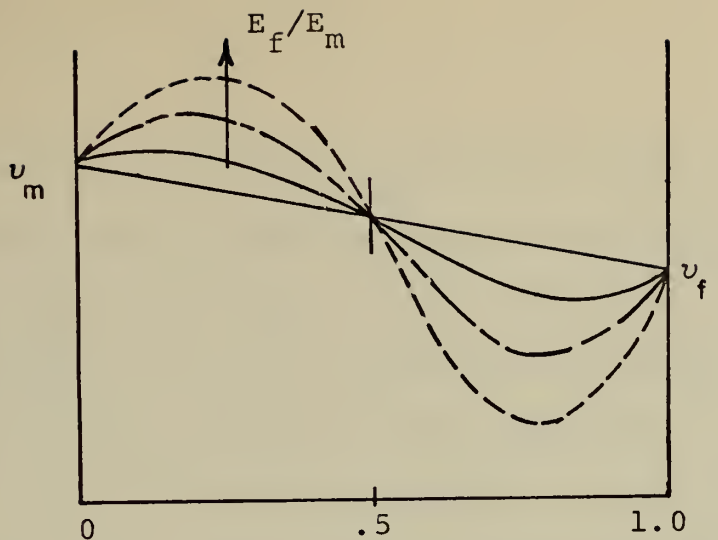


Figure (14). Effect of Constituent Stiffness on Transverse Poisson's Ratio.

In the course of attempting to correlate the results of this study with other theoretical results several alternative analytical methods were considered. Some of these were found to give results for Poisson's ratio comparable to other extreme values found in the literature. These alternative methods were discarded as erroneous. To assist in evaluating the various predicted values of v_T two of these methods will be discussed here.

i) If it is assumed that the composite exhibits the same stiffness in all directions the stress-strain relations become

$$\epsilon_x = \frac{1}{E} (\sigma_x - v_T \sigma_y)$$

$$\epsilon_y = \frac{1}{E} (\sigma_y - v_T \sigma_x)$$

$$\epsilon_z = - \frac{v_L}{E} (\sigma_x + \sigma_y) + \frac{1}{E} \sigma_z \quad (III-22)$$

Using the data of the various load cases these equations yield values for longitudinal Poisson's ratio, v_L , that follow a law of mixtures. As noted in the previous section

this concurs with most theoretical values. The transverse Poisson's ratio, however, takes on extremely small values, considerably less than .02 for 60% models. This method is not correct due to the inaccurate assumption regarding the stress-strain relations of the composite.

ii) It was also attempted to evaluate the transverse Poisson's ratio by simulating a tension test. A finite element analysis was carried out on the model shown in Fig. (15a). The boundary conditions were

$$\begin{aligned} u_y &= 0 \quad \text{on} \quad y = 0 \\ u_x &= 0 \quad \text{on} \quad x = 0 \\ u_x &= 1 \quad \text{on} \quad x = a \end{aligned}$$

This resulted in a displacement along the boundary as shown in Fig. (15b).

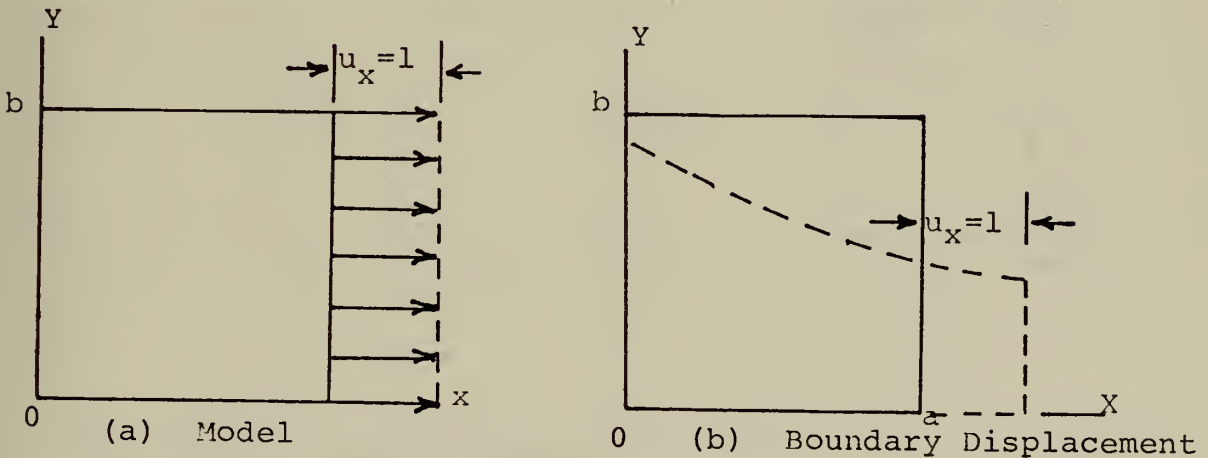


Figure (15). Simulated Tension Test of a Composite.

Consequently the Poisson's ratio, ν_T , varies along the boundary. In the problem considered the values ranged from approximately 0.15 to 0.7. The error in this method is that the rectangular boundaries of the basic block do

not remain rectangular, leading to violation of compatibility requirements.

The above result does however suggest a physical understanding of the Poisson's ratio found in this investigation. Figure (16a) demonstrates how the results of this study require the composite to act under a tensile load. Figure (16b) shows how the material would react if compatible boundary conditions were not enforced. In Fig. (16c) the stresses necessary to ensure the required compatible boundary conditions are shown. The stresses are such as to cause the displacements curve L_2 to coincide with L_1 . The integral of these stresses is zero, i.e., $S_y = 0$.

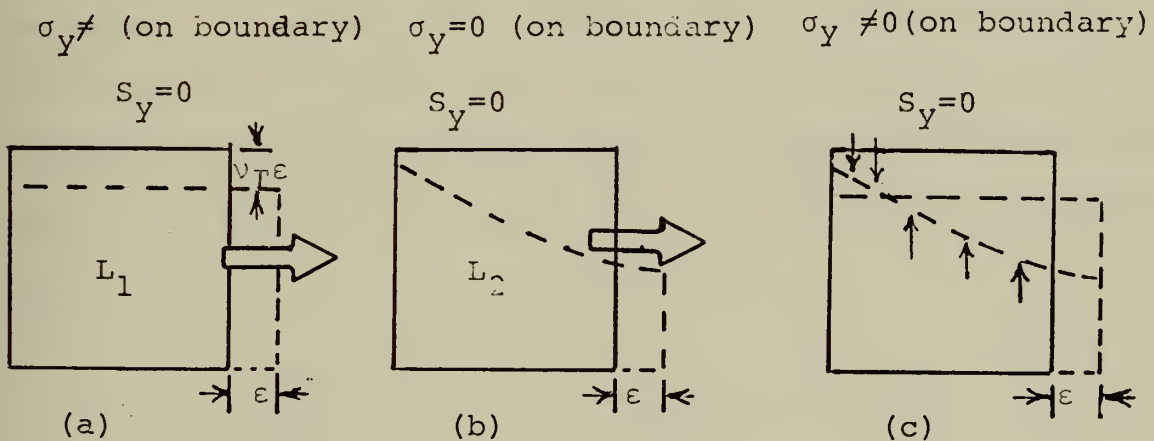


Figure (16). Transverse Poisson's Ratio.

6. Stress Concentration Factor (SCF)

Before examining the results obtained for stress concentration factors some consideration must first be given to the value and interpretation of such results. The primary value of SCF is in its relationship to the strength of a material. For a homogeneous material

initial yield will occur at the point of highest micro-stress, that is the location of the SCF. For identical materials with different SCF, which may occur as a result of loading conditions, initial yield will occur at a lower stress level in the material with the larger stress concentration factor.

For composite materials SCF requires further interpretation. Due to material discontinuity, stress distributions will differ in the matrix and filament materials. For this reason SCF should be calculated separately for filament and matrix regions of a composite. If the matrix is the larger no problem is posed, yield will occur in the matrix material. If the filament values are larger further investigation is necessary to ensure that initial yield is not occurring in the filament. If the ratio of filament to matrix stress concentration factor is less than the ratio of filament to matrix yield strength, yield will still occur in the matrix. That is

$$\frac{SCF_f}{SCF_m} / \frac{Y_{of}}{Y_{om}} < 1 \quad \text{yield in matrix}$$

$$\frac{SCF_f}{SCF_m} / \frac{Y_{of}}{Y_{om}} = 1 \quad \text{simultaneous yield in matrix and filament}$$

$$\frac{SCF_f}{SCF_m} / \frac{Y_{of}}{Y_{om}} > 1 \quad \text{yield in filament} \quad (III-23)$$

Caution should be exercised in interpreting stress concentration factors. Assuming that yield occurs in the matrix the macroscopic load required to cause yield may be related to the SCF as

$$SCF = \frac{Y_{O_m}}{S_c} \quad (III-24)$$

where S_c is the composite yield strength. This may represent a longitudinal, transverse, or longitudinal shear yield strength. For different materials with identical matrix yield strength, Y_{O_m} , therefore a smaller SCF will require a larger macroscopic load, S_c , to cause yield. Thus for such materials the SCF may be directly related to yield strength. An appealing aspect of this result is that for composites having identical matrix yield values, SCF offers an immediate evaluation of comparative yield strengths for the longitudinal, transverse, and longitudinal shear loading cases.

For any composite with initial yield occurring in the matrix, regardless of the matrix yield strength, the composite yield strength may be calculated for the three loading cases as

$$S_c = Y_{O_m} / SCF \quad (III-25)$$

As noted above SCF also allows a rapid check on which constituent first reaches yield.

For transverse and longitudinal shear loading the maximum SCF usually occurs in the matrix material. For

this reason any reference to SCF for these specific cases should be assumed to be a matrix property unless specifically stated to the contrary. No such generalization is warranted for the longitudinal loading problem.

Several authors have treated stress concentration factors extensively. Adams and Doner, [3] [6] using a finite difference technique, have provided a great deal of numerical data for both the transverse and longitudinal shear loading problems. For the transverse problem with a 55% Glass/Epoxy composite Adams and Doner calculated SCFX = 1.86. They also presented comparative data from solutions utilizing other analytical methods, ranging in value from 1.49 to 1.78. Analyses were not performed here for 55% volume composites, however a 47% model gave SCFX = 1.49, and a 60% model gave SCFX = 1.70. This data is included in Table VIII.

TABLE VIII. SCF FOR TRANSVERSE NORMAL LOADING

Method of Solution	$E_f/E_m=20$ $v_f=.3$ $v_m=.34$ $v_f=.55$		
	Stress Concentration Factor, SCFX		
Adams and Doner [6]			1.86
Wilson [13]			1.71
Pickett [14]			1.49
Foye [7]			1.78
Present analysis (47%)			1.49
Present analysis (60%)			1.70
Present analysis (50% estimate)			1.63

For the longitudinal shear problem Adams and Doner [3] gave results for SCFX of 40% and 55% models as 1.605 and 1.787 for Glass/Epoxy and 1.649 and 1.854 for Boron/Epoxy. As shown in Table IX these values bracket the present 47% solutions of 1.66 for Glass/Epoxy and 1.69 for Boron/Epoxy.

TABLE IX. SCF FOR LONGITUDINAL SHEAR LOADING

Material	Filament Volume	SCFX	Source
Glass/Epoxy	40%	1.605	Adams and Doner
Glass/Epoxy	47%	1.66	Present Analysis
Glass/Epoxy	55%	1.787	Adams and Doner
Boron/Epoxy	40%	1.649	Adams and Doner
Boron/Epoxy	47%	1.69	Present Analysis
Boron/Epoxy	55%	1.854	Adams and Doner

IV. PARAMETRIC ANALYSIS OF COMPOSITES

The purpose of this section is to analyze the effect that individual constituent material properties have on the mechanical properties of the composite. Properties considered include the modulus of elasticity, E , Poisson's ratio, ν , and yield strength, Y_0 , of both matrix and filament materials. In this study it is assumed that both filament and matrix materials are isotropic.

The goal is not to investigate every possible combination of material properties but rather to establish criteria and guidance for predicting composite properties associated with specific constituent properties.

The macroscopic properties that are considered as performance indices include the initial yield strength, the specific strength, longitudinal and transverse stiffness, shear modulus, stress concentration factors and specific moduli.

To determine how constituent properties effect composite behavior, parameter variations were carried out on fictitious materials. Variations were performed by starting with some actual properties, primarily those of a Boron/Aluminum or Graphite/Epoxy composite, and independently varying the particular property in question.

A. EFFECT OF FILAMENT VOLUME

To evaluate the effect of filament volume on composite properties several groups of 40%, 50%, and 60% filament volume models were investigated. These included

- 1) Boron/NARMCO Epoxy
- 2) High modulus graphite (MODMOR I)/4617 Epoxy
- 3) High strength graphite (MODMOR II)/NARMCO Epoxy
- 4) MODMOR II/4617 Epoxy

For MODMOR I/NARMCO Epoxy additional models of 30% and 70% were also utilized. The material properties for all materials are listed in Table II.

In a composite material subjected to a constant longitudinal strain the macroscopic stress is related to the microscopic axial stresses as

$$S_c = v_f \sigma_f + v_m \sigma_m \quad (\text{IV-1})$$

where v_f and v_m represent the volume fraction of filament and matrix materials. An assumption of this study is that the filament and matrix are perfectly bonded. For longitudinal loading the strain will be constant over any transverse cross section, thus;

$$\epsilon_c = \epsilon_f = \epsilon_m \quad (\text{IV-2})$$

Within the elastic region the stress strain relations give

$$E_L = v_f E_f + v_m E_m \quad (\text{IV-3})$$

The longitudinal stiffness of a composite should be described then by a linear relation, the so called law of mixtures.

This line passes through the matrix modulus at 0% filament volume ($E_L = E_m$ when $v_f = 0$) and through the filament modulus at 100% filament volume ($E_L = E_f$ when $v_f = 1$), as shown in Fig. (17) for MODMOR I/NARMCO Epoxy.

For the case of transverse stiffness the relationship is not linear with respect to filament volume. For loading in the X or Y direction a constant strain applied at the boundary will not result in a uniform strain throughout the material. This is due to the change in material composition for cross sections perpendicular to the direction of loading. At zero filament volume the material has the properties of the matrix, that is the composite transverse modulus, E_T , must equal the matrix modulus, E_m . At 100% filament volume the material will have the properties of the filament and the composite transverse modulus, E_T , will equal the filament modulus, E_f . The transverse stiffness, E_T , versus filament volume, v_f , curve must go through

$$E_T = E_m \quad \text{at} \quad v_f = 0$$

and increase monotonically, terminating at

$$E_T = E_f \quad \text{at} \quad v_f = 1.$$

All cases investigated followed this pattern. The results for MODMOR I/NARMCO Epoxy are plotted in Fig. (17). The increasing slope of the curve indicates that an increase in filament volume has a more significant effect on transverse stiffness at higher filament volume percentages. For example, for a MODMOR I/NARMCO Epoxy composite a 15% increase in filament volume, v_f , from 35% to 50% results in a 42% increase in composite transverse stiffness, E_T . A similar 15% increase

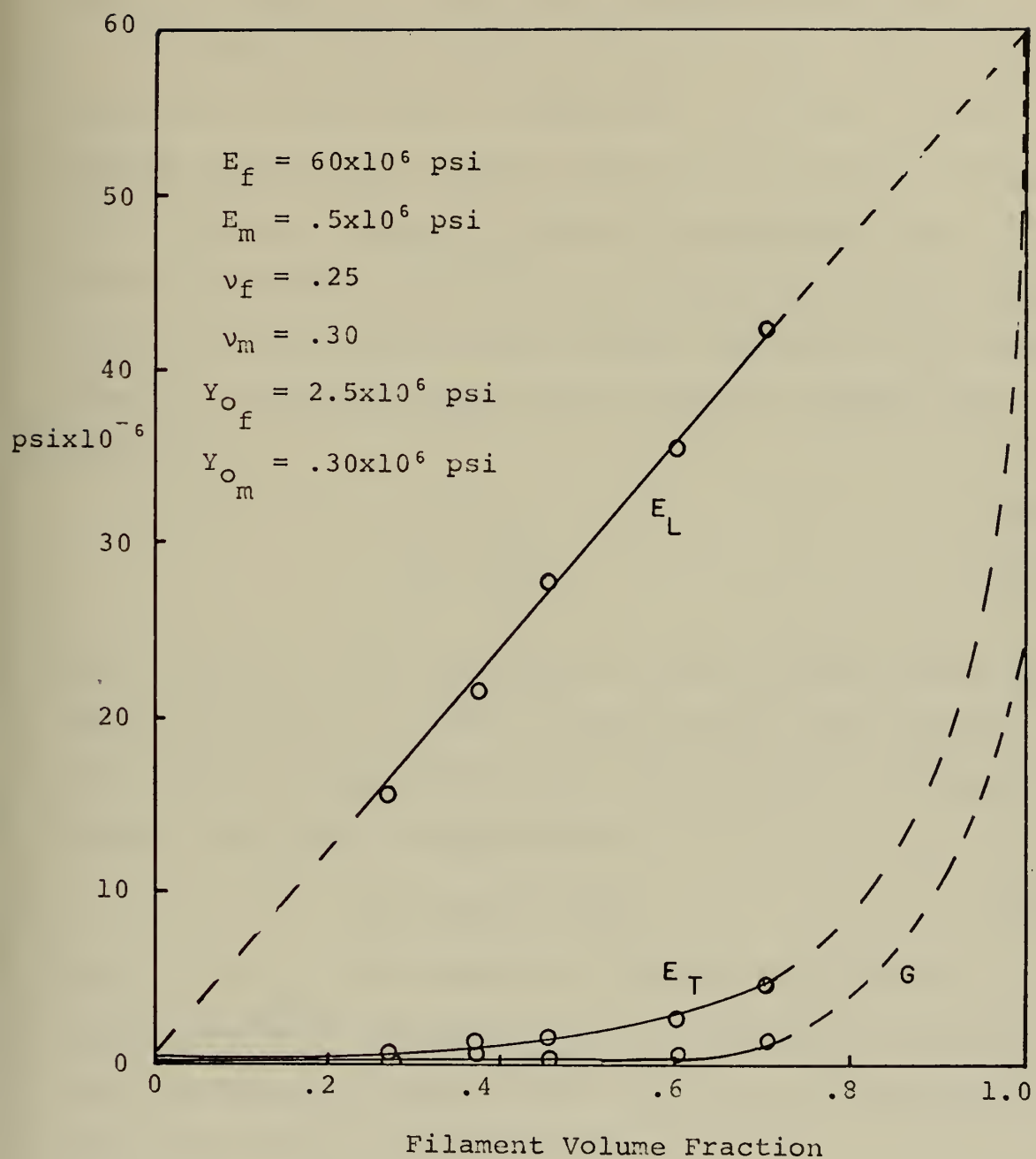


Figure (17). Composite Elastic Properties vs. Filament Volume

in v_f from 60% to 75% results in a 75% increase in composite transverse stiffness. For composite shear modulus, G , a change in cross sectional material properties indicates a behavior similar to that of the transverse stiffness.

In longitudinal loading problem III, the stress concentration factor SCFZ is calculated. The unit strain applied results in a uniform stress in the matrix material and a uniform stress of a different magnitude in the filament material. For the same constituent material and identical unit strain these stresses should not vary with changes in filament volume since they must satisfy the relations

$$\sigma_f = E_f \epsilon \quad (\text{IV-4})$$

$$\sigma_m = E_m \epsilon \quad (\text{IV-5})$$

The resultant surface traction, S_z , the average value of the microstresses σ_f and σ_m acting on the cross section, will change proportionally with the increase in filament volume, according to the equation

$$S_z = v_f \sigma_f + v_m \sigma_m \quad (\text{IV-6})$$

Thus as $(\sigma_z)_{\max}$, the numerator of SCFZ, Eq. (III-11), remains constant, the denominator S_z increases lineally with increasing filament volume, v_f , and the stress concentration factor itself decreases.

For a homogeneous material the uniform stress throughout the entire block would equal the applied stress and SCFZ

would equal one. The curve for SCFZ versus filament volume should therefore pass through the points $SCFZ (v_f = 0) = 1$, and $SCFZ (v_f = 1) = 1$.

Consider the case of the SCFZ in the filament. The addition of a small amount of filament material to a 0% model would result in a negligible change in the surface traction. That is, for unit strain

$$\epsilon_z = 1.0 \quad (IV-7)$$

$$S_z \approx \sigma_m = E_m \epsilon = E_m \quad (IV-8)$$

The maximum filament stress in this case would be

$$\sigma_{z_f} = E_f \epsilon = E_f \quad (IV-9)$$

For a small filament volume the filament SCFZ would be

$$SCFZ = \frac{\sigma_f}{\sigma_m} = \frac{E_f}{E_m} \quad (IV-10)$$

Figure (18) for Boron/6061 Aluminum shows this graphically. The points at 0% and 100% filament volume are established in accordance with the above discussion while the other points are results of the analysis.

For the matrix SCFZ the maximum stress will remain constant while the average surface traction increases with increase of v_f , as noted in Eq. (IV-6). For the matrix case therefore the curve will originate at $SCFZ (v_f = 0) = 1$, and decrease to the point where, with little matrix material remaining,

$$SCFZ \approx \frac{E_m}{E_f} \quad (IV-11)$$

Recall from section II-B-6 that if the ratio of the filament SCF to the matrix SCF is less than the ratio of filament to matrix yield strengths, Y_{o_f}/Y_{o_m} , yield will occur in the matrix. This will determine in each individual case which of the stress concentration factors discussed above is pertinent.

SCFX and SCFXZ increase directly with filament volume, as shown in Fig. (18). These stress concentrations occur in the matrix at the interface.

B. EFFECT OF FILAMENT YOUNG'S MODULUS

To evaluate the effect of variations in the modulus of elasticity of the filament, E_f , on the composite mechanical properties four computer analyses were made. Each analysis used a 50% filament volume model with material properties as listed in Table X.

TABLE X. FILAMENT YOUNG'S MODULUS VARIATION

Analysis	E_f (psix 10^{-6})	v_f	Y_{o_f} (psix 10^{-5})	E_m (psix 10^{-6})	v_m	Y_{o_m} (psix 10^{-4})
1	30	.2	4.8	10.	.3	.3
2	40	.2	4.8	10.	.3	.3
3	60	.2	4.8	10.	.3	.3
4	70	.2	4.8	10.	.3	.3

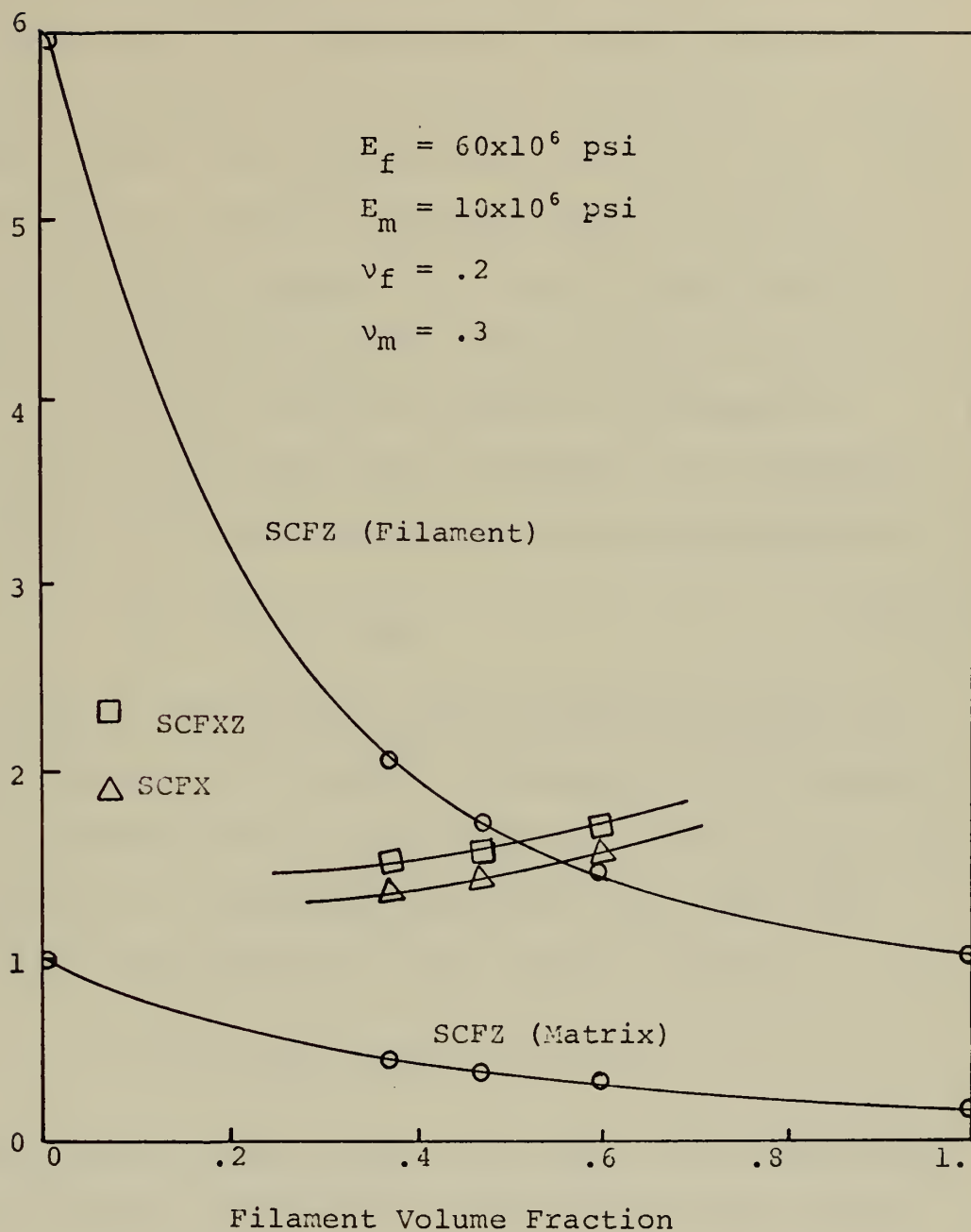


Figure (18). Stress Concentration Factor vs. Filament Volume.

Figure (19) displays the transverse stiffness, longitudinal stiffness, and shear modulus of the composite as a function of fiber modulus. This figure shows that the most significant effect of increasing the filament modulus is the linear increase in the composite longitudinal stiffness, E_L . This relates with matrix modulus variation and will be treated in greater detail in the following two sections.

The relationship between the composite longitudinal stiffness, E_L , and the filament Young's modulus, E_f , is linear. In fact for the same reasons as discussed in section IV-A for filament volume variation, the relationship can be accurately described by a rule of mixtures as

$$E_L = v_f E_f + v_m E_m \quad (IV-12)$$

The plot of the composite shear modulus variation of Fig. (19) appears to be linear, although it will be shown that this variation must be non-linear. Consider that, for the combination of materials considered here, when the composite is homogeneous $E_f = 10 \times 10^6$ psi. Hence

$$G_c = G_f = G_m = 3.84 \times 10^6 \text{ psi}$$

The shear modulus curve of Fig. (19) must vary considerably from its apparent linear form to pass through this point, as shown in Fig. (25).

As would be expected, considering the linear variation of longitudinal stiffness, the longitudinal yield strength also increased linearly with filament modulus increase.

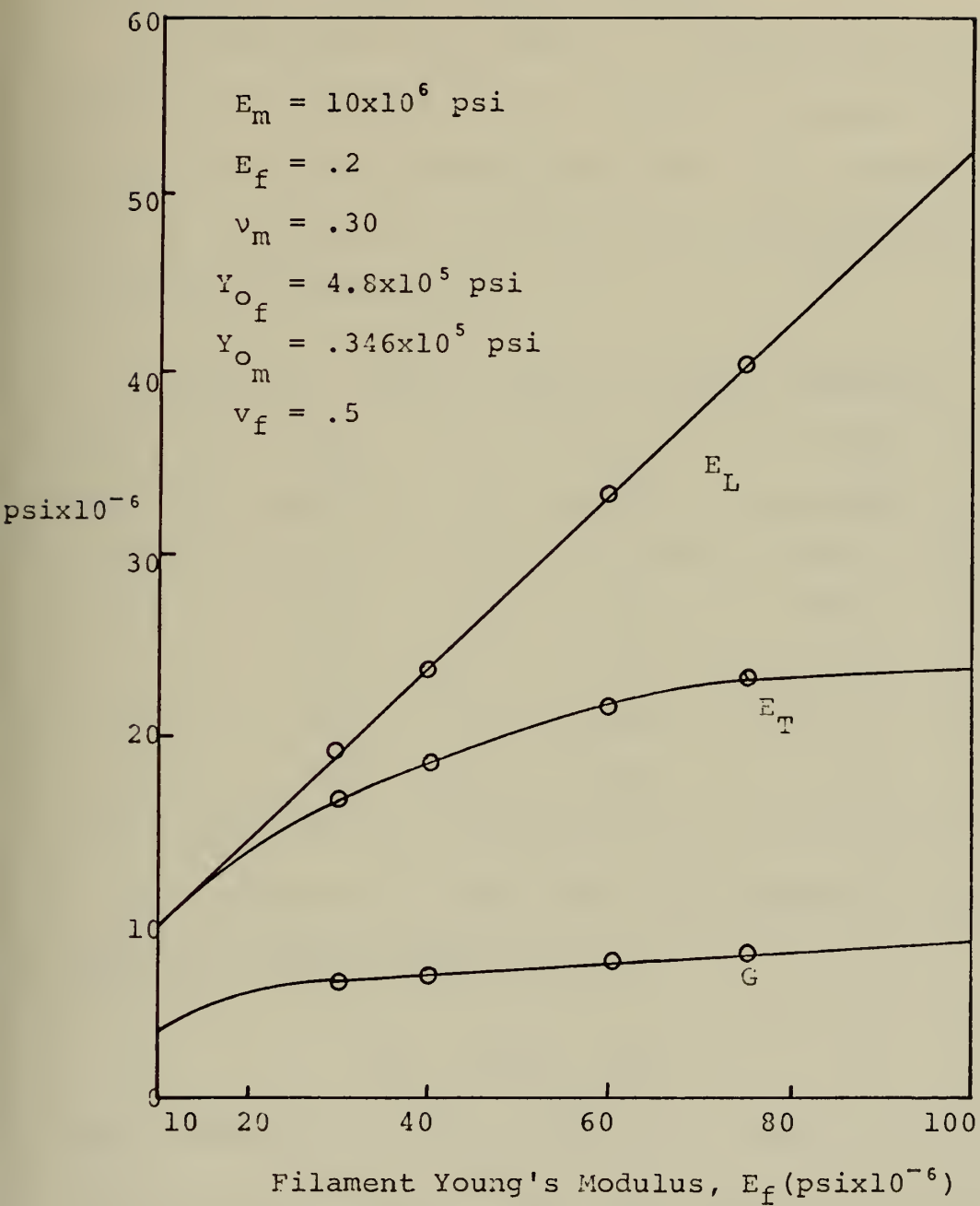


Figure (19). Composite Elastic Properties vs. Filament Modulus of Elasticity.

Variation in transverse and longitudinal shear strength was negligible for the range of E_f considered, $E_f = 30-75 \times 10^6$ psi.

C. EFFECT OF MATRIX YOUNG'S MODULUS

To investigate the effect of variation of the matrix modulus of elasticity on the composite mechanical properties a series of four analyses were made. All analyses were made with a 50% filament volume model with constituent properties as shown in Table XI.

TABLE XI. MATRIX YOUNG'S MODULUS VARIATION

Analysis	E_f (psix 10^{-6})	v_f	Y_{of} (psix 10^{-5})	E_m (psix 10^{-6})	v_m	Y_{Om} (psix 10^{-5})
1	60.	.2	4.8	10.	.3	.346
2	60.	.2	4.8	7.	.3	.346
3	60.	.2	4.8	5.	.3	.346
4	60.	.2	4.8	2.5	.3	.346

As established in Eq. (IV-3) the composite longitudinal stiffness varies lineally as

$$E_L = v_f E_f + v_m E_m$$

Thus the variation of E_L with matrix modulus is also linear as shown in Fig. (20). From this figure it is seen that the variation of E_m has a greater effect on the transverse stiffness and shear modulus than on longitudinal stiffness. An increase of 400% in the matrix modulus of elasticity results in percentage increases of

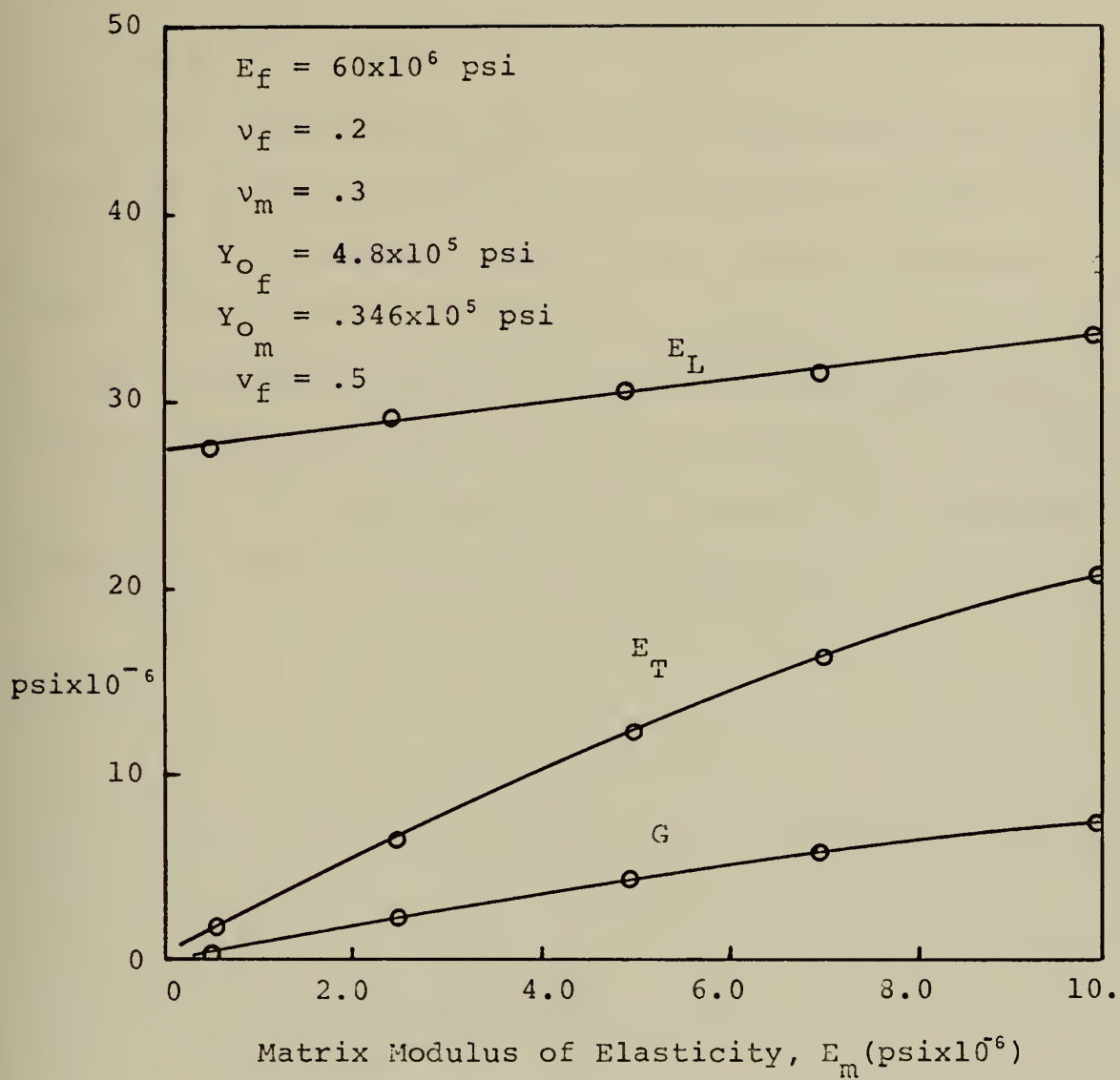


Figure (20). Composite Elastic Properties vs. Matrix Modulus of Elasticity.

- i) $E_L = 14\%$
- ii) $E_T = 207\%$
- iii) $G = 222\%$

This also resulted in an increase in transverse and longitudinal shear yield strength. The complementary effect of this result with that of the filament modulus variation will be discussed in the following section.

An interesting aspect of the variation of the matrix Young's modulus is that, despite the increase in longitudinal stiffness, the longitudinal yield strength, S_L , decreases. The reason for this may be seen in Fig. (21).

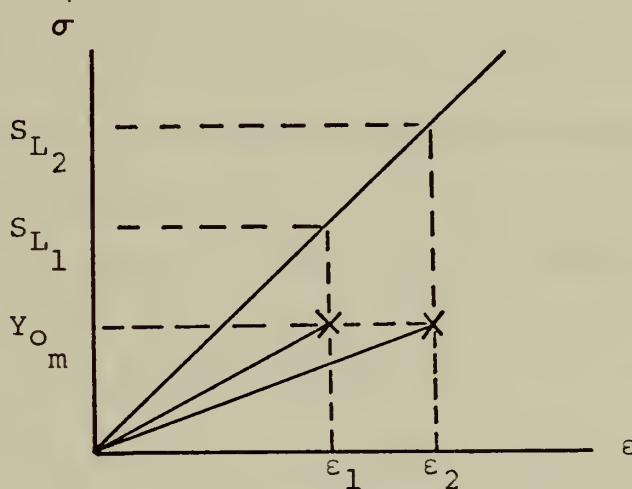


Figure (21). Effect of Matrix Stiffness on Longitudinal Yield Strength.

For two matrix materials with similar initial yield points one with the lower Young's modulus will require a larger strain to reach yield. Due to the relatively small effect of matrix stiffness on composite longitudinal stiffness, E_L , assume that E_L is the same for both cases. The larger strain, ϵ_2 , will result in a larger composite yield strength, S_{L_2} .

D. EFFECT OF CONSTITUENT PROPERTY RATIO

The results noted for filament and matrix stiffness variation may be conveniently correlated through use of non-dimensional parameters. For example, composite longitudinal stiffness, E_L , may be normalized with respect to filament stiffness, i.e., E_L/E_f , and plotted against the constituent modulus ratio E_m/E_f . Figure (22) is such a representation. Longitudinal stiffness may be expressed as

$$E_L = v_f E_f + v_m E_m \quad (\text{IV-13})$$

Dividing through by E_f and rearranging terms yields

$$E_L/E_f = v_f (1 - E_m/E_f) + E_m/E_f \quad (\text{IV-14})$$

Equation (IV-14) describes the configuration of the non-dimensional longitudinal stiffness curve. The following points are significant:

i) when $E_m = E_f$, i.e., a homogeneous material,

$$E_L/E_f = E_m/E_f = 1. \quad (\text{IV-15})$$

ii) when $E_m = 0$, i.e., zero matrix stiffness,

$$E_L/E_f = v_f (1) = v_f \quad (\text{IV-16})$$

Equations (IV-15) and (IV-16) were used to determine the extreme points of Fig. (22). The points noted on this figure are the results of this investigation for a filament volume fraction, $v_f = .5$. For comparison some other curves were drawn using the endpoints determined by Eqs. (IV-15) and

(IV-16). The non-dimensional longitudinal stiffness curve for any filament volume must fall in the triangular region of Fig. (22) formed by the $v_f = 0$ curve and the $v_f = 1.0$ curve.

The comparative effect of filament Young's modulus and matrix Young's modulus variations on composite longitudinal stiffness may be examined by consideration of Eq. (IV-13). Taking partial derivatives of this equation with respect to the individual independent quantities yields

$$\frac{\partial E_L}{\partial E_m} = v_m \quad (\text{IV-17})$$

and

$$\frac{\partial E_L}{\partial E_f} = v_f \quad (\text{IV-18})$$

Thus the effect of constituent stiffness variation on longitudinal stiffness is directly related to the volume fraction of the constituent. For the 50% filament volume case this is seen to be true as Figs. (19) and (20) show that filament and matrix stiffness variation, respectively, result in identical slopes of 0.5 when plotted versus longitudinal stiffness.

These comments concerning comparative effects of matrix and filament stiffness variation refer to the change per unit stiffness of constituent. The actual range of longitudinal stiffness due to matrix and filament stiffness variation is considerably different however. Consider Fig. (23), a non-dimensional longitudinal stiffness curve for some arbitrary filament volume fraction, v_f .

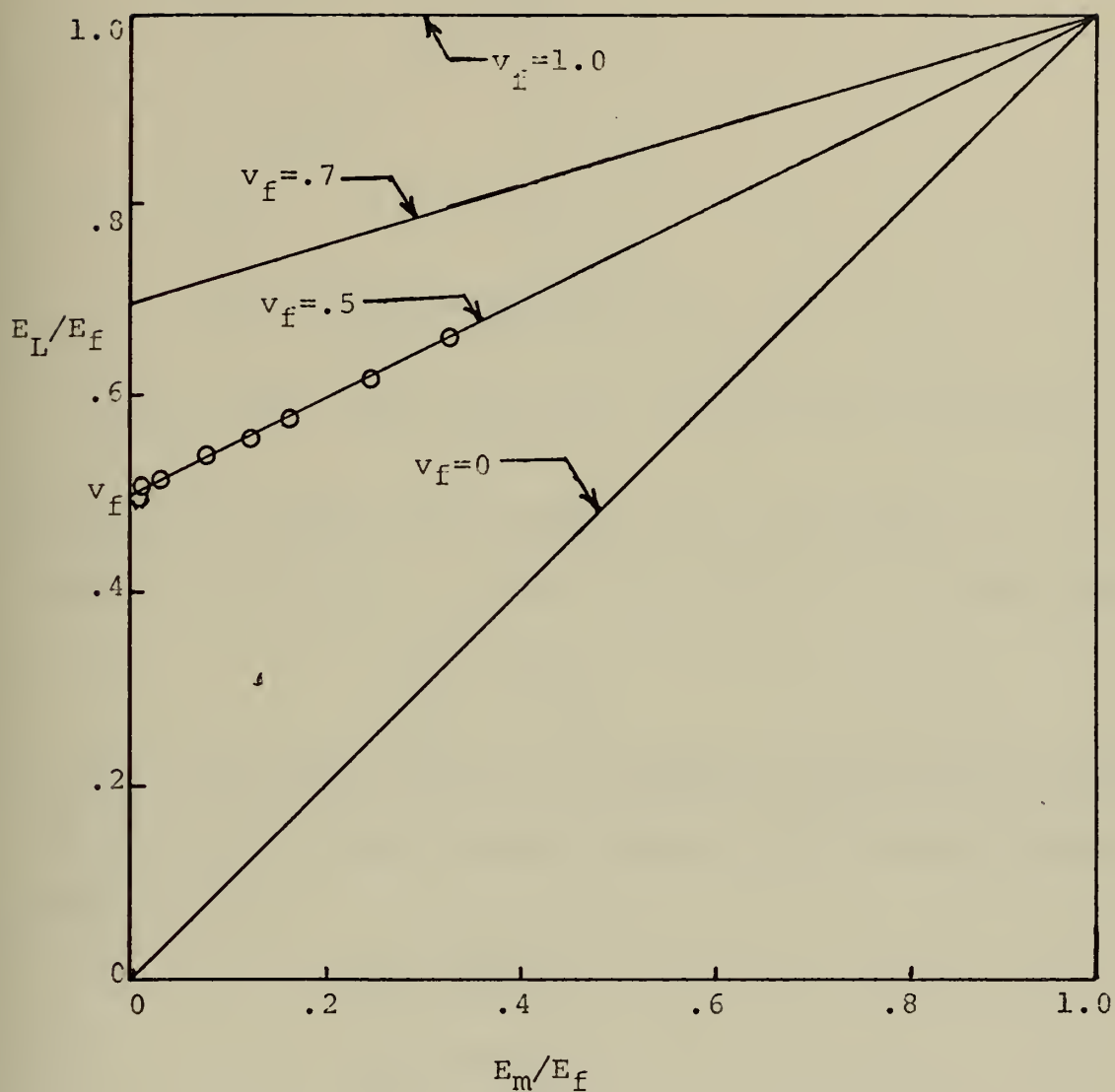


Figure (22). Effect of Constituent Stiffness on Longitudinal Stiffness.

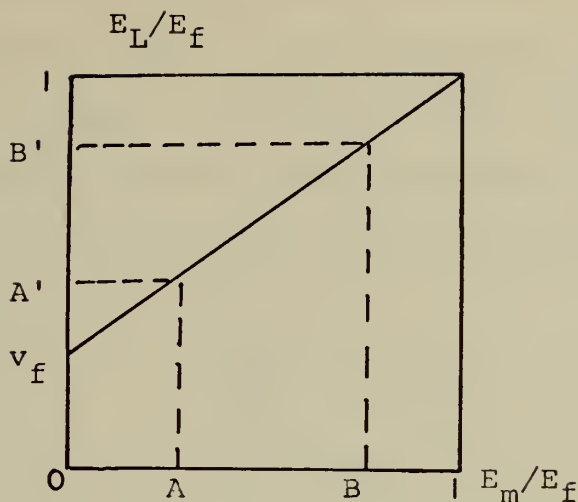


Figure (23). Non-Dimensional Longitudinal Stiffness.

For a given constituent moduli ratio, say point A, a specific ratio, E_L/E_f , results at point A'. At this point

$$E_{L_A} = A'E_{f_A}$$

If the constituent ratio is increased to point B by increasing the matrix modulus while holding the filament modulus constant then

$$E_{f_A} = E_{f_B}$$

$$E_{L_B} = B'E_{f_B}$$

The ratio of longitudinal stiffness for these two hypothetical composites is

$$\frac{E_{L_B}}{E_{L_A}} = \frac{B'E_{f_B}}{A'E_{f_A}} = \frac{B'}{A'} = \frac{(E_L/E_f)_B}{(E_L/E_f)_A} \quad (IV-19)$$

Thus variation in the matrix modulus results in a change in composite longitudinal stiffness in direct proportion to the

change in non-dimensional stiffness, E_L/E_f . In general the maximum range of non-dimensional stiffness, E_L/E_f , is from the value of filament volume fraction, v_f , to 1.0. The maximum increase in longitudinal stiffness E_L , due solely to a variation of matrix modulus is

$$\left(\frac{E_{LB}}{E_{LA}} \right)_{\max} = \frac{1.0}{v_f}$$

For the 50% filament volume case of Fig. (22) this maximum increase is a factor of

$$\left(\frac{E_{LB}}{E_{LA}} \right)_{\max} = \frac{1.0}{.5} = 2.0$$

If the constituent ratio of Fig. (23) is increased to point B by decreasing the filament modulus while holding the matrix modulus constant, then

$$\begin{aligned} E_{fB} &< E_{fA} \\ E_{LA} &= A'E_{fA} & E_{LB} &= B'E_{fB} \\ \frac{E_{LA}}{E_{LB}} &= \frac{A'E_{fA}}{B'E_{fB}} \end{aligned} \quad (IV-20)$$

Thus the increase in longitudinal stiffness with variation of the filament modulus is dependent on the non-dimensional stiffness, E_L/E_f , and the ratio of filament moduli, E_{fA}/E_{fB} .

For actual filament materials the range for the filament modulus is approximately 10×10^6 to 60×10^6 psi. Consider a constant matrix material, for example aluminum. For the 50% filament volume case of Fig. (22) the range of E_L/E_f corresponding to this range of filament modulus is 50 to 1.0. For this 50% case the variation in longitudinal stiffness due to variation in the filament modulus alone is

$$\left(\frac{E_{L_A}}{E_{L_B}} \right)_{\max} = \left(\frac{.50}{1.0} \right) \left(\frac{60}{10} \right) = 3.0$$

Variation of the filament modulus is thus seen to result in a much greater range of longitudinal stiffness than does the variation of the matrix modulus of elasticity because of the greater range of E_f as compared to E_m .

Figure (24) is a non-dimensional representation of the effect of constituent stiffness, E_m/E_f , on a normalized composite transverse stiffness, E_T/E_f . Note that the curve approaches $E_T = 0$ as E_m/E_f approaches zero. This indicates that when the matrix material is extremely soft in comparison to the filament that the macroscopic transverse stress required to produce a unit displacement of the block boundary, as in load case I, is virtually zero. In the limit, when $E_m = 0$, then $E_T = 0$. Thus it is theoretically possible to produce a composite with a value of transverse stiffness approaching zero.

Comparison of Figs. (19) and (20) shows that the slope of the E_T vs. matrix stiffness curve is greater than that

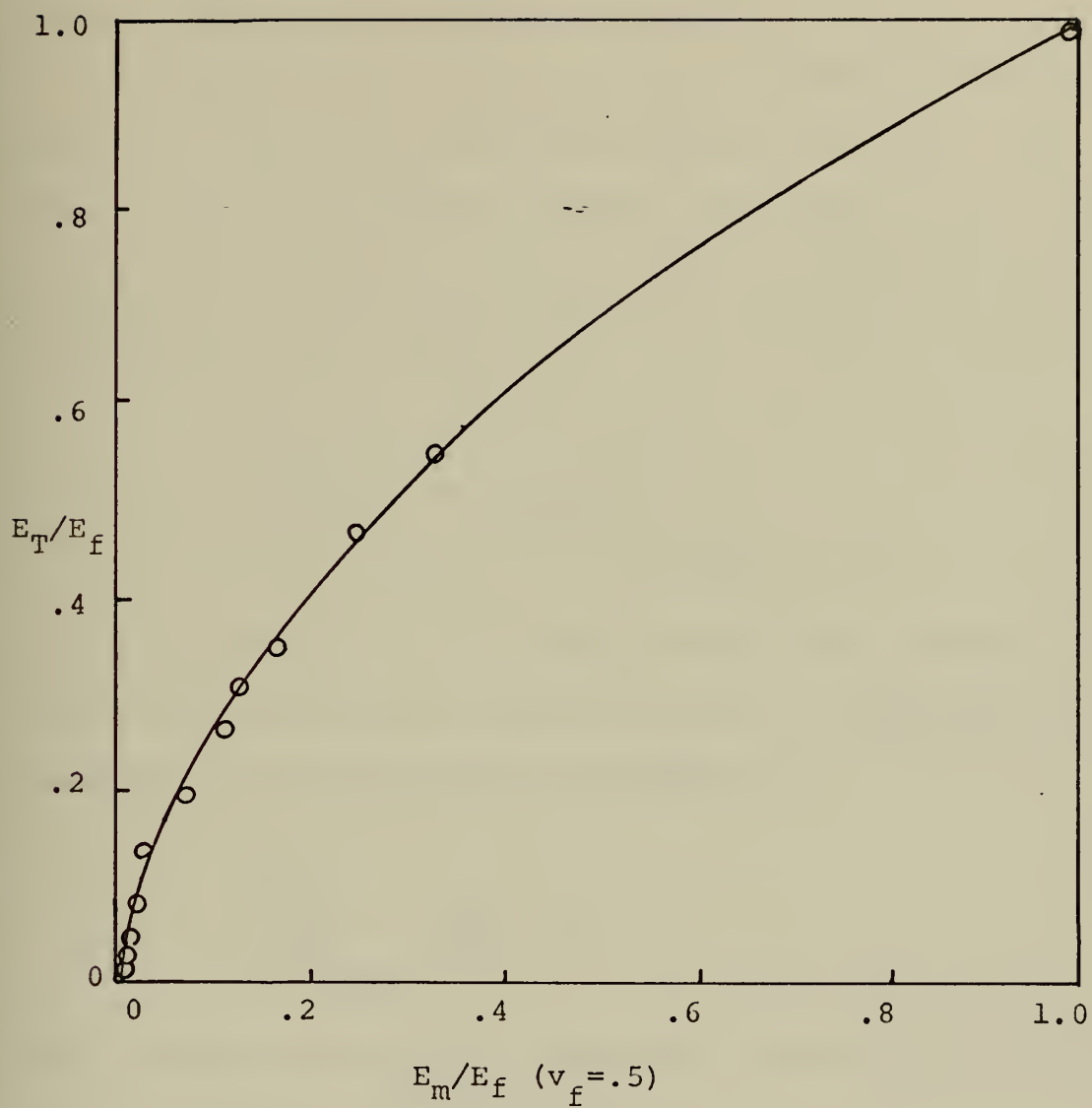


Figure (24). Effect of Constituent Stiffness on Transverse Stiffness.

of the E_T vs. filament stiffness curve. Therefore on a unit stiffness basis, variation of matrix Young's modulus is more effective than variation of filament Young's modulus on the composite transverse stiffness.

By considering a non-dimensional transverse stiffness curve and following the same technique as for the non-dimensional longitudinal stiffness the range of the transverse stiffness due to matrix Young's modulus variation, analogous to Eq. (IV-19), is

$$\left(\frac{E_{TB}}{E_{TA}} \right)_{\max} = \left[\frac{(E_T/E_f)_B}{(E_T/E_f)_A} \right]_{\max} \quad (\text{IV-21})$$

The range of E_T/E_f , as is seen in Fig. (24), is zero to one. Thus the theoretical maximum increase of transverse stiffness due to matrix Young's increase is

$$\left(\frac{E_{TB}}{E_{TA}} \right)_{\max} = \frac{1.0}{0} = \infty$$

The maximum variation in transverse modulus due to variation of the filament stiffness alone is

$$\left(\frac{E_{TA}}{E_{TB}} \right)_{\max} = \left[\frac{(E_T/E_f)_A}{(E_T/E_f)_B} \frac{E_{fA}}{E_{fB}} \right]_{\max} \quad (\text{IV-22})$$

For common filament materials the range of filament modulus is approximately 10×10^6 to 60×10^6 psi. Consider a constant matrix material, for example aluminum. For the 50%

filament volume case of Fig. (24) the range of E_T/E_f corresponding to this range of filament modulus is .349 to 1.0. Thus the maximum variation in transverse stiffness due to variation of the filament modulus alone is

$$\left(\frac{E_{TA}}{E_{TB}} \right)_{\max} = \left(\frac{.349}{1.0} \right) \left(\frac{60.}{10.} \right) = 2.094$$

The range of transverse stiffness due to matrix Young's modulus variation is greater therefore than that due to filament Young's modulus variation.

Figure (25) is a plot of the normalized composite shear modulus, G/G_f , versus the ratio of constituent shear moduli, G_m/G_f . This curve substantiates earlier contentions that shear modulus variation with respect to constituent moduli is non-linear. Again this curve approaches zero as the constituent moduli ratio approaches zero.

Again comparing Figs. (19) and (20) it is seen that the slope of the composite shear modulus versus matrix stiffness is greater than the slope of the composite shear modulus versus filament stiffness curve. This indicates that, per unit of constituent stiffness, the matrix material has a greater effect on composite shear modulus.

By considering a non-dimensional shear modulus curve and following the same technique as for the non-dimensional longitudinal stiffness, the range of shear modulus variation due to matrix shear modulus variation, analogous to Eq. (IV-19), is

$$\left(\frac{G_B}{G_A} \right)_{\max} = \left[\frac{(G/G_f)_B}{(G/G_f)_A} \right]_{\max} \quad (\text{IV-23})$$

The range of G/G_f , as seen in Fig. (25), is from zero to 1.0. Thus the theoretical maximum value of Eq. (IV-23) is

$$\left(\frac{G_B}{G_A} \right)_{\max} = \frac{1.0}{0} = \infty$$

If the ratio G_m/G_f is increased by changing the filament modulus the maximum range attainable is

$$\left(\frac{G_A}{G_B} \right)_{\max} = \left[\frac{(G/G_f)_A}{(G/G_f)_B} \frac{G_{fA}}{G_{fB}} \right]_{\max} \quad (\text{IV-24})$$

For common filament materials the range of shear modulus is approximately 4.0×10^6 to 25.0×10^6 psi. For a constant matrix material, for example aluminum, the range of G/G_f of Fig. (25) corresponding to this range of filament shear modulus is .31 to 1.0. These values are for a 50% filament volume case. For this case the Eq. (IV-24) becomes

$$\left(\frac{G_A}{G_B} \right)_{\max} = \left(\frac{.31}{1.0} \right) \left(\frac{25}{4} \right) = 1.94$$

Variation of the matrix shear modulus thus results in a greater range of composite shear modulus than does variation of filament shear modulus.

The effect of Poisson's ratio will be discussed in the next section.

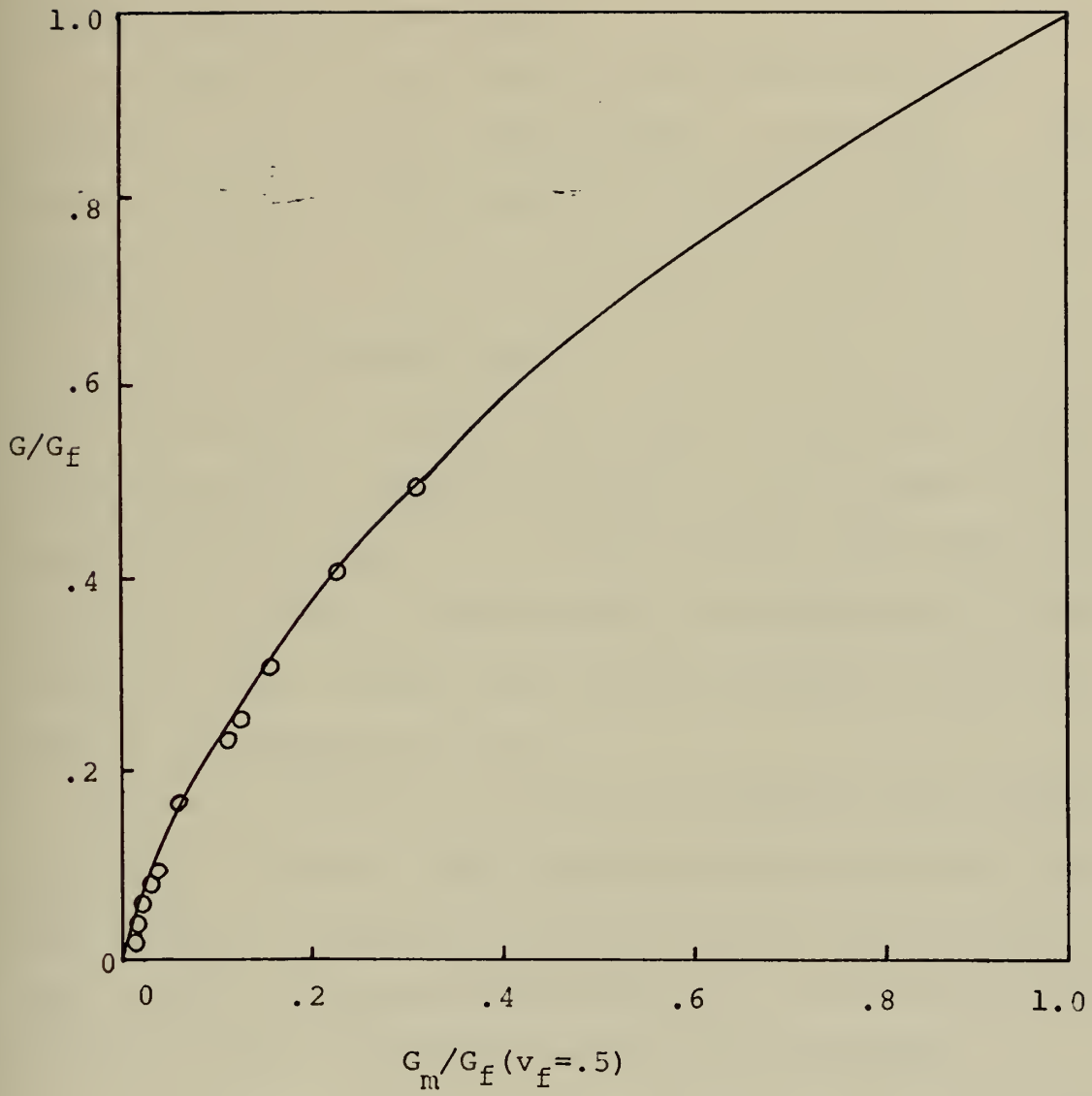


Figure (25). Effect of Constituent Shear Modulus on Composite Shear Modulus.

The primary advantage of the non-dimensional representations is that valid comparisons may be made between composites without necessarily holding the Young's modulus of one constituent constant.

It should be noted that the non-dimensional plots presented here are for a 50% filament volume model. Different filament volume models will result in different curves.

E. EFFECT OF POISSON'S RATIO

Two series of computer analyses were made for evaluation of the effects on composite behavior due to change of Poisson's ratio of the filament, ν_f . Four analyses were made using a fictitious material approximating the properties of Boron/Aluminum while varying the filament Poisson's ratio from .15 to .30 in increments of .05.

Another series of analyses was conducted with MODMOR I graphite and epoxy. This was done because Poisson's ratio for graphite filaments is not accurately specified and it was desired to determine whether or not this would significantly effect the results of this investigation.

In both cases no significant effect was noted on any composite mechanical property. All observed variations were less than 1%.

The effect of the variation of matrix Poisson's ratio was evaluated through a series of three analyses. Constituent properties similar to Boron/6061 Aluminum were used while varying the matrix Poisson's ratio from .30 to .35. Again

no significant effect on composite mechanical properties was noted. It is expected however that changes in Poisson's ratio will produce more significant changes for post yield behavior.

F. EFFECT OF MATRIX YIELD STRENGTH

To investigate the effect of the matrix yield strength, Y_{O_m} , on composite mechanical properties, a series of four computer analyses were made. All used a 50% Boron filament volume model with constituent properties as listed in Table XII.

TABLE XII. MATRIX YIELD STRENGTH VARIATION

Analysis	E_f (psix 10^{-6})	v_f	Y_{O_f} (psix 10^{-5})	E_m (psix 10^{-6})	v_m	Y_{O_m} (psix 10^{-5})
1	60.	.2	4.8	10.	.3	.346
2	60.	.2	4.8	10.	.3	.230
3	60.	.2	4.8	10.	.3	.130
4	60.	.2	4.8	10.	.3	.030

The yield point of a material has no effect on the elastic properties of that material. It merely defines the limit of elastic behavior. Thus the variation of matrix yield strength had no effect on the composite stiffness or shear modulus. This is as expected considering the comparison in section III-B-4 of two aluminum alloy matrix materials.

Figure (26) shows hypothetical stress-strain curves for the composite (curve A) and the matrix (curve B). For a given matrix yield strength, say $Y_{O_m}^1$, a specific composite macroscopic yield strength, S_C^1 , is defined. If, as stated, the yield point of a material does not effect the elastic properties, then the stress-strain curves remain the same, independent of the yield strength variation. For a given increase in matrix yield strength, say a 50% increase to $Y_{O_m}^2$, plane geometry shows that an identical increase, on a percentage basis, must occur in the composite yield strength. Figure (27) confirms this hypothesis.

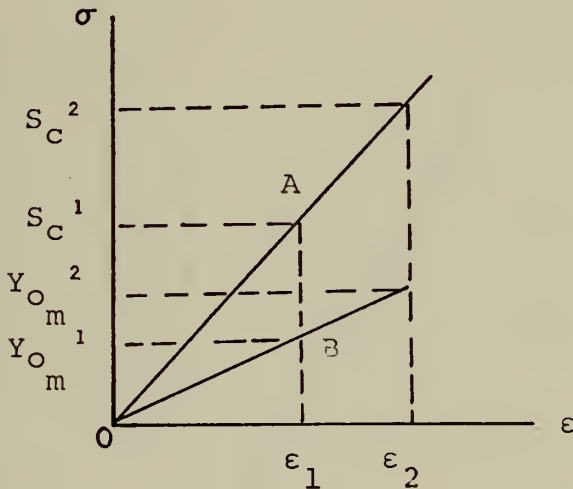


Figure (26). Effect of Matrix Yield Strength Variation.

It should be noted that the above discussion assumes that yield occurs in the matrix, as is true for most, but not all, composites.

The implication of this phenomenon is that there is no variation in the shape of the initial yield surface due

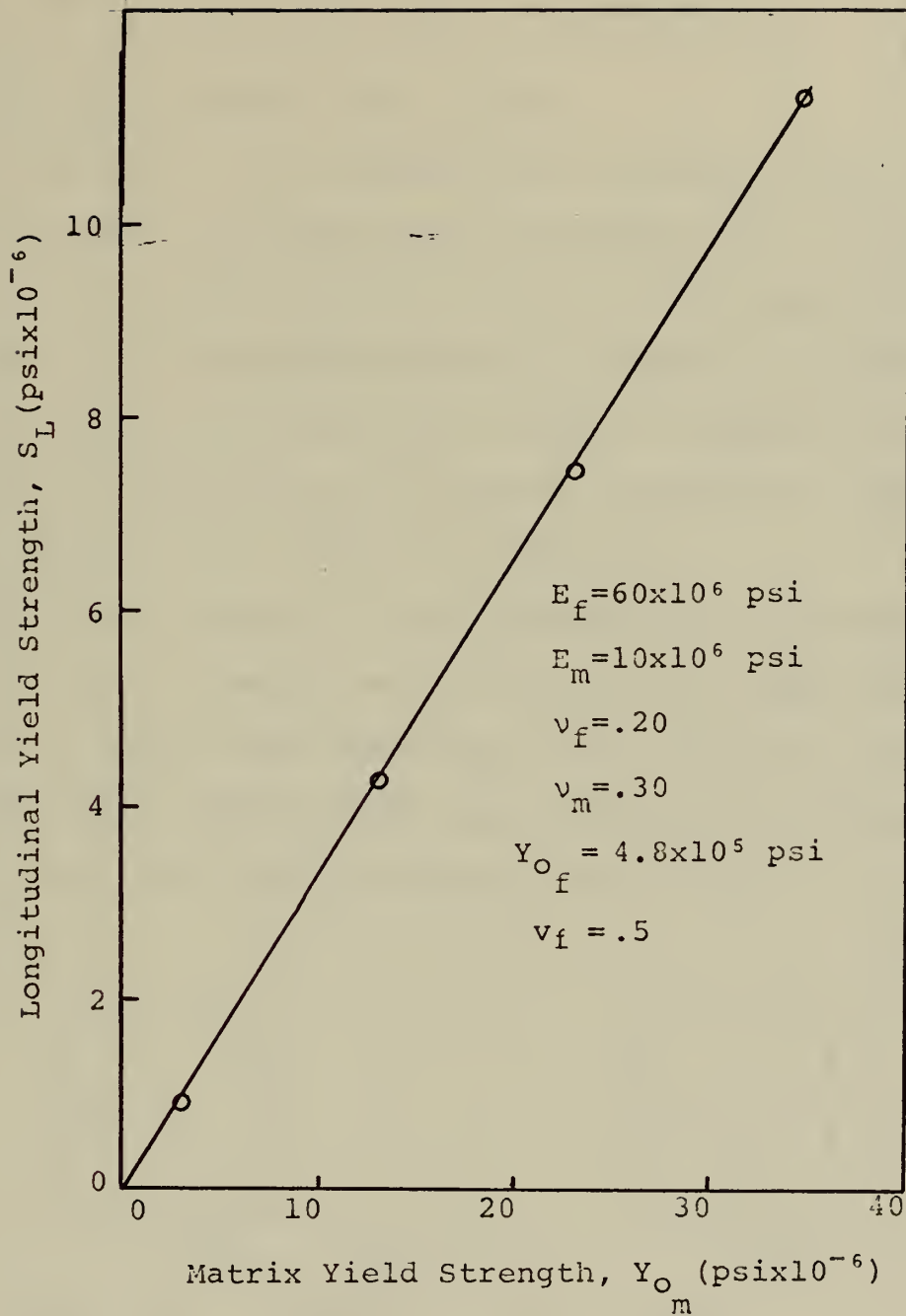


Figure (27). Effect of Matrix Yield Strength on Composite Yield Strength.

solely to variation in the matrix yield strength. That is, the initial yield surface changes in size only. This can be seen in Figs. (C-1) and (C-2) of Appendix C.

G. EFFECT OF FILAMENT CROSS SECTION

The majority of the computations included in this investigation are based on longitudinal filaments with a circular cross section. This was done because it is assumed that this particular cross section would be the easiest to produce. The question arises as to the effect change of shape of filament cross section would have on composite properties. Such changes might be the result of fabrication.

To provide an answer to this question two elliptical cross sectional filaments were investigated. These were identical ellipses with major/minor axes ratio of 1.25 to 1.0. One model had the major axis oriented along the x-axis and one along the y-axis, as seen in Fig. (28).



Figure (28). Elliptical Cross Sections.

The rule of mixtures and the comments of section IV-A leading to its use are independent of cross section shape. Elliptical and circular cross section filaments of the same volume should therefore produce identical results for the

longitudinal composite stiffness, E_L . In the three cases investigated, 50% models of Boron/6061 Aluminum, Boron/NARMCO Epoxy, and S-glass/NARMCO Epoxy, this was found to be true. The variation in E_L was less than 1% in all cases, as may be seen from Table XIII.

TABLE XIII. EFFECT OF FILAMENT CROSS SECTION ON LONGITUDINAL STRENGTH AND STIFFNESS

	Circular		Elliptical	
	E_L (psix 10^6)	S_L (psix 10^4)	E_L (psix 10^6)	S_L (psix 10^4)
Boron/6061 Aluminum	37.08	11.4	37.25	10.1
Boron/NARMCO Epoxy	28.23	16.71	28.57	14.5
S-glass/NARMCO Epoxy	6.05	3.47	6.105	3.04

The transverse composite stiffness reacted as expected. In all cases E_T increased in the direction of the major elliptical axis and decreased in the direction of the minor axis as noted in Table XIV. This seems reasonable since more of the stiff filament material is oriented in the direction of the major axis. On a percentage basis the increase in transverse stiffness in the direction of the major axis was approximately twice that of the decrease in the direction of the minor axis.

An interesting result of the cross section variation that is evident in Table XIV is that the transverse strength changed in a manner opposite to that of the transverse stiffness. That is, the transverse strength increased in the direction of the minor axis and decreased in the direction

of the major axis. This result may be understood by considering the micromechanics of the problems in question. For ease of discussion call the transverse load case with the major axis oriented along the x-axis load case IA, and that with the major axis along the y-axis as load case IB. These load cases are shown in Fig. (29). Using this notation, the analysis results require, for transverse normal loading, at yield

$$S_{x_A} < S_{x_B} \quad (IV-25)$$

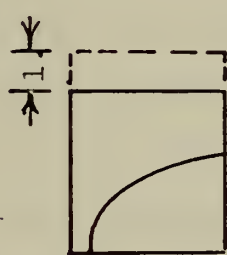
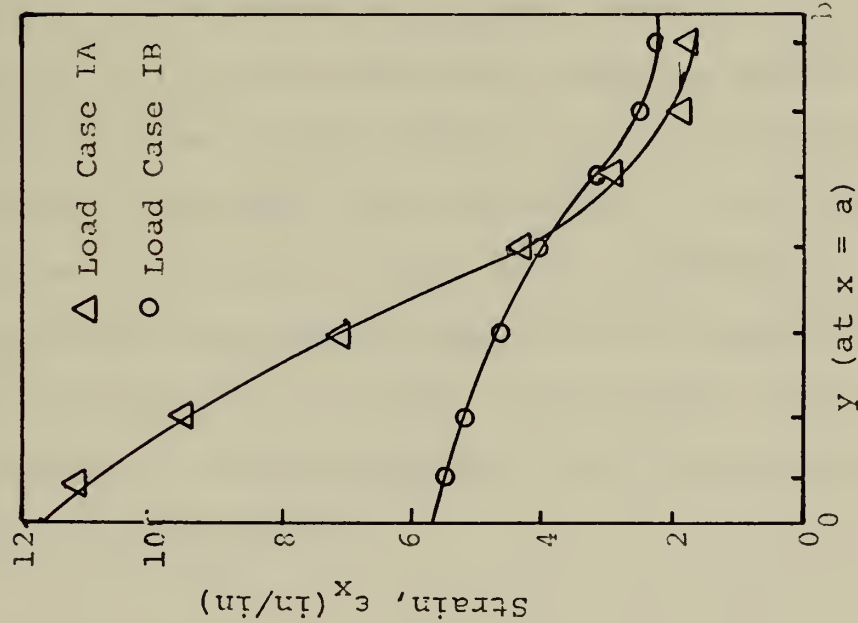
The definition of macrostresses requires that the integral of the microstresses along the boundary be related as

$$\int \sigma_A < \int \sigma_B \quad (IV-26)$$

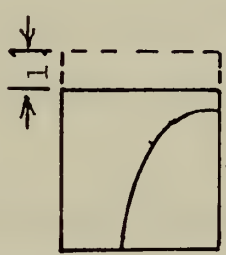
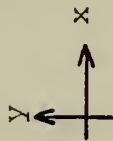
TABLE XIV. EFFECT OF FILAMENT CROSS SECTION ON TRANSVERSE STRENGTH AND STIFFNESS

	Circular		Elliptical			
	E_T	S_T	Major Axis		Minor Axis	
	E_T	S_T	E_T	S_T	E_T	S_T
Boron/6061 Aluminum	24.4	3.0	26.6	3.5	23.0	2.5
Boron/NARMCO Epoxy	1.64	.24	2.05	.19	1.46	.30
S-glass/NARMCO Epoxy	1.52	.245	1.83	.195	1.38	.295
E_T (psix10 ⁶)	S_T (psix10 ⁴)					

Figure (29) shows the stress and strain distribution on the x-boundary ($x = a$) for a unit displacement for load cases IA and IB. In both cases yield occurs in the matrix at a point near the interface, along the x-axis. Both cases



Y



$E_f = 12 \times 10^6$ psi

$E_{f1} = .5 \times 10^6$ psi

$\nu_f = .2$

$\nu_m = .3$

$\nu_f = .5$

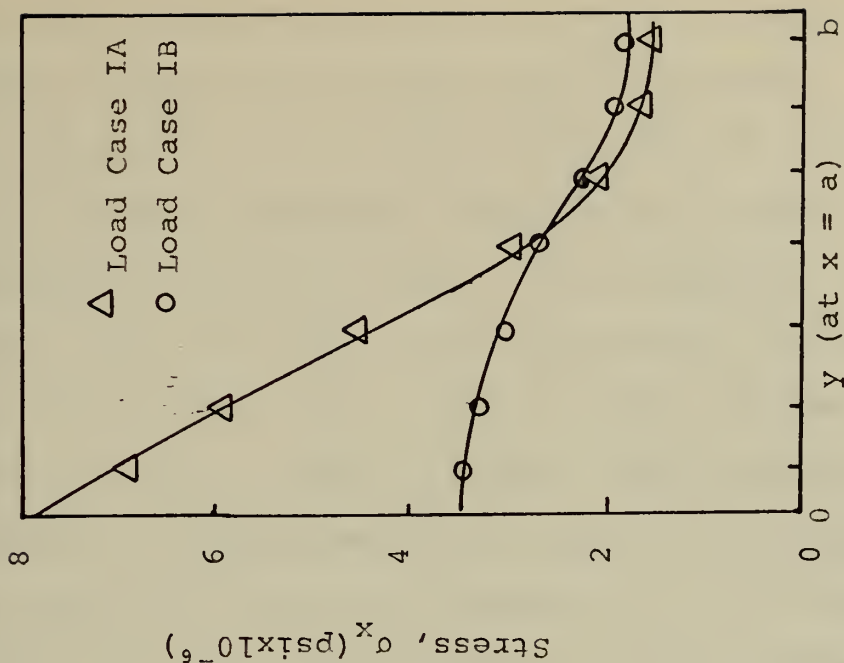
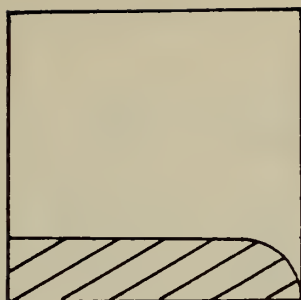


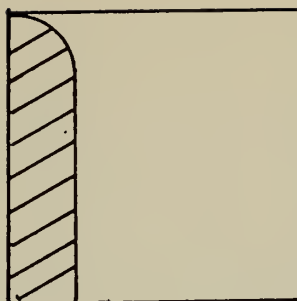
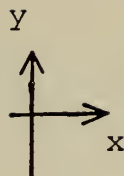
Figure (29). Stress and Strain Distribution on the Boundary of a Transversely Loaded Elliptical Filament.

also show little variation in stress or strain along the x-axis between the interface and the boundary. For example, for load case A, i.e., major axis along the x-axis, problem I for a 50% S-glass/Epoxy model gives a stress, σ_x , at the interface of $.664 \times 10^6$ psi. At the boundary ($x = a$) σ_x equals $.688 \times 10^6$ psi. The same material for load case B gave an interface value of σ_x as $.366 \times 10^6$ psi and a boundary value of $.389 \times 10^6$ psi. Thus the strain to cause yield will be approximately the same at the yield point, i.e., the interface, and at the boundary ($x = a, y = 0$). If the strain and stress curves of Fig. (29) are scaled to give identical strain values at the boundary ($x = a, y = 0$) the more uniform distribution of case IB will result in a larger value of the integral of the stress. This confirms Eqs. (IV-25) and (IV-26).

It seems therefore that the stiffness of the composite depends on the degree of filament material alignment in a particular direction while the strength depends on the maximum filament cross section in a direction perpendicular to that of the load. The inference of this is that the optimum cross-section shape would approximate that of a plane whose orientation depends on the desired properties. This is shown in Fig. (30). The filament shape can not be a rectangle as the square ends would induce prohibitive stress concentrations.



For Maximum E_x



For Maximum S_x

Figure (30). Approximate Optimum Cross Section for Particular Properties.

In the case of circular cross section filaments the transverse properties are the same in the y-direction as in the x-direction. Thus transverse yield strength in the y-direction would be numerically equivalent to that in the x-direction. This is shown in Fig. (31a). Again assume the convenient designation of load case A as that of the elliptical cross section with the major axis along the x-axis, and load case B with the major axis along the y-axis. The results of these two load cases may be interpreted as transverse strength in different directions of the same model as shown in Fig. (31b).

On a percentage basis the change in transverse strength due to cross section variation was considerable, ranging from 15% for Boron/Aluminum to 23% for Boron/NARMCO Epoxy. Of more significance however is the fact that the vector sum of S_x and S_y is independent of the filament cross section. This indicates, in vector notation, for Fig. (31)

$$\tilde{S} = \tilde{S}_{x_c} + \tilde{S}_{y_c} = \tilde{S}_{x_e} + \tilde{S}_{y_e} \quad (\text{IV-27})$$

Or, alternatively,

$$(S_{x_c}^2 + S_{y_c}^2) = (S_{x_e}^2 + S_{y_e}^2) \tag{IV-28}$$

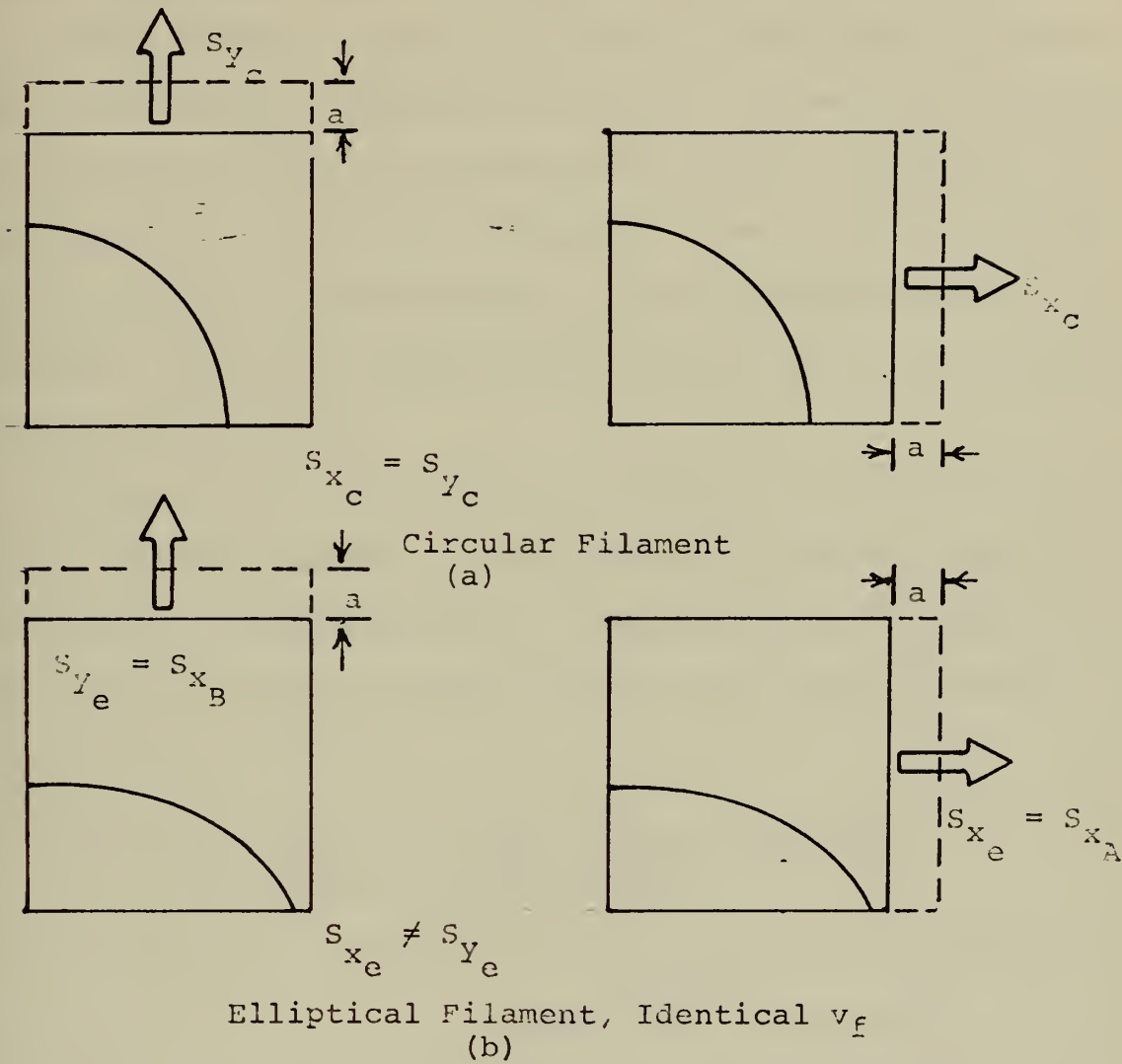


Figure (31). Transverse Strength Relation to Filament Cross Section.

This indicates that any increase in strength in one direction is directly offset by a decrease of the strength in the perpendicular direction.

In each case there was a noticeable increase in the stress concentration factors SCFX and SCFXZ, although SCFZ remained relatively constant. The net result was a reduction in the longitudinal yield strength of the elliptical cross section

compared to the circular cross section. The decrease was approximately 12% in each case. The implication is that a circular cross section is the most effective, with respect to a given filament volume, in terms of longitudinal strength. Adams and Doner [6] reported that stress concentration factors are directly related to the maximum radius of curvature of the filament. For a given filament volume a circular cross section results in the smallest possible maximum radius of curvature. This also implies that the circular cross section is the most efficient.

Another significant result evident in the analysis of the elliptical filament is the effect of filament shape on the composite shear modulus, G . Normalized with respect to the circular composite shear modulus the results obtained are listed in Table XV.

TABLE XV. EFFECT OF CROSS SECTION VARIATION
ON COMPOSITE SHEAR MODULUS

Composite	G_{ell}/G_c		$v_f = .5$
	Major Axis Orientation		
	x	y	
Boron/6061 Aluminum	1.345	.555	
Boron/NARMCO Epoxy	1.21	.326	
S-glass/NARMCO Epoxy	1.15	.398	

The shape of the filament cross section could be used to good advantage by a designer with detailed knowledge of

the expected loading of the structure under design. Such large variations in some composite properties due to relatively small departures from a circular cross section also make it extremely dangerous to load a "circular" filament near its expected transverse or shear strength. Small manufacturing errors can lead to large strength discrepancies.

V. COMPARISON OF MATERIAL COMBINATIONS

The preceeding sections have investigated the effect of various constituent properties on the properties of the composite. The goal was to be able to predict the comparative properties of various actual material combinations. In this section several functional material combinations are analyzed. Theoretical mechanical properties are compared and the results are correlated with the guide lines developed in the preceeding sections.

Forty, fifty, and sixty percent filament volume models are compared for the following combinations of materials,

- i) MODMOR II/NARMCO Epoxy
- ii) MODMOR II/4617 Epoxy
- iii) MODMOR I/4617 Epoxy
- iv) Boron/6061 Aluminum

For MODMOR I/NARMCO Epoxy and E-glass/Epoxy, 30% and 70% filament volume models were also considered. Single models of S-glass/NARMCO Epoxy, THORNEL 25/4617 Epoxy, THORNEL 40/4617 Epoxy, and Boron/2024 Aluminum were also investigated.

Primary measures of structural efficiency of a material are the specific strength and specific moduli of the material. These are defined in section I-B, however their importance necessitate further explanation.

In general, design of a particular structure requires certain material properties of strength and/or stiffness. In modern technology the weight of a structure has gained

equal importance with mechanical properties. It is significant to note that all common structural materials, when considered on a stiffness to weight basis, are remarkably similar. Wood, steel, aluminum, and titanium fall within the range of 92.0×10^6 psi/(lb/in³) to 105.5×10^6 psi/(lb/in³) for specific Young's modulus. Similarly for specific ultimate strength these common materials range from 4.60×10^5 to 8.33×10^5 psi/(lb/in³). This data is summarized in Table XVI. Thus for a composite to be valuable from a structural standpoint it must exceed these values for specific mechanical properties.

TABLE XVI. SPECIFIC ULTIMATE STRENGTH AND SPECIFIC YOUNG'S MODULUS FOR COMMON STRUCTURAL MATERIALS

Material	Specific Ultimate Strength psi/(lb/in ³)x10 ⁻⁵	Specific Modulus psi/(lb/in ³)x10 ⁻⁶
Steel	5.16	105.5
Aluminum	6.64	104.2
Titanium	8.33	97.2
Magnesium	5.00	101.6
Wood	4.60	92.0

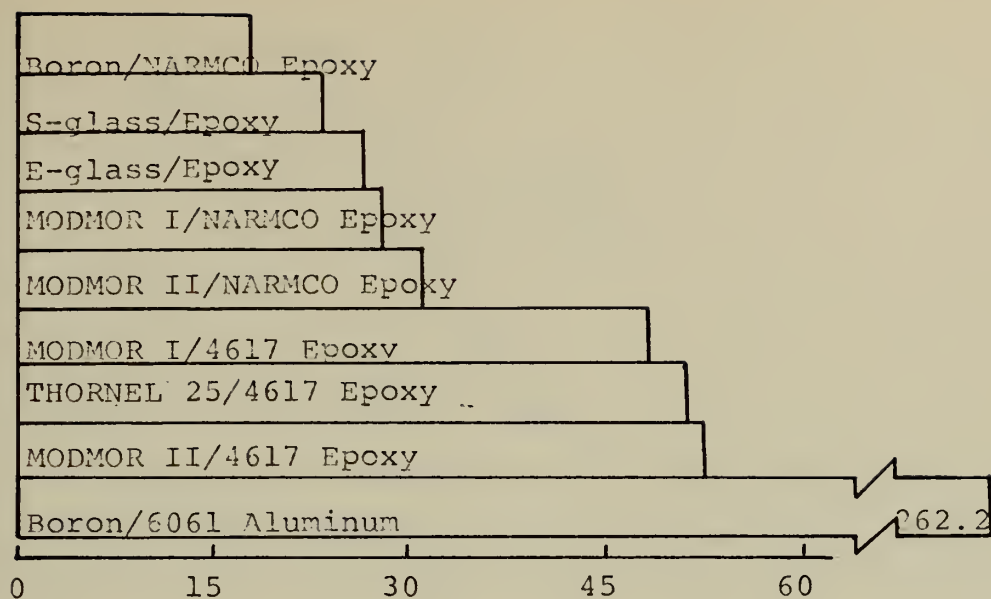
Figure (32) shows the transverse stiffness, E_T , and the specific transverse stiffness, E_T/ρ , where ρ is the composite specific weight. These results are for the 50% filament volume models considered. In the preceeding sections transverse stiffness was found to depend primarily on the matrix modulus of elasticity. The results of Fig.

(32a) show that the transverse stiffness of materials with similar matrix properties showed little variation. For example, those composites with a matrix of NARMCO epoxy had comparable values of transverse stiffness regardless of filament properties. The aluminum matrix was so much stiffer than any other matrix material studied that the performance of Boron/Aluminum far exceeds that of the other composites.

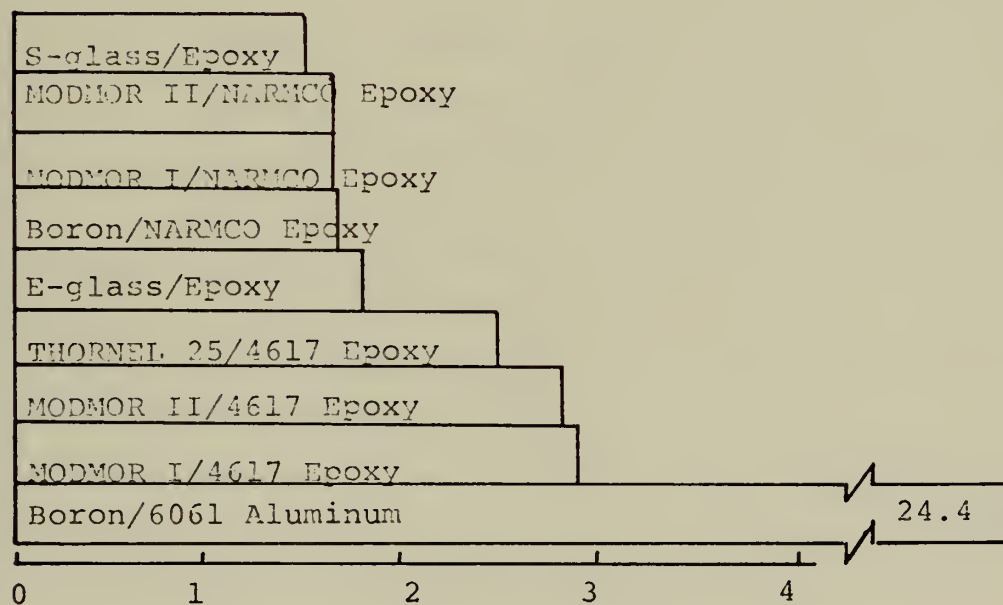
Figure (32b) shows the specific transverse stiffness. Note that the smallest value of composite specific transverse stiffness is approximately 80% greater than that normally associated with structural materials.

Figure (33) shows the composite transverse strength, S_T , and specific transverse strength, S_T/ρ . The constituent property that showed the most influence on transverse strength was the matrix modulus of elasticity. Figure (33a) reinforces this judgement by showing negligible variation in transverse strength among those composites utilizing identical matrix materials. Progressively stiffer matrix materials produced greater transverse yield strength regardless of the filament material.

Figure (33b) shows the specific transverse yield strength for the composites considered. Note that not all of the material combinations exceeded the stated value of 8.33×10^5 in. for common structural materials. One reason for this is that the quoted values for common structural materials are ultimate strengths rather than



Specific Transverse Stiffness (in x 10⁷)
50% Filament Model
(b)



Transverse Stiffness (psi x 10⁶)
50% Filament Model
(a)

Figure (32). Transverse Stiffness Comparison.

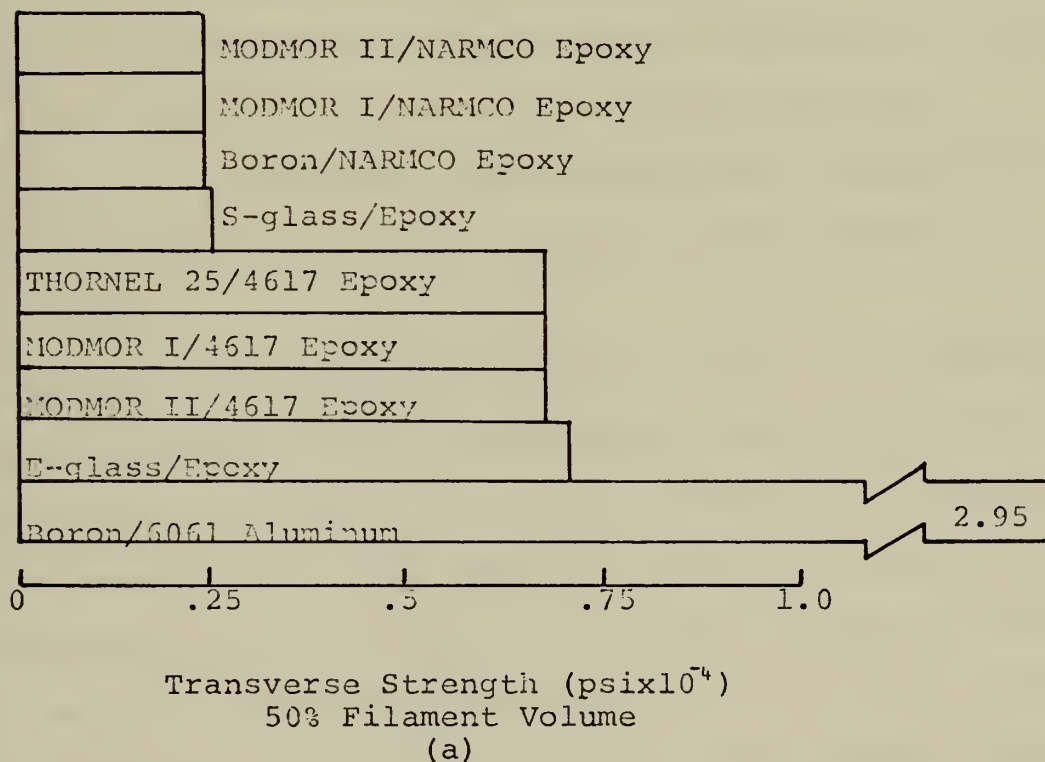
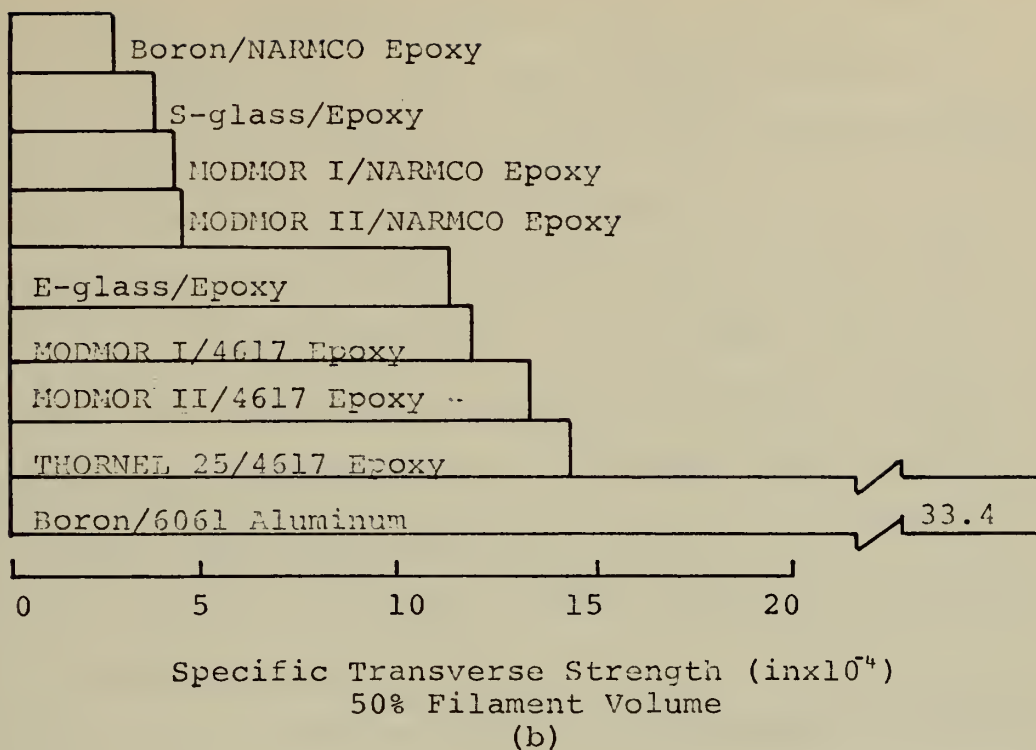


Figure (33). Transverse Strength Comparison.

yield strengths. Another reason is that the composite lamina are designed such that their primary strength is in the longitudinal direction whereas most standard structural materials are considered isotropic.

Figure (34) is a plot of longitudinal stiffness and specific longitudinal stiffness. It has been shown in this study that composite longitudinal stiffness can be accurately predicted by a law of mixtures. For the 50% case of Fig. (34a) the composites should be in order of increasing sum of matrix and filament moduli of elasticity. This is seen to be true.

Figure (34b) shows the specific longitudinal stiffness. Note that the graphite/epoxy combinations are considerably more efficient than the Boron/Aluminum combinations despite the large stiffness advantage of aluminum over epoxy.

Figure (35) shows the longitudinal yield strength and specific longitudinal yield strength of the various composites.

The relative longitudinal yield strength of a composite is somewhat more difficult to predict than are the other properties. Increasing the filament modulus or the matrix yield strength has been shown to increase the composite longitudinal yield strength. Increasing the matrix modulus of elasticity decreases longitudinal yield strength. There is no set method however for predicting the combined effect of such changes.

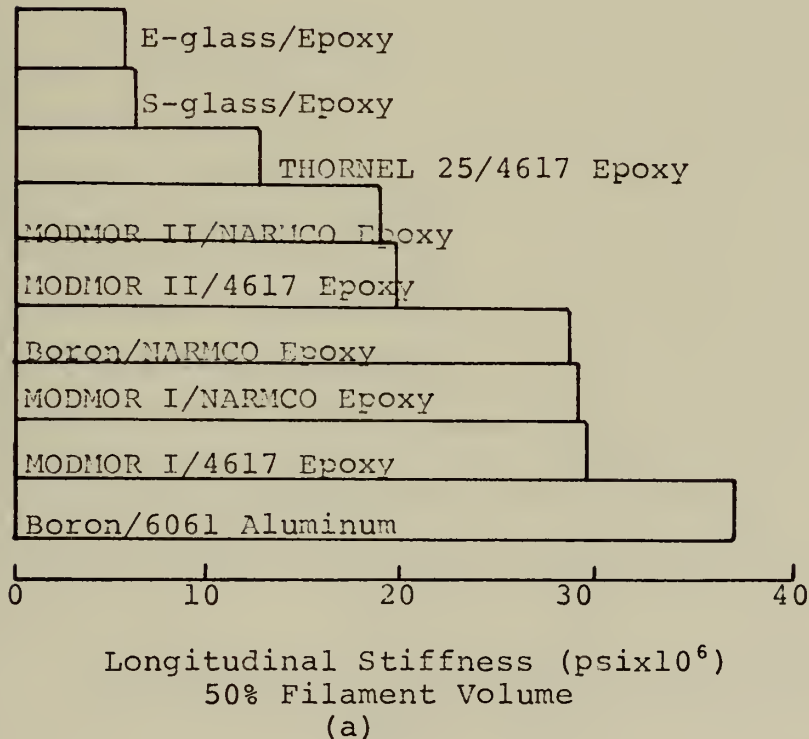
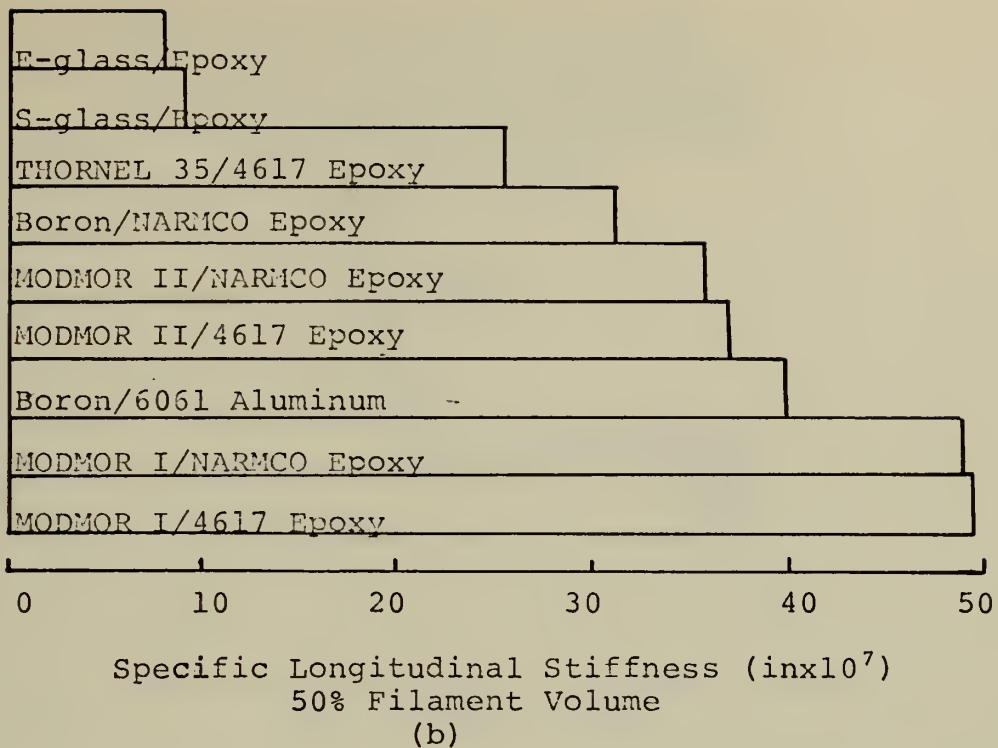


Figure (34). Longitudinal Stiffness Comparison.

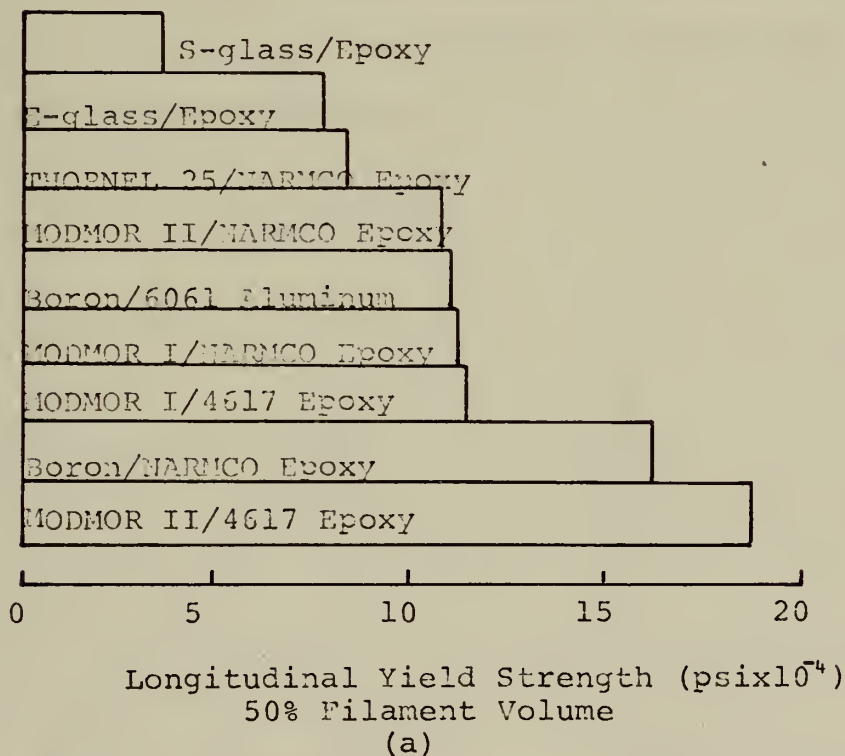
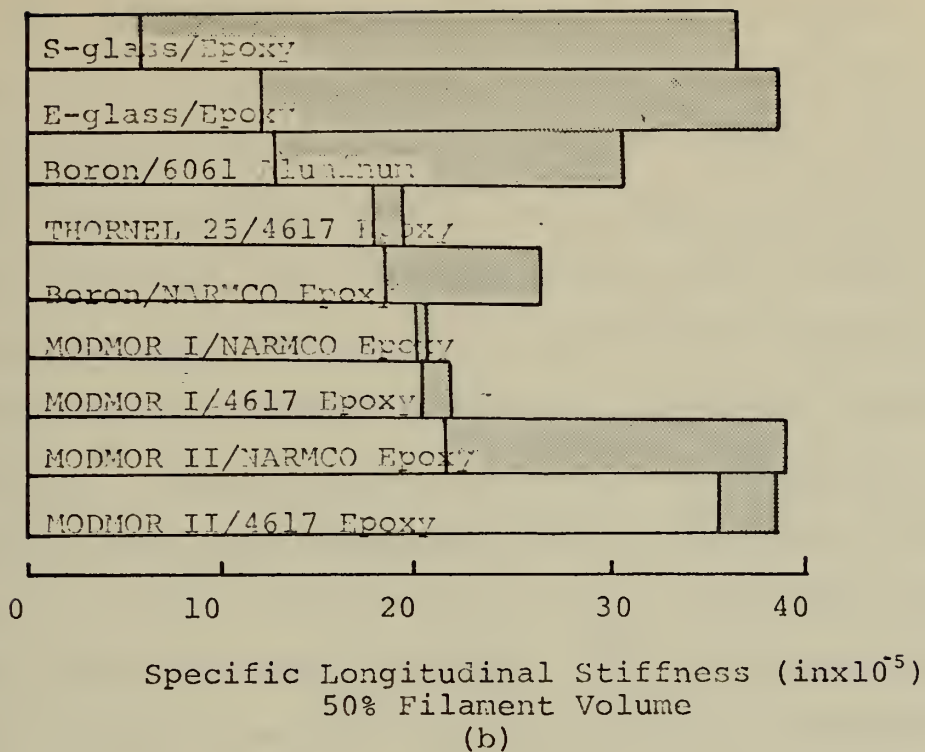


Figure (35). Longitudinal Strength Comparison.

The MODMOR II (graphite)/Epoxy models indicate a case where the matrix yield strength was of greater significance than the matrix modulus increase. The 4617 Epoxy had a greater modulus, which should decrease the yield strength, and a greater matrix yield strength which should increase the composite longitudinal strength. The net result was a marked increase in composite yield strength. Considering the variations individually, as in Fig. (36), this indicates that the increase in matrix yield strength, say from $Y_{O_m}^1$ to $Y_{O_m}^2$, increased the composite yield strength from S_L^1 to S_L^2 . This is shown in Fig. (36). The decrease in matrix modulus results in a composite stress-strain curve with a smaller slope. For the same matrix yield strength, $Y_{O_m}^2$, the composite yield is S_L^3 . The results of the analysis shows that

$$S_L^1 < S_L^3 < S_L^2 \quad (V-1)$$

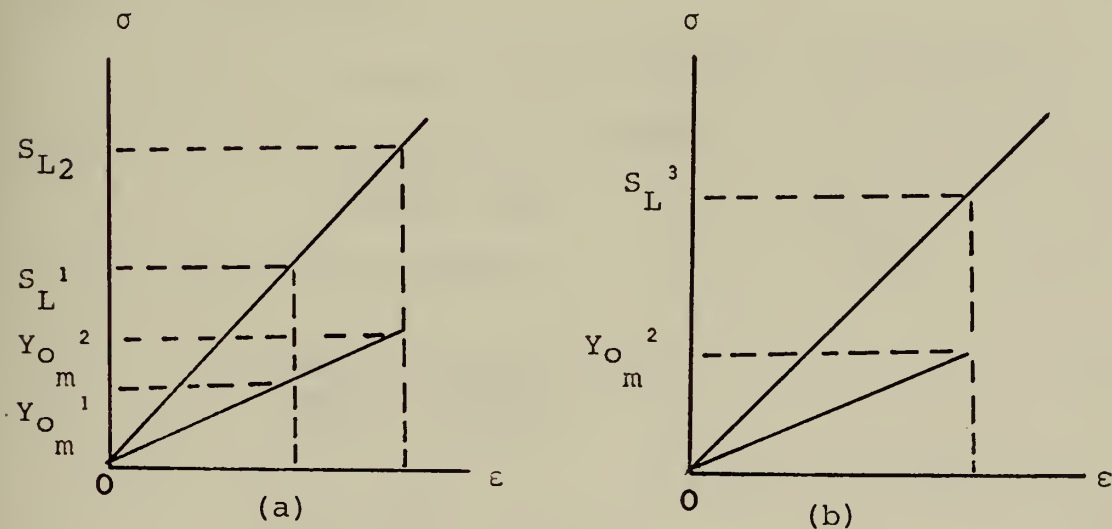


Figure (36). Combined Effect of Matrix Modulus and Matrix Yield (MODMOR II/Epoxy)

The two boron analyses represent the opposite case. The change in matrix modulus prevails over the change in matrix yield strength as the epoxy composite has a yield strength considerably larger than that of the Boron/Aluminum composite.

It should be noted that the longitudinal yield strength of the graphite composite MODMOR I/4617 Epoxy is considerably less than that of the MODMOR II/4617 Epoxy. This is significant in that the Young's modulus of MODMOR I is 50% greater than that of MODMOR II. This apparently contradicts the guidelines presented in this study. The reason for this is that the conclusions of this investigation are based on the assumption that initial yield occurs in the matrix rather than the filament. Due to the relatively low yield strength of MODMOR I initial yield actually occurs in the filament. This is predicted by considering the stress concentration factors as outlined in section III-B-6. Explicitly, for MODMOR I/4617 Epoxy,

Filament yield strength	2.5×10^5 psi
Matrix yield strength	$.08 \times 10^5$ psi
Filament SCFZ	2.106
Matrix SCFZ	.0524

$$\frac{SCFZ_f}{SCFZ_m} = \frac{2.106}{.0524} = 40.2 \quad (V-2)$$

$$\frac{Y_o_f}{Y_o_m} = \frac{2.5}{.08} = 31.25 \quad (V-3)$$

$$\frac{SCFZ_f}{SCFZ_m} > \frac{Y_{of}}{Y_{om}} \quad (V-4)$$

Which meets the criteria of section III-B-6 for initial yield occurring in the filament.

Figure (35b) represents the specific longitudinal yield strength. The unshaded area of the bar chart represents the specific yield strength from the yield calculations of this analysis. The shaded region of the figure represents an estimate of specific ultimate strength. The ultimate strength was estimated by use of the equation

$$S_{ult} = v_f Y_{of} + v_m \sigma_{m_{ult}} \quad (V-5)$$

As discussed in section III-B-4 $\sigma_{m_{ult}}$ is the stress in the matrix at the ultimate strain of the filament. Again it should be noted that this relation assumes that the matrix remains elastic up to the failure of the filament. Generally this is not true. Using the method of Lin, Salinas, and Ito [9] the theoretical ultimate tensile strength of a 50% Boron/Aluminum composite was found to be 243,000 psi. This compares with an estimate using Eq. (V-5) of 305,000 psi, a difference of greater than 20%. While the discrepancy is rather large the results are considered to be worthy of inclusion as a relative measure of the range between yield and failure.

For MODMOR I, MODMOR II/4617 Epoxy and THORNEL 25 (all graphite filaments) yield actually occurred in the filament.

This is the reason that the specific ultimate and specific yield strength are virtually coincident.

Also of importance in a manufacturing process is the cost of the materials. Table XVIII shows strength per unit cost data for selected materials. Cost data was obtained from Refs. [25] and [26]. The extremely high strength to cost ratio for glass filament serves to explain why glass composites are in such wide use despite their relatively low transverse yield strength. The present interest in graphite filaments can certainly be justified by the strength/cost increase anticipated in the near future.

TABLE XVII. COMPARATIVE STRENGTH PER UNIT COST

Filament	Epoxy Matrix	$v_f = 0.5$
	Strength/Unit Cost (in-lb/dollar $\times 10^{-4}$)	
Boron		.98
Graphite		2.01
Graphite (1974)		4.02
Glass		42.48

Numerous other factors also enter into a material selection process. Ease of handling and fabrication, special processing requirements, and specific desirable properties such as thermal expansion may be such factors. Consideration of these factors is beyond the scope of this investigation.

VI. CONCLUSIONS AND RECOMMENDATIONS

A. CONCLUSIONS

In this investigation a finite element analysis of the microscopic and macroscopic stresses of a composite material has been carried out. The stresses were used to calculate the initial yield surface for unidirectional composite materials. The results of these analyses were then used to determine the mechanical properties of a laminate of composite material. Parametric studies of the effect of various constituent properties on the composite mechanical properties were then carried out. Table XVIII summarizes the results of these parameter variations.

These results are based on the assumption that initial yield takes place in the matrix material. The effects noted in this table are those associated with a change of the specified constituent property only, that is, with all other constituent properties held constant. Caution must be exercised in attempting to predict the effects of changes in more than one constituent property.

Other results included:

i) Composite Transverse Poisson's Ratio, ν_T . This value exceeded that of either constituent. By adjusting the ratio of filament Young's modulus to matrix Young's modulus, E_m/E_f , the designer may achieve extreme values of transverse Poisson's ratio.

TABLE XVIII. EFFECT OF CONSTITUENT PROPERTIES ON COMPOSITE PROPERTIES

Macroscopic Property	Change Required in Constituent Property to Increase Macroscopic Property (+ increase; - decrease)							
	E_f	ν_f	Y_{Of}	E_m	ν_m	Y_{Om}	E_m/E_f	ν_f
Longitudinal Strength S_L	+			-		+		+
Longitudinal Stiffness E_L	+			+				+
Transverse Strength S_T	+			+		+		+
Transverse Stiffness E_T	+			+				+
Longitudinal Shear Strength, S_{xy}				+		+		
Longitudinal Shear Modulus, G	+			+				+
Longitudinal Poisson's Ratio, ν_L		+			+			-
Transverse Poisson's Ratio, ν_T		+			+		-	-

ii) Longitudinal Initial Yield Strength, S_L . For initial yield occurring in the matrix material the longitudinal yield strength may be predicted by

$$S_L = v_f \sigma_f + v_m Y_{O_m}$$

where Y_{O_m} is the yield strength of the matrix material, σ_f^* is the stress in the filament at the yield strain of the matrix, and v_f and v_m are filament and matrix volume fractions, respectively.

iii) Initial Yield Location. The computer program utilized in this investigation gives results which include the location of the yield point for any macroscopic stress state. For load case III it may be determined whether the composite fails in the matrix or the filament by considering the stress concentration factor in the longitudinal direction, SCFZ. If the ratio of SCFZ in the filament to that in the matrix is less than the ratio of filament yield strength to matrix yield strength then yield will occur in the matrix. That is, if

$$SCFZ_f / SCFZ_m < Y_{O_f} / Y_{O_m}$$

yield will occur in the matrix. This determines the applicability of the longitudinal yield equation noted above and does not require the application of any particular yield criteria.

iv) Filament Cross Section Effects. Variations from a circular filament cross section have significant influence on composite properties. Shear modulus and transverse

properties change considerably. Due to the distribution of microscopic stresses on the block boundaries an elliptical cross section has greater transverse strength in the direction of the minor axis.

B. RECOMMENDATIONS

i) The logical extension of this investigation is consideration of inelastic loading. The analysis used in this study is a special case of the elastic-plastic analysis of Lin, Salinas, and Ito. [9] [10]

ii) Further effort seems warranted in the evaluation of filament cross section effects. Through use of cross sectional shapes and filament distribution it should be possible to exert control over transverse and shear properties.

iii) The wide variation in the literature of theoretical transverse Poisson's ratio certainly suggests an urgent need for accurate experimental results as well as a comprehensive survey of analytical techniques.

APPENDIX A: YIELD LOCUS CALCULATIONS

The analytical method employed in this investigation 8 requires that the macroscopic stress state of the composite be one of plane stress. It is also required that the rectangular form of the basic block, Figs. (2) and (3), be maintained under deformation. To ensure these results four distinct loading cases are superposed. These load cases and their boundary conditions are shown in Fig. (4). Load cases I and II are plane strain states with $\epsilon_z = 0$. Load case III is a generalized plane strain case with $\epsilon_z = 1.0$. Load cases I, II, and III, are superposed to give $S_y = 0$. Load case IV is a state of longitudinal shear. All four cases have $S_{xy} = S_{yz} = 0$. Rectangular shapes of the basic block result from all load cases.

Using finite element methods with linear strain triangles [12] the four loading cases are individually analyzed to obtain the microstresses and their associated macrostresses. The microstresses are designated σ_{ij} with a subscript denoting the stress component and a superscript for the load case. For example, for load case I the microstresses obtained are

$$\sigma_x^I, \sigma_{xy}^I, \sigma_y^I, \sigma_z^I \quad (A-1)$$

Similar results are obtained for problems II and III. The macrostresses for load case I are designated

$$S_x^I, S_z^I, S_y^I \quad (A-2)$$

and similarly for load cases II and III.

Load case IV yields microstress results for

$$\sigma_{xz}^{IV} \quad \text{and} \quad \sigma_{yz}^{IV} \quad (A-3)$$

and macrostresses

$$S_{xz}^{IV} \quad \text{and} \quad S_{yz}^{IV} \quad (A-4)$$

In the notation of Lin, Salinas and Ito [8] the microstresses of a combined loading state may be related to the macrostresses as

$$\begin{matrix} \{\sigma\} & = & [A] & \{S\} \\ 4 \times 1 & & 4 \times 3 & 3 \times 1 \end{matrix} \quad (A-5)$$

and

$$\begin{matrix} \{\bar{\sigma}\} & = & [\bar{A}] & \{\bar{S}\} \\ 2 \times 1 & & 2 \times 2 & 2 \times 1 \end{matrix} \quad (A-6)$$

Where

$$\{\sigma\}^T = \langle \sigma_x \sigma_y \sigma_{xy} \sigma_z \rangle \quad (A-7)$$

$$\{S\}^T = \langle S_x S_y S_z \rangle \quad (A-8)$$

$$\{\bar{\sigma}\}^T = \langle \sigma_{xz} \sigma_{yz} \rangle \quad (A-9)$$

$$\{\bar{S}\}^T = \langle S_{xz} S_{yz} \rangle \quad (A-10)$$

$$[A] = \begin{bmatrix} A_{11} & A_{12} & A_{13} \\ A_{21} & A_{22} & A_{23} \\ A_{31} & A_{32} & A_{33} \\ A_{41} & A_{42} & A_{43} \end{bmatrix} \quad (A-11)$$

$$[\bar{A}] = \begin{bmatrix} A_{11} & A_{12} \\ A_{21} & A_{22} \end{bmatrix} \quad (A-12)$$

The matrix A may be related to the results of load cases I, II and III as

$$\begin{bmatrix} \sigma_x^I & \sigma_x^{II} & \sigma_x^{III} \\ \sigma_y^I & \sigma_y^{II} & \sigma_y^{III} \\ \sigma_{xy}^I & \sigma_{xy}^{II} & \sigma_{xy}^{III} \\ \sigma_z^I & \sigma_z^{II} & \sigma_z^{III} \end{bmatrix} = \begin{bmatrix} A_{11} & A_{12} & A_{13} \\ A_{21} & A_{22} & A_{23} \\ A_{31} & A_{32} & A_{33} \\ A_{41} & A_{42} & A_{43} \end{bmatrix} \begin{bmatrix} S_x^I & S_x^{II} & S_x^{III} \\ S_y^I & S_y^{II} & S_y^{III} \\ S_z^I & S_z^{II} & S_z^{III} \end{bmatrix} \quad (A-13)$$

For convenience this may be written

$$\begin{matrix} [T] & = & [\bar{A}] [\psi] \\ 4 \times 3 & & 4 \times 3 \quad 3 \times 3 \end{matrix} \quad (A-14)$$

The matrix A can then be evaluated as

$$\begin{matrix} [\bar{A}] & = & [T] [\psi]^{-1} \\ 4 \times 3 & & 4 \times 3 \quad 3 \times 3 \end{matrix} \quad (A-15)$$

Thus the combined microstresses, $[\sigma]$, due to any uniform transverse or longitudinal deformation may be evaluated by substituting the results of Eq. (A-15) into Eq. (A-5) as

$$\begin{matrix} \{\sigma\} & = & [T] [\psi]^{-1} \{S\} \\ 4 \times 1 & & 4 \times 3 \quad 3 \times 3 \quad 3 \times 1 \end{matrix} \quad (A-16)$$

In a similar manner for load state IV and an analogous load case V associated with S_{23} shear loading, the matrix \bar{A} may be evaluated as

$$[\bar{A}]_{2 \times 2} = \begin{bmatrix} \sigma_{xz}^{IV} & \sigma_{xz}^V \\ \sigma_{yz}^{IV} & \sigma_{yz}^V \end{bmatrix} \begin{bmatrix} \frac{1}{S_{xz}^{IV}} & 0 \\ 0 & \frac{1}{S_{yz}^V} \end{bmatrix} \quad (A-17)$$

This may be written as

$$[\bar{A}]_{2 \times 2} = [\bar{T}]_{2 \times 2} [\bar{\psi}]_{2 \times 2}^{-1} \quad (A-18)$$

From Eqs. (A-6) and (A-18) the microstresses, $\{\bar{\sigma}\}$, may be related to any specified shear loading as

$$\{\bar{\sigma}\}_{2 \times 1} = [\bar{T}]_{2 \times 2} [\bar{\psi}]_{2 \times 2}^{-1} \{\bar{S}\}_{2 \times 1} \quad (A-19)$$

The derivation of Eqs. (A-16) and (A-19) is independent of the load state. For the particular case of plane macroscopic stress treated in this investigation the macroscopic stress vectors become

$$\begin{aligned} \{S\}^T &= \langle S_x \quad 0 \quad S_z \rangle \\ \{\bar{S}\}^T &= \langle S_{xz} \quad 0 \rangle \end{aligned} \quad (A-20)$$

Equations (A-16) and (A-19) may be evaluated for the point by point microstresses associated with a plane macroscopic load condition as specified by Eq. (A-20).

Von Mises yield criterion is assumed to govern initial yield. This requires that

$$\begin{aligned} \bar{J} = & \sigma_{xz}^2 + \sigma_{yz}^2 + \sigma_{xy}^2 + \frac{1}{3} [\sigma_x^2 + \sigma_y^2 + \sigma_z^2 \\ & - \sigma_x \sigma_y - \sigma_y \sigma_z - \sigma_z \sigma_x] = \frac{1}{3} Y_o^2 \end{aligned} \quad (A-21)$$

Y_o is the elastic limit of the material for the tensile stress state.

Equations (A-16), (A-19), (A-20), and (A-21) may be combined to form a yield equation for plain macroscopic loading in terms of the macrostresses and the point dependent components of the A matrix. This equation is

$$\begin{aligned}
 & \left[A_{33}^2 + \frac{1}{3}(A_{13}^2 + A_{23}^2 + A_{43}^2 - A_{13}A_{23} - A_{23}A_{43} - A_{43}A_{13}) \right] S_z^2 \\
 & + \left[2A_{31}A_{33} + \frac{2}{3}(A_{11}A_{13} + A_{21}A_{23} + A_{41}A_{43}) \right. \\
 & \left. - \frac{1}{3}(A_{11}A_{23} + A_{13}A_{21} + A_{21}A_{43} + A_{23}A_{41} + A_{41}A_{13} + A_{43}A_{11}) \right] S_z S_x \\
 & + \left[A_{31}^2 + \frac{1}{3}(A_{11}^2 + A_{21}^2 + A_{41}^2 - A_{11}A_{21} - A_{21}A_{41} - A_{41}A_{11}) \right] S_x^2 \\
 & + (\bar{A}_{11}^2 \bar{A}_{21}^2) S_{xz}^2 - \frac{1}{3} Y_0^2 = 0 \tag{A-22}
 \end{aligned}$$

For given values of S_x and S_{xz} Eq. (A-22) may be solved for the value of S_z necessary to cause yield. Each point within the fundamental block will give a different value of S_z dependent on its microstress state. Each combination of S_x and S_{xz} yields two values of S_z at each point, a maximum and a minimum. The minimum of the maximum values and the maximum of the minimum values determine two yield points for the given values of S_x and S_{xz} . Continuing in this manner the initial yield surface for a composite subjected to a macroscopic plane stress state is calculated.

APPENDIX B: CONSTITUTIVE EQUATIONS
FOR A HOOKEAN FIBROUS COMPOSITE MATERIAL

The well known equations of elasticity relating stress components and strain components in terms of two independent elastic constants represents a special case of generalized Hooke's Law for isotropic materials. Here we derive the Hookean stress-strain relations for a lamina of an anisotropic fiber reinforced composite material.

The generalized Hookean stress-strain law relating stress and strain may be written in matrix form as

$$\begin{bmatrix} \epsilon_x \\ \epsilon_y \\ \epsilon_z \\ \epsilon_{xy} \\ \epsilon_{yz} \\ \epsilon_{xz} \end{bmatrix} = \begin{bmatrix} a_{11} & a_{12} & a_{13} & a_{14} & a_{15} & a_{16} \\ a_{21} & a_{22} & a_{23} & a_{24} & a_{25} & a_{26} \\ a_{31} & a_{32} & a_{33} & a_{34} & a_{35} & a_{36} \\ a_{41} & a_{42} & a_{43} & a_{44} & a_{45} & a_{46} \\ a_{51} & a_{52} & a_{53} & a_{54} & a_{55} & a_{56} \\ a_{61} & a_{62} & a_{63} & a_{64} & a_{65} & a_{66} \end{bmatrix} \begin{bmatrix} S_x \\ S_y \\ S_z \\ S_{xy} \\ S_{yz} \\ S_{xz} \end{bmatrix} \quad (B-1)$$

In a more compact notation this may be written

$$\begin{matrix} \{\epsilon\} & = & [A] & \{S\} \\ 6 \times 1 & & 6 \times 6 & 6 \times 1 \end{matrix} \quad (B-2)$$

The ϵ_{ij} terms are engineering strain components and the S_{ij} are stress components.

Thus the generalized stress-strain relations contain 36 unknown Hookean constants,

$$a_{ij} \quad (i, j = 1, 2, 3, 4, 5, 6) \quad (B-3)$$

Consideration of the strain-energy density function [27] establishes symmetry of the matrix of Hookean constants

$$a_{ij} = a_{ji} \quad (B-4)$$

and reduces the maximum number of independent elastic constants to 21. Further reductions in the number of elastic constants depends on the number of planes of symmetry present in the material.

When the elastic constants at a point have the same values for every pair of co-ordinate systems which are mirror images of each other in a certain plane that plane is called a plane of elastic symmetry. This means that if a certain plane, say the (x_1, x_2) plane in co-ordinate system (x_1, x_2, x_3) is a plane of elastic symmetry then the reflection of this system, (x'_1, x'_2, x'_3) , where

$$\begin{aligned}x'_1 &= x_1 \\x'_2 &= x_2 \\x'_3 &= -x_3\end{aligned}\tag{B-5}$$

must have the same elastic constants. If you could actually "see" the elastic properties this means that the properties would appear identical at every point regardless of which side of the plane you were viewing. Alternatively Sines [28] suggests that if you could actually see these properties they would look the same even if the observer stood on his head, that is rotated 180° about his line of sight. This invariance is utilized to evaluate the elastic constants.

Consider the reference system (x_1, x_2, x_3) of Fig. (B-1). If the plane (x_1, x_2) is a plane of elastic symmetry a reflection through the x_3 axis may be carried out without effecting the elastic constants. This new reference system is designated by the primed axes of Fig. (B-1).

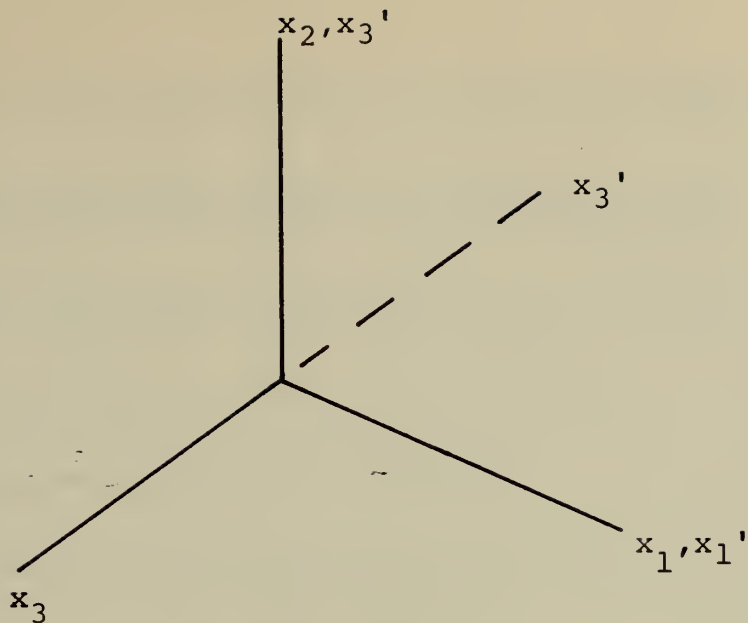


Figure (B-1). Reflection of a Plane of Symmetry (x_1, x_2).

The general equations governing the transformation of axes are

$$\begin{aligned}
 \epsilon'_x &= l_1^2 \epsilon_x + m_1^2 \epsilon_y + n_1^2 \epsilon_z + l_1 m_1 \epsilon_{xy} + m_1 n_1 \epsilon_{yz} + n_1 l_1 \epsilon_{zx} \\
 \epsilon'_y &= l_2^2 \epsilon_x + m_2^2 \epsilon_y + n_2^2 \epsilon_z + l_2 m_2 \epsilon_{xy} + m_2 n_2 \epsilon_{yz} + n_2 l_2 \epsilon_{zx} \\
 \epsilon'_z &= l_3^2 \epsilon_x + m_3^2 \epsilon_y + n_3^2 \epsilon_z + l_3 m_3 \epsilon_{xy} + m_3 n_3 \epsilon_{yz} + n_3 l_3 \epsilon_{zx} \\
 \epsilon'_{xy} &= 2 l_1 l_2 \epsilon_x + 2 m_1 m_2 \epsilon_y + 2 n_1 n_2 \epsilon_z + (l_1 m_2 + m_1 l_2) \epsilon_{xy} \\
 &\quad + (m_1 n_2 + n_1 m_2) \epsilon_{yz} + (n_1 l_2 + l_1 n_2) \epsilon_{zx} \\
 \epsilon'_{yz} &= 2 l_2 l_3 \epsilon_x + 2 m_2 m_3 \epsilon_y + 2 n_2 n_3 \epsilon_z + (l_2 m_3 + m_2 l_3) \epsilon_{xy} \\
 &\quad + (m_2 n_3 + n_2 m_3) \epsilon_{yz} + (n_2 l_3 + l_2 n_3) \epsilon_{zx} \\
 \epsilon'_{zx} &= 2 l_3 l_1 \epsilon_x + 2 m_3 m_1 \epsilon_y + 2 n_3 n_1 \epsilon_z + (l_3 m_1 + l_1 m_3) \epsilon_{xy} \\
 &\quad + (m_3 n_1 + n_3 m_1) \epsilon_{yz} + (n_3 l_1 + l_3 n_1) \epsilon_{zx}
 \end{aligned} \tag{B-6}$$

for strain components and

$$S'_x = l_1^2 S_x + m_1^2 S_y + n_1^2 S_z + 2l_1 m_1 S_{xy} + 2m_1 n_1 S_{yz} + 2n_1 l_1 S_{zx}$$

$$S'_y = l_2^2 S_x + m_2^2 S_y + n_2^2 S_z + 2l_2 m_2 S_{xy} + 2m_2 n_2 S_{yz} + 2n_2 l_2 S_{zx}$$

$$S'_z = l_3^2 S_x + m_3^2 S_y + n_3^2 S_z + 2l_3 m_3 S_{xy} + 2m_3 n_3 S_{yz} + 2n_3 l_3 S_{zx}$$

$$S'_{xy} = l_1 l_2 S_x + m_1 m_2 S_y + n_1 n_2 S_z + (l_1 m_2 + m_1 l_2) S_{xy}$$

$$+ (m_1 n_2 + n_1 m_2) S_{yz} + (n_1 l_2 + l_1 n_2) S_{zx} \quad (B-7)$$

$$S'_{yz} = l_2 l_3 S_x + m_2 m_3 S_y + n_2 n_3 S_z + (l_2 m_3 + m_2 l_3) S_{xy}$$

$$+ (m_2 n_3 + n_2 m_3) S_{yz} + (n_2 l_3 + l_2 n_3) S_{zx}$$

$$S'_{zx} = l_3 l_1 S_x + m_3 m_1 S_y + n_3 n_1 S_z + (l_3 m_1 + m_3 l_1) S_{xy}$$

$$+ (m_3 n_1 + n_3 m_1) S_{yz} + (n_3 l_1 + l_3 n_1) S_{zx}$$

for stress components. The terms

$$l_i, m_i, n_i \quad (i = 1, 2, 3) \quad (B-8)$$

are direction cosines defined by the following table:

	1	2	3
1'	l_1	m_1	n_1
2'	l_2	m_2	n_2
3'	l_3	m_3	n_3

This indicates that $l_1 \cos (x'_1, x_1)$ etc. For the reflection of Fig. (B-1) the direction cosines are:

	1	2	3
1'	1	0	0
2'	0	1	0
3'	0	0	-1

Using these direction cosines to evaluate the transformation relations Eqs. (B-6) and (B-7) yields

$$\begin{aligned}
 S'_x &= S_x & \epsilon'_x &= \epsilon_x \\
 S'_y &= S_y & \epsilon'_y &= \epsilon_y \\
 S'_z &= S_z & \epsilon'_z &= \epsilon_z \\
 S'_{xy} &= -S_{xy} & \epsilon'_{xy} &= -\epsilon_{xy} \\
 S'_{yz} &= -S_{yz} & \epsilon'_{yz} &= -\epsilon_{yz} \\
 S'_{zx} &= S_{zx} & \epsilon'_{zx} &= \epsilon_{zx}
 \end{aligned} \tag{B-9}$$

The stress-strain relation in the new co-ordinate system may be written

$$\langle \epsilon'_x \ \epsilon'_y \ \epsilon'_z \ \epsilon'_{xy} \ \epsilon'_{yz} \ \epsilon'_{zx} \rangle^T = \underset{6 \times 6}{[A]} \langle S_x \ S_y \ S_z \ S_{xy} \ -S_{yz} \ -S_{zx} \rangle^T \tag{B-10}$$

The elastic constants are then evaluated by equating the transformed strains to the original strains in accordance with Eq. (B-9). Consider for example $\epsilon'_x = \epsilon_x$. In detail this requires that

$$\begin{aligned}
 a_{11}S_x + a_{12}S_y + a_{13}S_z - a_{14}S_{xy} - a_{15}S_{yz} + a_{16}S_{zx} = \\
 a_{11}S_x + a_{12}S_y + a_{13}S_z + a_{14}S_{xy} + a_{15}S_{yz} + a_{16}S_{zx}
 \end{aligned} \tag{B-11}$$

The constants are invariant with transformation, requiring that

$$\begin{aligned}
 -a_{15} S_{yz} &= a_{15} S_{yz} \\
 -a_{14} S_{xy} &= a_{14} S_{xy}
 \end{aligned} \tag{B-12}$$

For a non zero stress condition this can be true only if

$$a_{15} = a_{14} = 0 \tag{B-13}$$

Carrying this out for the other relations of Eq. (B-9) shows that

$$a_{15} = a_{14} = a_{24} = a_{25} = a_{34} = a_{35} = a_{46} = a_{56} = 0 \tag{B-14}$$

Thus a single plane of elastic symmetry reduces the number of independent elastic constants to 13.

If a material has three orthogonal planes of symmetry a reflection of a second plane may be carried out without changing the Hookean coefficients. Reflecting the (x_2, x_3) plane through the x_1 axis results in the transformed axes of Fig. (B-2). In this case the

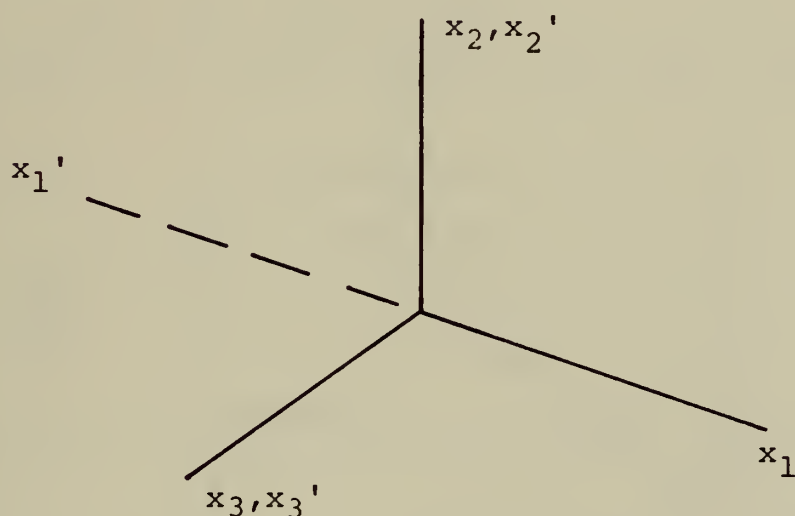


Figure (B-2). Reflection of a Plane of Symmetry (x_2, x_3)

direction cosines are given by

	1	2	3
1'	-1	0	0
2'	0	1	0
3'	0	0	1

The transformation relations Eqs. (B-6) and (B-7) give

$$\begin{array}{ll}
S'_x = S_x & \epsilon'_x = \epsilon_x \\
S'_y = S_y & \epsilon'_y = \epsilon_y \\
S'_z = S_z & \epsilon'_z = \epsilon_z \\
S'_{xy} = -S_{xy} & \epsilon'_{xy} = -\epsilon_{xy} \\
S'_{yz} = S_{yz} & \epsilon'_{yz} = \epsilon_{yz} \\
S'_{zx} = -S_{zx} & \epsilon'_{zx} = -\epsilon_{zx}
\end{array} \tag{B-15}$$

Using these relations it may be shown that

$$a_{26} = a_{16} = a_{36} = a_{45} = 0 \tag{B-16}$$

The matrix of elastic constants may now be written

$$\begin{array}{l}
[A]_o \\
6 \times 6
\end{array} = \begin{bmatrix}
a_{11} & a_{12} & a_{13} & 0 & 0 & 0 \\
& a_{22} & a_{23} & 0 & 0 & 0 \\
& & a_{33} & 0 & 0 & 0 \\
& & & a_{44} & 0 & 0 \\
\text{symmetric} & & & & a_{55} & 0 \\
& & & & & a_{66}
\end{bmatrix} \tag{B-17}$$

where the subscript o indicates that this matrix is defined for an orthotropic material. There are now nine independent elastic constants.

Further reductions in the number of independent elastic constants depend upon the number of planes of isotropy, if any, present in the material. A plane of isotropy is one in which the elastic constants are invariant with respect to direction within the plane.

Assume that a plane of isotropy does exist, the (x_1, x_2) plane of Fig. (B-3). This indicates that the Hookean

coefficients are independent of the orientation of the (x_1, x_2) axes within this plane. An infinite number of orientations could be chosen within this plane to assist in evaluating the remaining unknowns. A 45 degree rotation, shown in Fig. (B-3), was selected for ease of calculation.

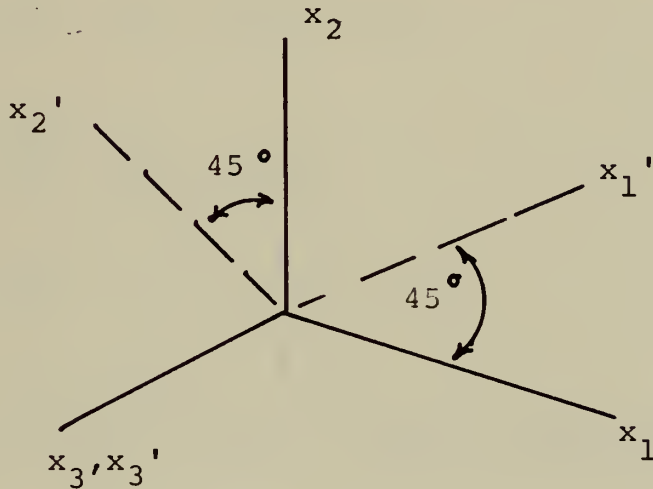


Figure (B-3). 45 Degree Rotation of Plane (x_1, x_2)

The direction cosines for such a case are:

	1	2	3
1'	$\frac{1}{\sqrt{2}}$	$\frac{1}{\sqrt{2}}$	0
2'	$\frac{1}{\sqrt{2}}$	$-\frac{1}{\sqrt{2}}$	0
3'	0	0	1

Again using the transformation relations Eqs. (B-6) and (B-7) one obtains

$$\epsilon'_x = \frac{1}{2} \epsilon_x + \frac{1}{2} \epsilon_y + \frac{1}{2} \epsilon_{xy}$$

$$\epsilon'_y = \frac{1}{2} \epsilon_x + \frac{1}{2} \epsilon_y - \frac{1}{2} \epsilon_{xy}$$

$$\epsilon'_x = \epsilon_z \tag{B-18}$$

$$\epsilon'_{xy} = \epsilon_x - \epsilon_y$$

$$\epsilon'_{yz} = -\frac{1}{\sqrt{2}} \epsilon_{yz} + \frac{1}{\sqrt{2}} \epsilon_{zx}$$

$$\epsilon'_{zx} = \frac{1}{\sqrt{2}} \epsilon_{yz} + \frac{1}{\sqrt{2}} \epsilon_{zx}$$

$$s'_x = \frac{1}{2} s_x + \frac{1}{2} s_y + s_{xy}$$

$$s'_y = \frac{1}{2} s_x + \frac{1}{2} s_y - s_{xy}$$

$$s'_z = s_z \quad (B-18)$$

$$s'_{xy} = \frac{1}{2} s_x - \frac{1}{2} s_y$$

$$s'_{yz} = -\frac{1}{\sqrt{2}} s_{yz} + \frac{1}{\sqrt{2}} s_{zx}$$

$$s'_{zx} = \frac{1}{\sqrt{2}} s_{yz} + \frac{1}{\sqrt{2}} s_{zx}$$

Using these relations it may be shown that

$$a_{55} = a_{66}$$

$$a_{11} = a_{22}$$

$$a_{13} = a_{23} \quad (B-19)$$

$$a_{44} = 2(a_{11} - a_{12})$$

A material exhibiting one such plane of isotropy is called a transversely isotropic material. There are five remaining independent elastic constants and the matrix of elastic constants may be written

$$\begin{bmatrix} A_{TI} \end{bmatrix}_{6 \times 6} = \begin{bmatrix} a_{11} & a_{12} & a_{13} & 0 & 0 & 0 \\ & a_{11} & a_{13} & 0 & 0 & 0 \\ & & a_{33} & 0 & 0 & 0 \\ & & & 2(a_{11} - a_{12}) & 0 & 0 \\ & \text{symmetric} & & & a_{55} & 0 \\ & & & & & a_{55} \end{bmatrix} \quad (B-20)$$

where the subscript TI signifies transversely isotropic.

The stress-strain relations for this case may be written

$$\begin{matrix} \{ \epsilon \} & = & \begin{bmatrix} A_{TI} \end{bmatrix} & \{ S \} \\ 6 \times 1 & & 6 \times 6 & 6 \times 1 \end{matrix} \quad (B-21)$$

One of the assumptions of this study is that a composite material may be considered to be homogeneous in a macroscopic sense. This assumption allows the composite to be considered as a transversely isotropic material, and Eqs. (B-21) are the constitutive equations for a composite material. Introducing the engineering constants these equations become

$$\begin{aligned} \epsilon_x &= \frac{1}{E_T} (S_x - \nu_T S_y) - \frac{\nu_L}{E_L} S_z \\ \epsilon_y &= \frac{1}{E_T} (S_y - \nu_T S_x) - \frac{\nu_L}{E_L} S_z \\ \epsilon_z &= -\frac{\nu_L}{E_L} (S_x + S_y) + \frac{1}{E_L} S_z \\ \epsilon_{xy} &= \frac{1}{G_T} S_{xy} \\ \epsilon_{yz} &= \frac{1}{G_L} S_{yz} \\ \epsilon_{zx} &= \frac{1}{G_L} S_{xz} \\ G_T &= \frac{E_T}{2(1 + \nu_T)} \end{aligned} \quad (B-22)$$

E_T and G_T are the Young's modulus and shear modulus in the transverse direction, in the plane of isotropy. E_L and G_L are corresponding values in the longitudinal direction, perpendicular to the plane of isotropy. Poisson's ratio

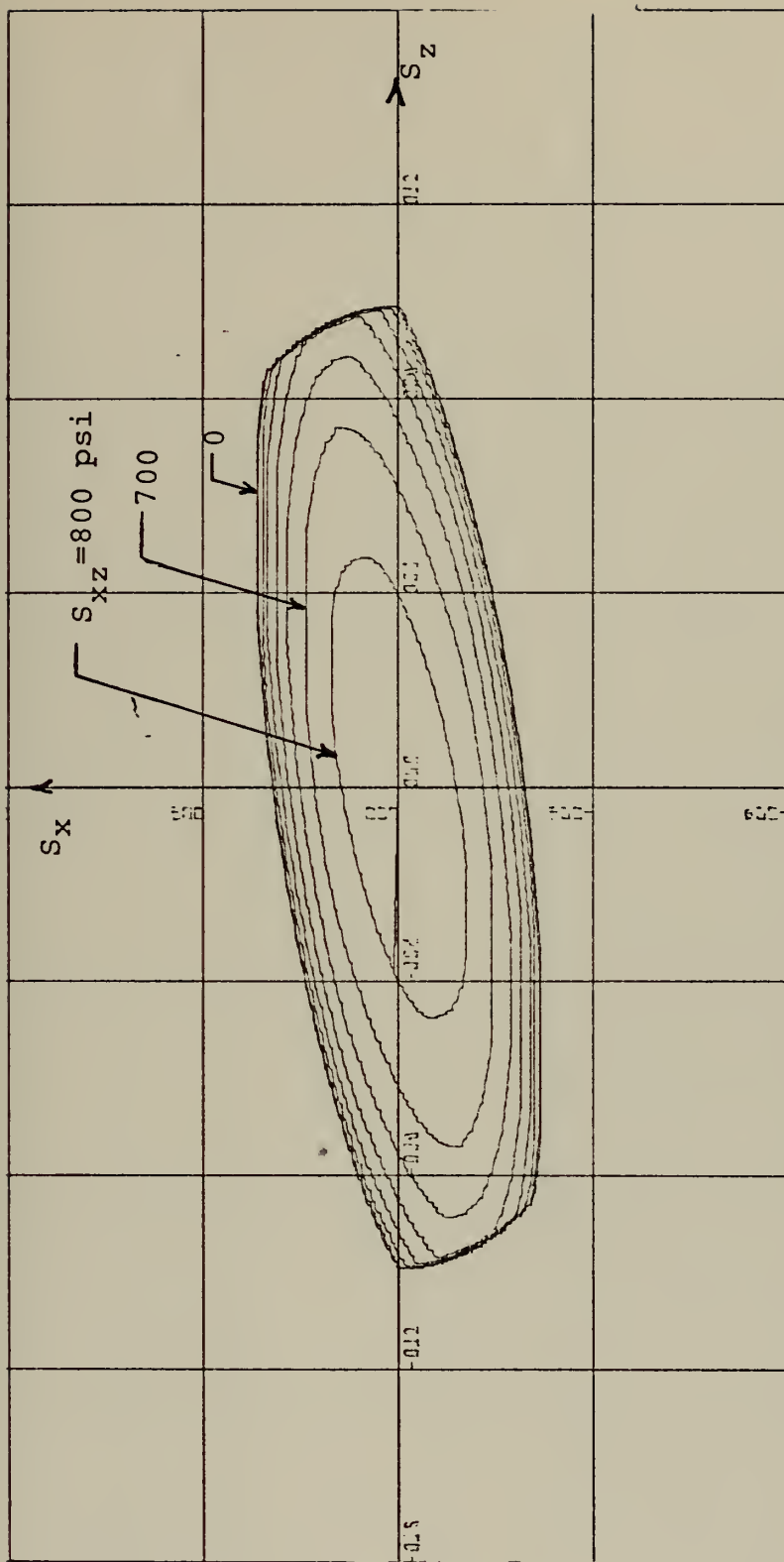
ν_T signifies the contraction in the plane of isotropy due to tension in the same plane. Poisson's ratio ν_L represents the contraction in the plane of isotropy due to tension in the longitudinal direction. The transverse shear modulus is a dependent quantity.

APPENDIX C: YIELD LOCI

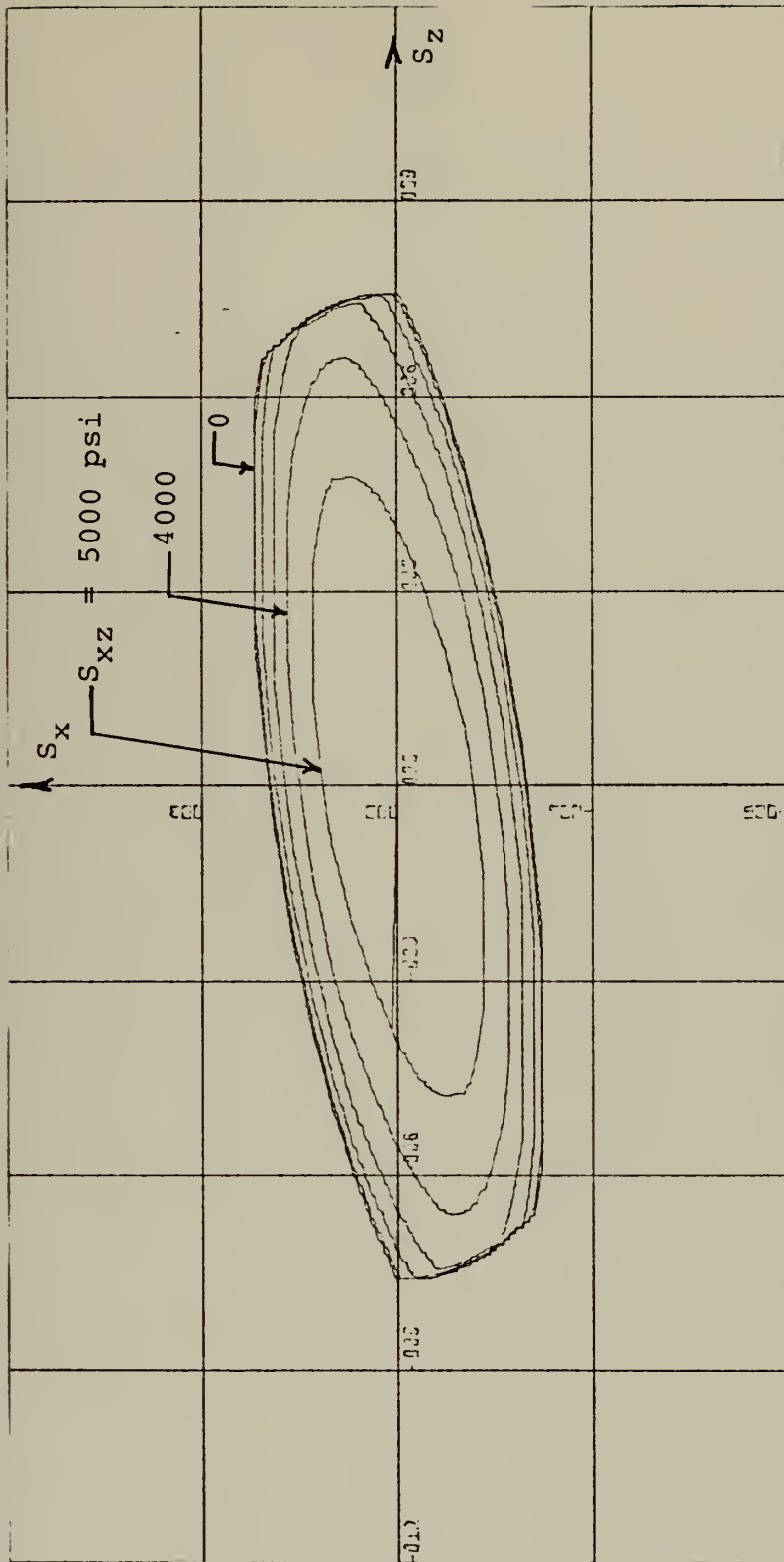
The figures included in this section represent the yield loci that were generated during the course of this investigation. Each plot is labelled with the constituent materials, filament volume fraction, v_f , and S_x and S_z scales. The outermost locus for all cases corresponds to $S_{xz} = 0$. The S_{xz} increment between successive loci is also noted on each plot.

Those plots that were used in the parametric analysis are labelled in terms of the parameter being investigated. All other properties are held constant.

Note that in some cases the S_x and S_z scales are different from one another. This occurs when the matrix materials are quite soft in comparison to the filament material. The transverse strength is so much less than the longitudinal strength that the surface plots nearly as a straight line if the same scales are used for both axes.



S_x scale = 4×10^3 psi/in S_{xz} increment = 100 psi
 S_z scale = 4×10^3 psi/in
 Figure (C-1). Matrix Yield Strength Variation, $Y_o = 3 \times 10^3$ psi_m



S_x scale = 3×10^4 psi/in

S_{xz} increment = 1000 psi

S_z scale = 3×10^4 psi/in

Figure (C-2). Matrix Yield Strength Variation, $Y_{Om} = 2.3 \times 10^4$ psi

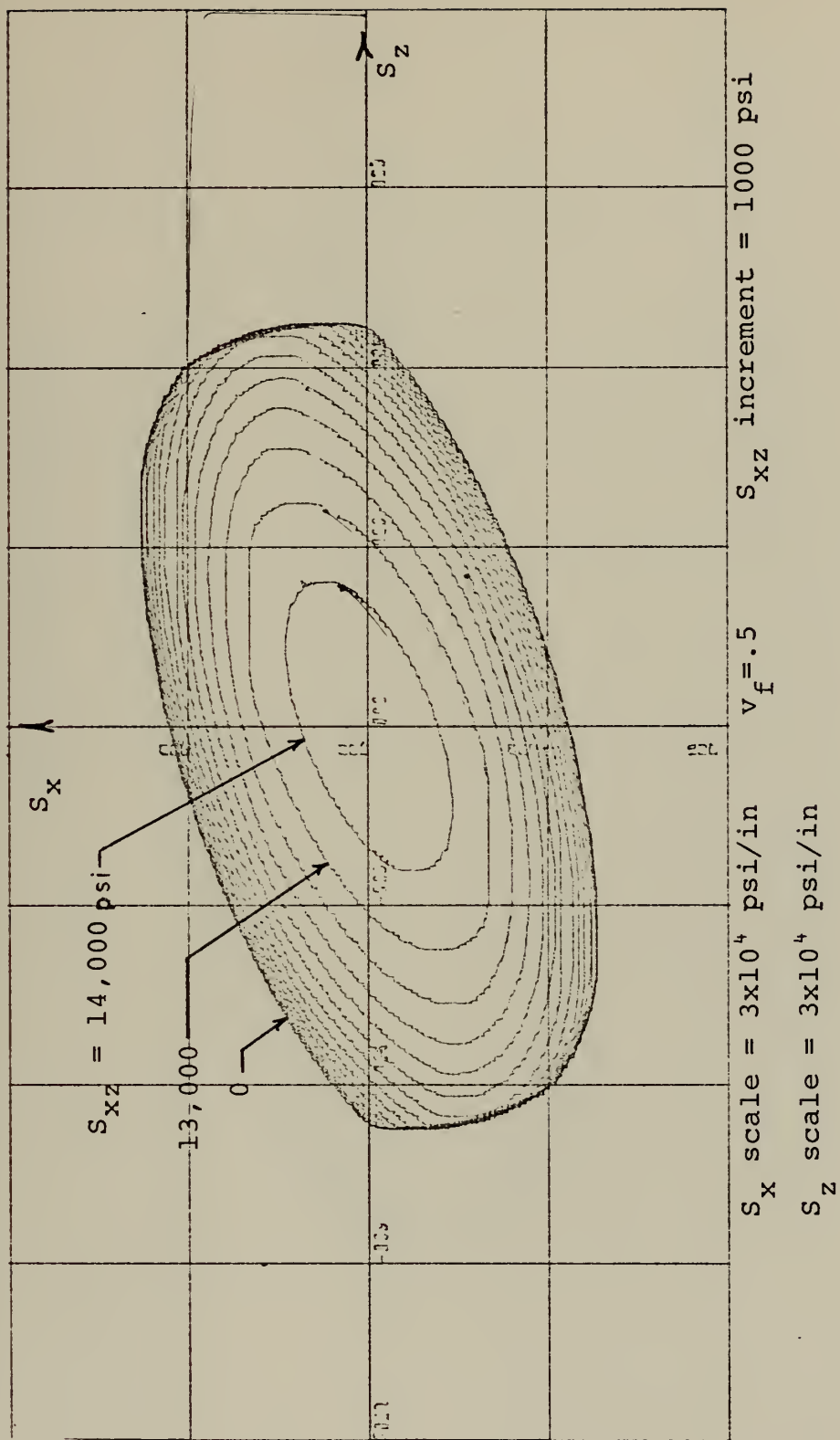
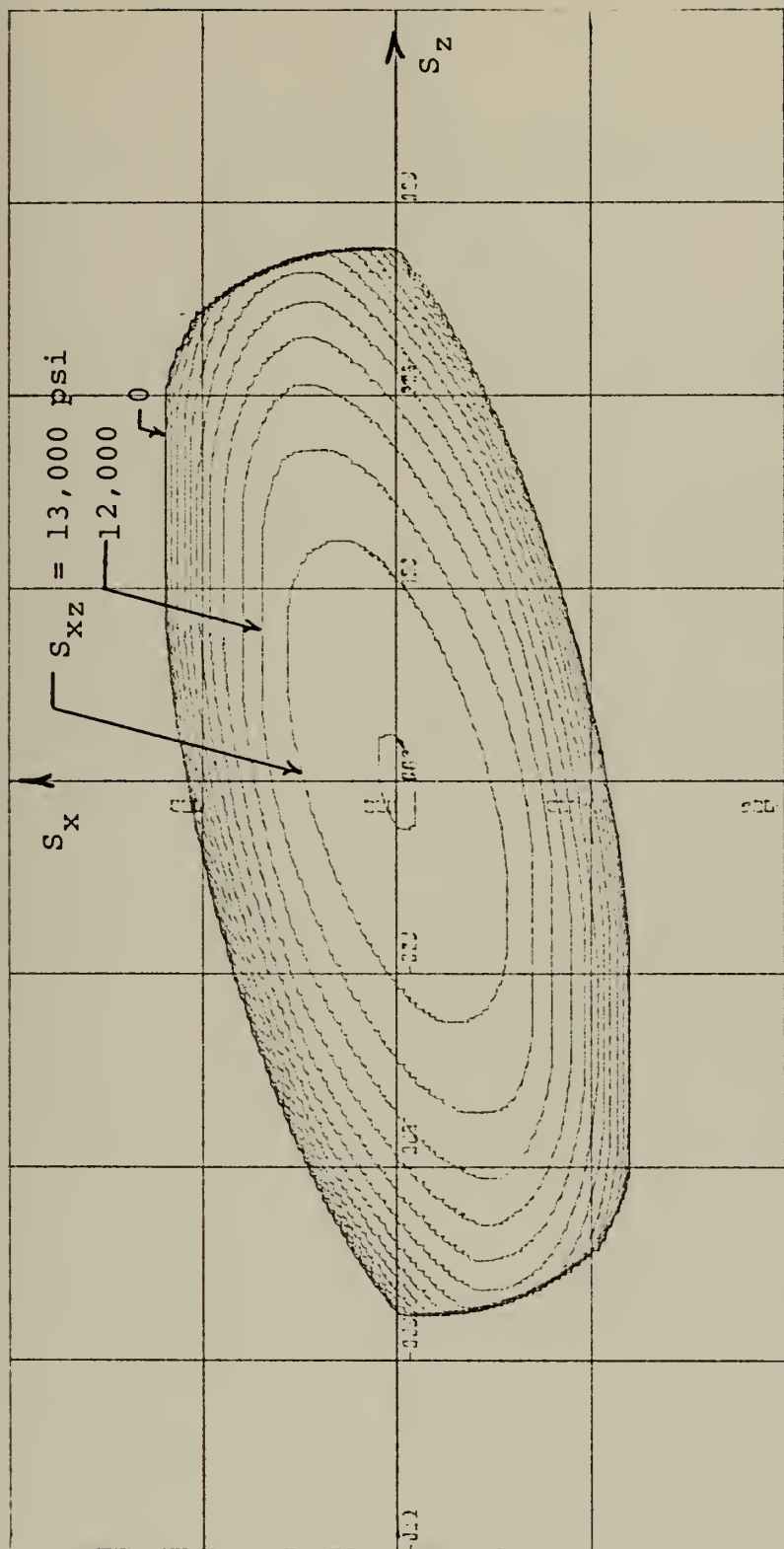


Figure (C-3). Filament Stiffness Variation, $\epsilon_f = 30 \times 10^6$ psi



S_x scale 3×10^4 psi/in $\nu_f = .5$ S_{xz} increment = 1000 psi

S_z scale 3×10^4 psi/in

Figure (C-4). Filament Stiffness Variation, $E_f = 40 \times 10^6$ psi

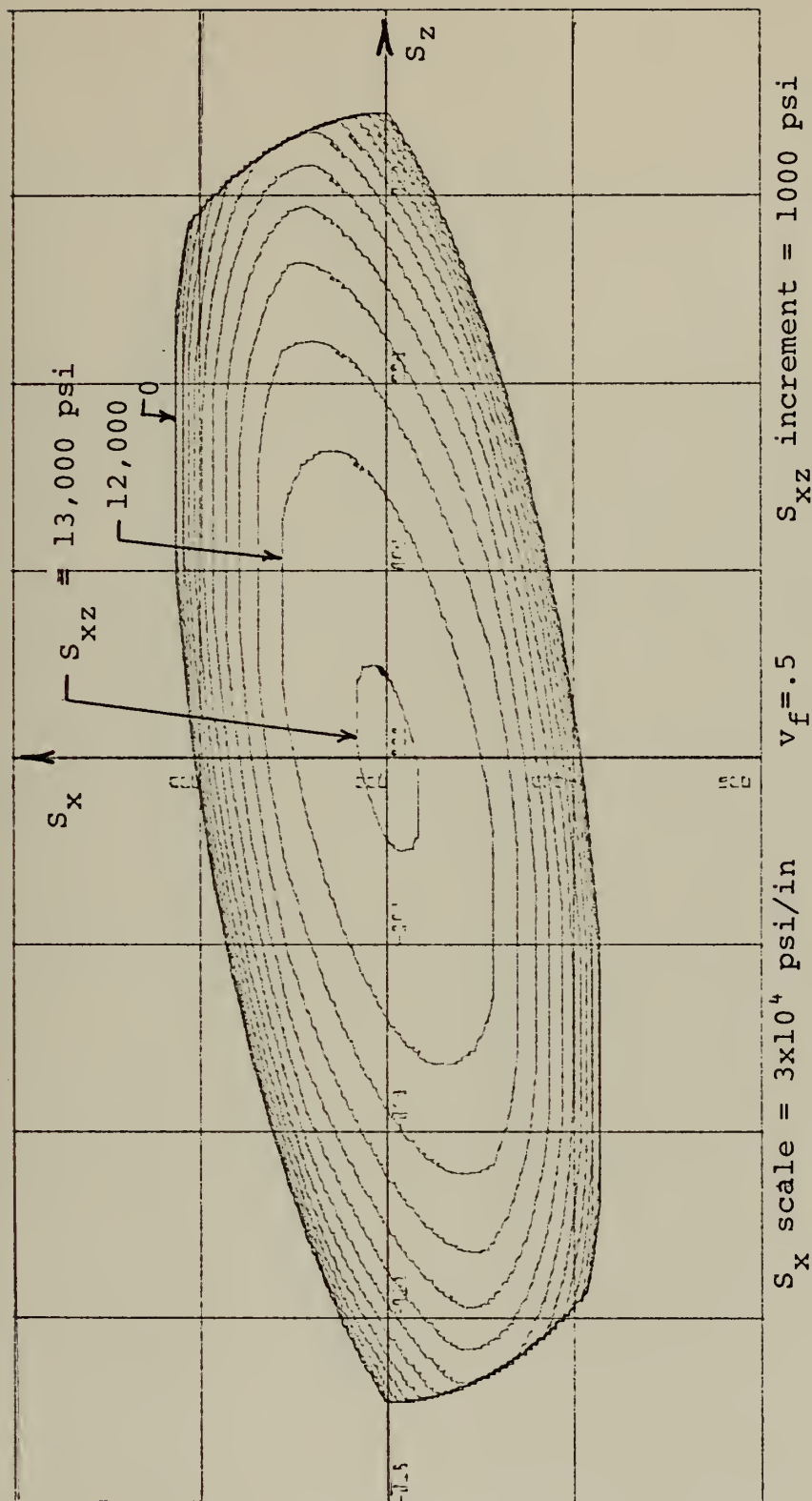
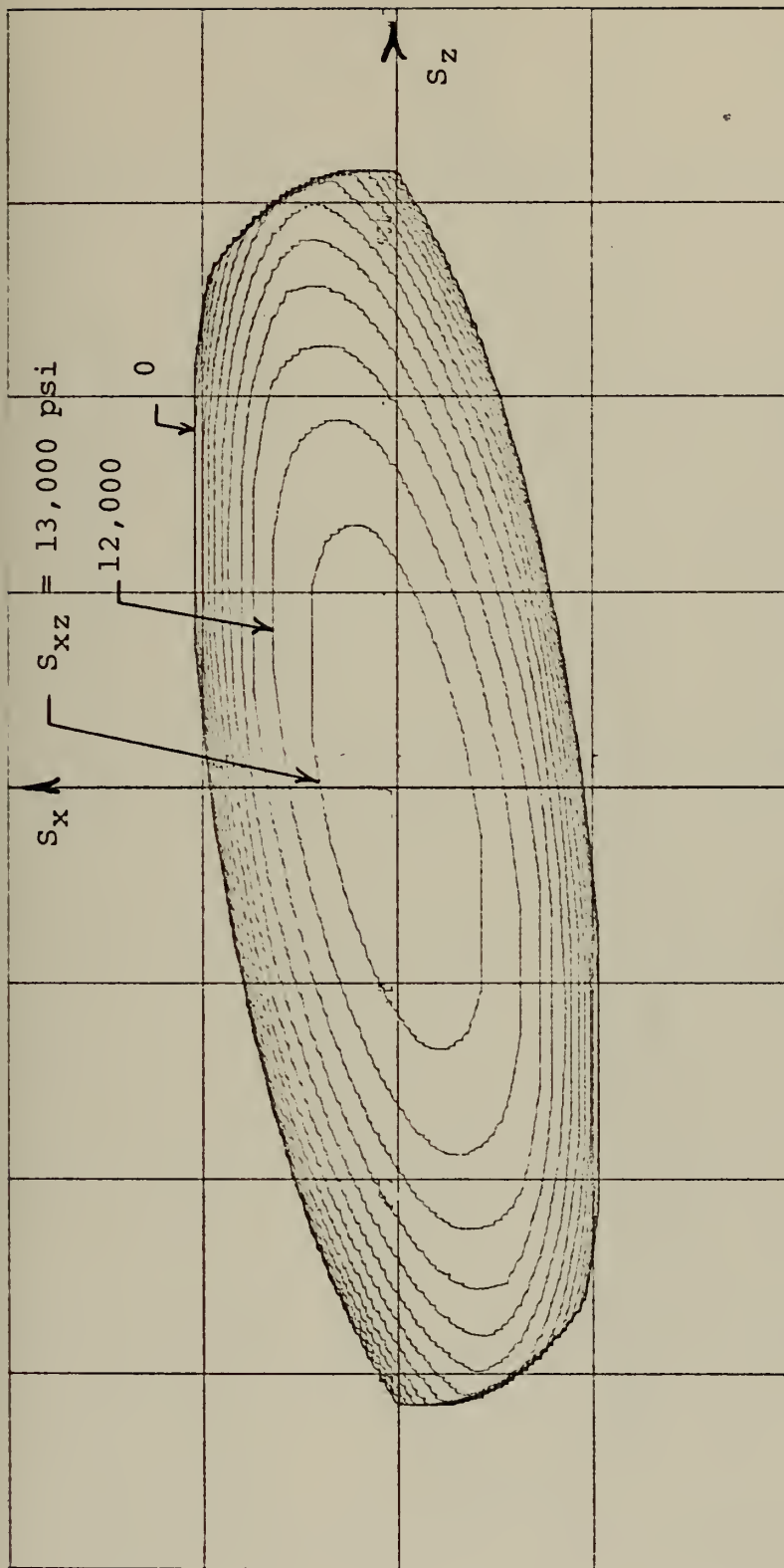


Figure (C-5). Filament Stiffness Variation, $E_f = 75 \times 10^6 \text{ psi}$

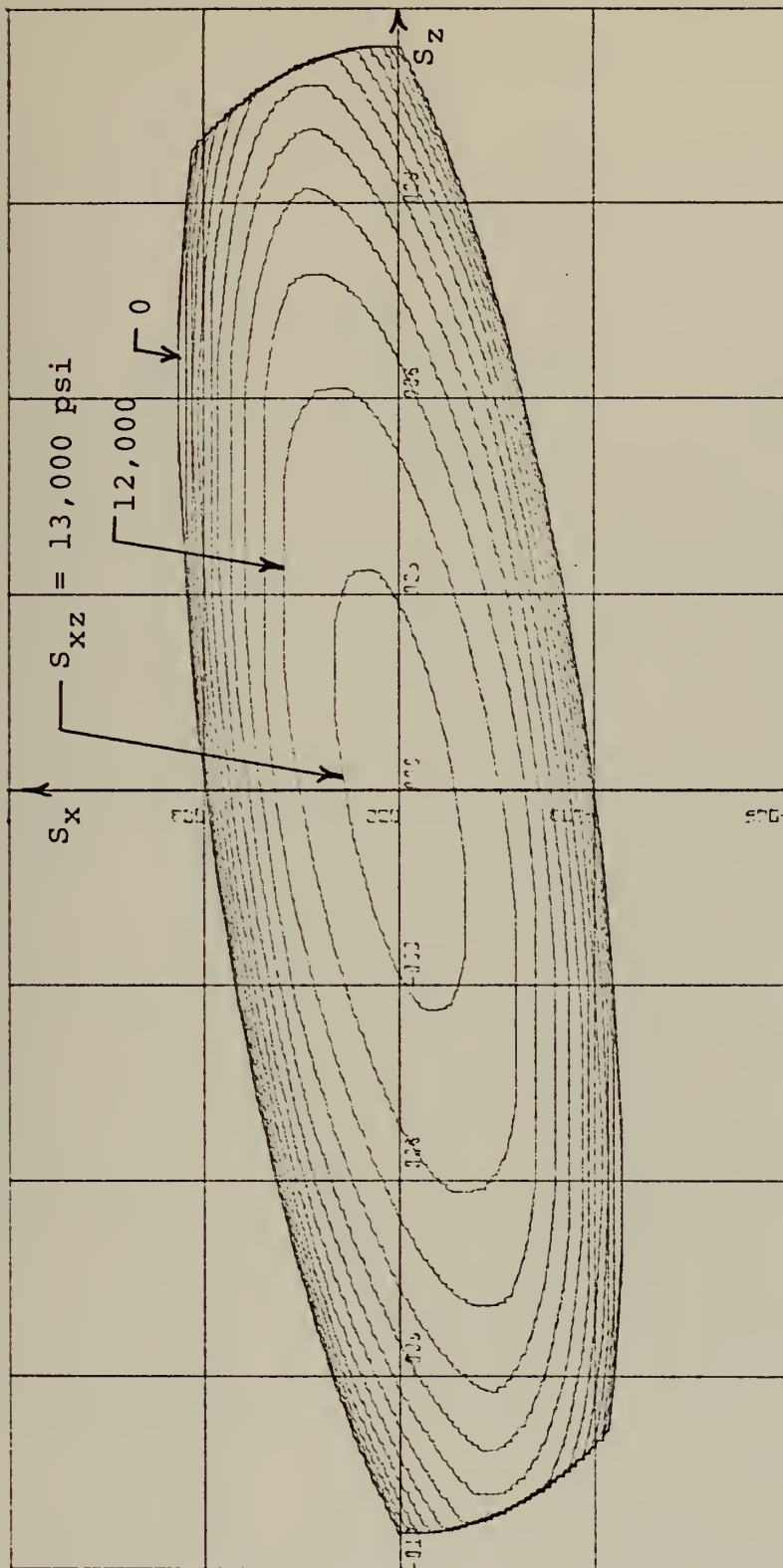


S_{xz} increment = 1000 psi

S_x scale = 3×10^4 psi/in

S_z scale = 3×10^4 psi/in

Figure (C-6).. Boron/6061 Aluminum, $v_f = .4$



S_x scale = 3×10^4 psi/in

S_z scale = 3×10^4 psi/in

S_{xz} increment = 1000 psi

Figure (C-7). Boron/6061 Aluminum, $v_f = .5$

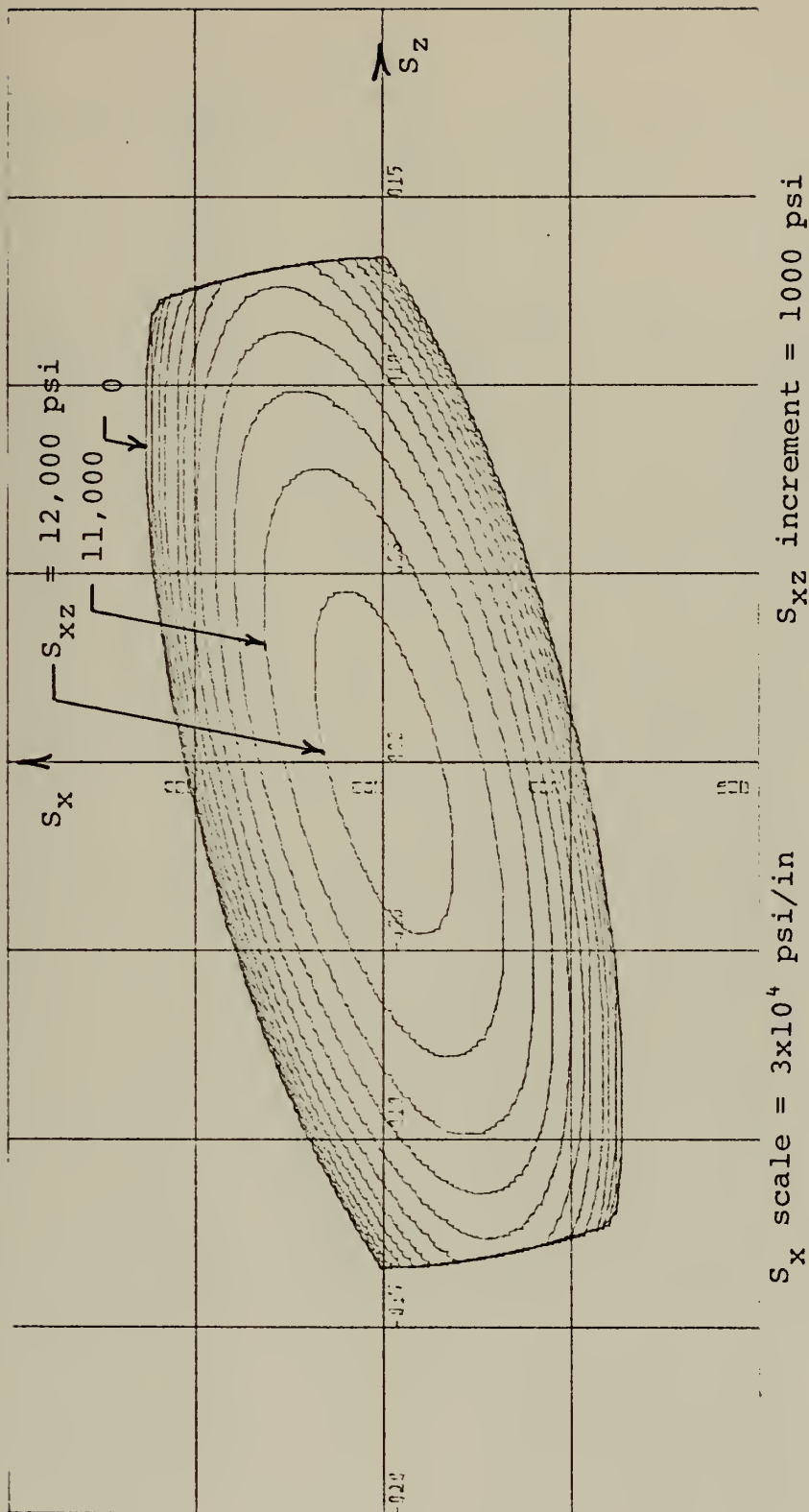
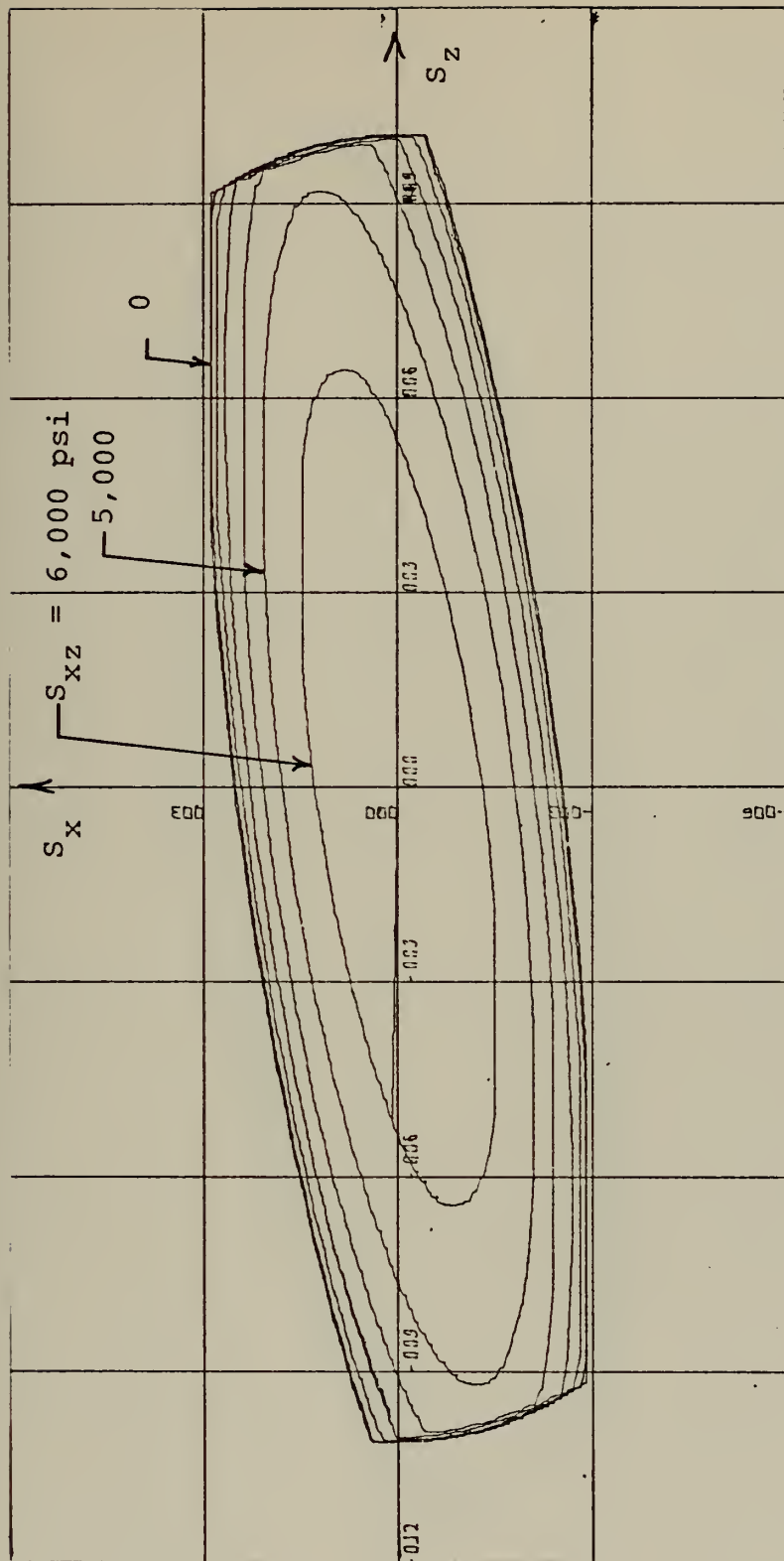
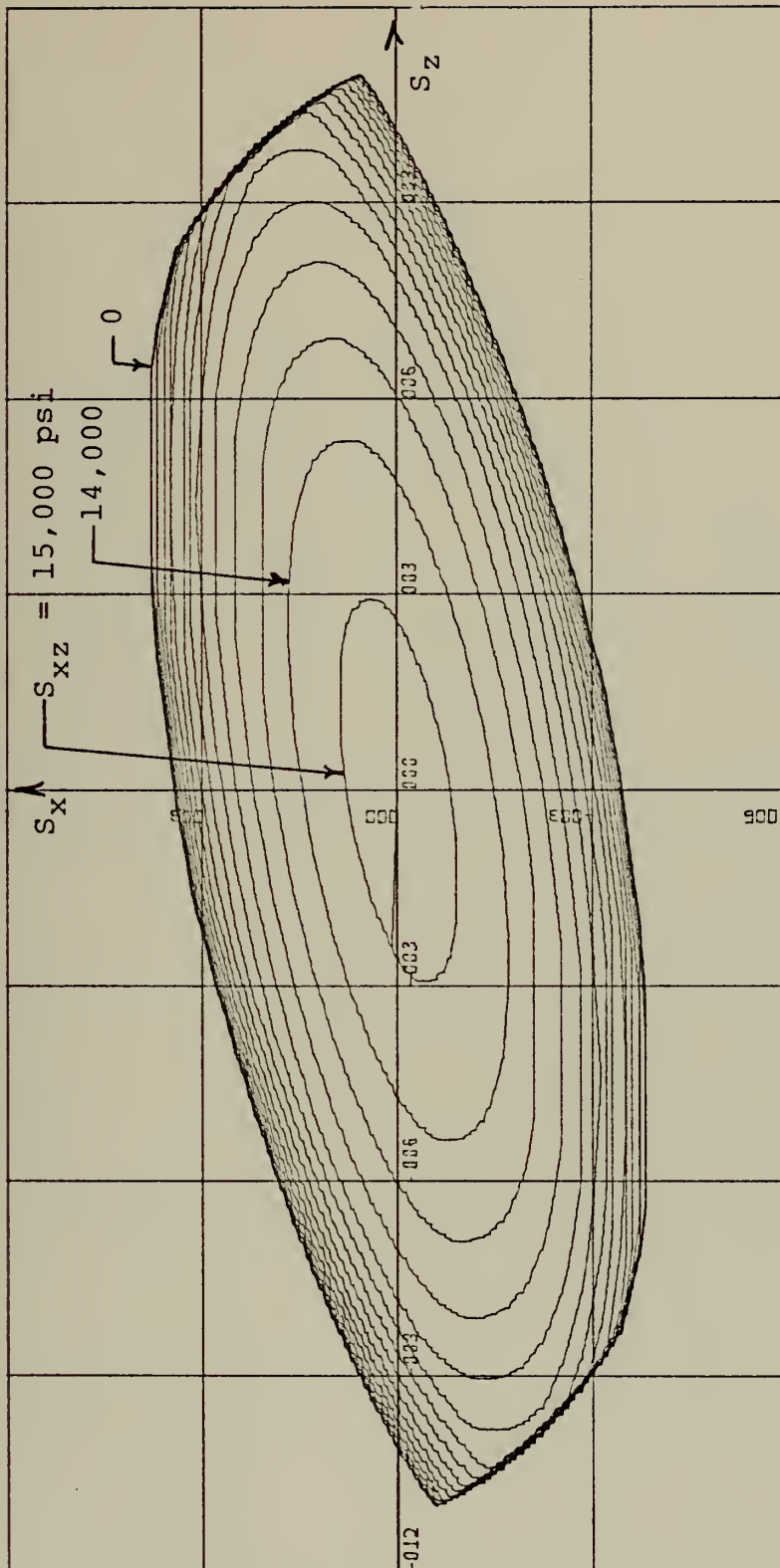


Figure (C-8). Boron/6061 Aluminum, $v_f = .6$



S_x scale = 3×10^4 psi/in Major Axis X-axis S_{xz} increment = 1000 psi
 S_z scale = 3×10^4 psi/in

Figure (C-9). Boron/6061 Aluminum, Elliptical



S_x scale = 3×10^4 psi/in Major Axis Y-axis S_{xz} increment = 1000 psi
 S_z scale = 3×10^4 psi/in

Figure (C-10). Boron/6061 Aluminum, Elliptical

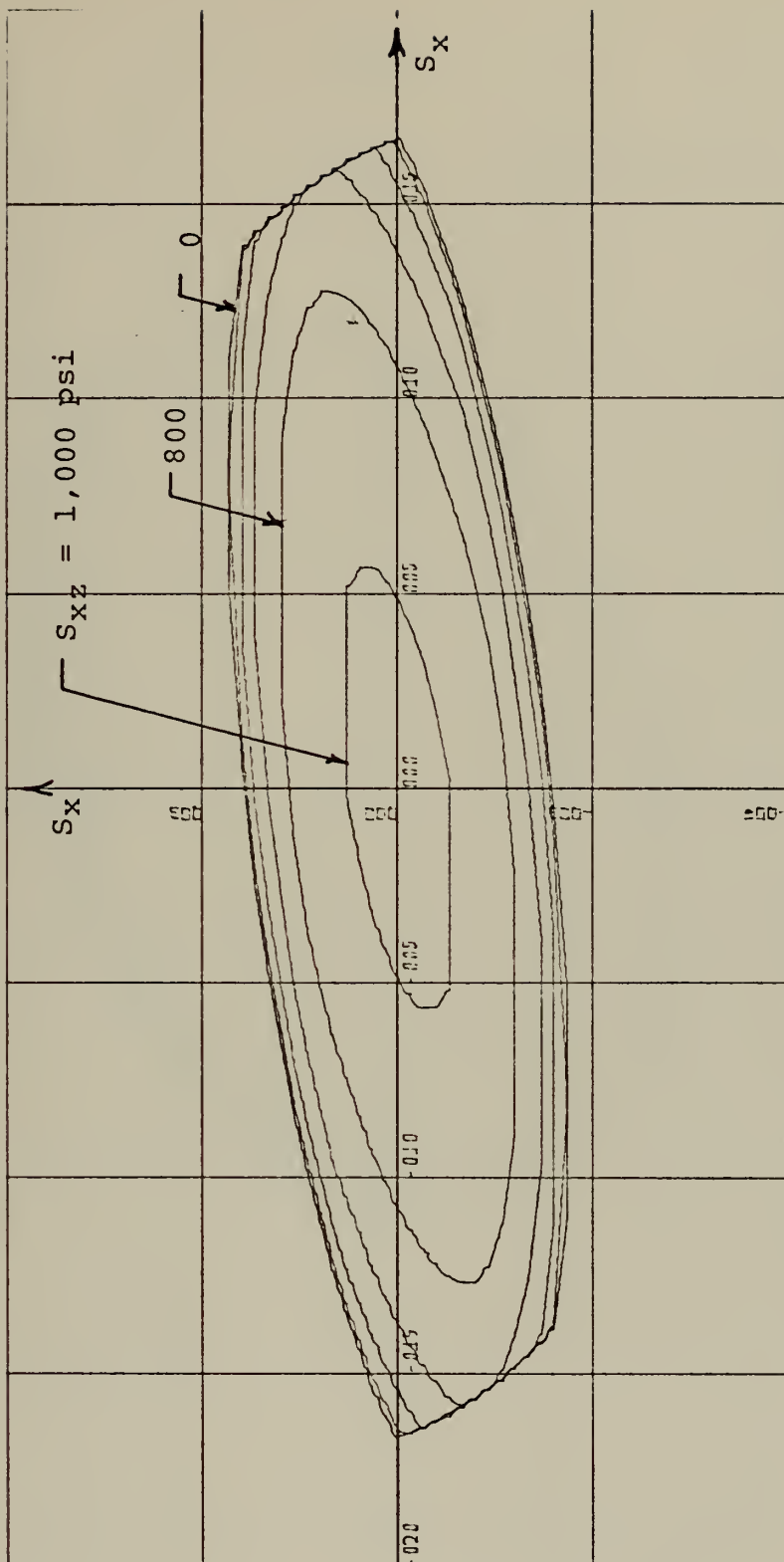
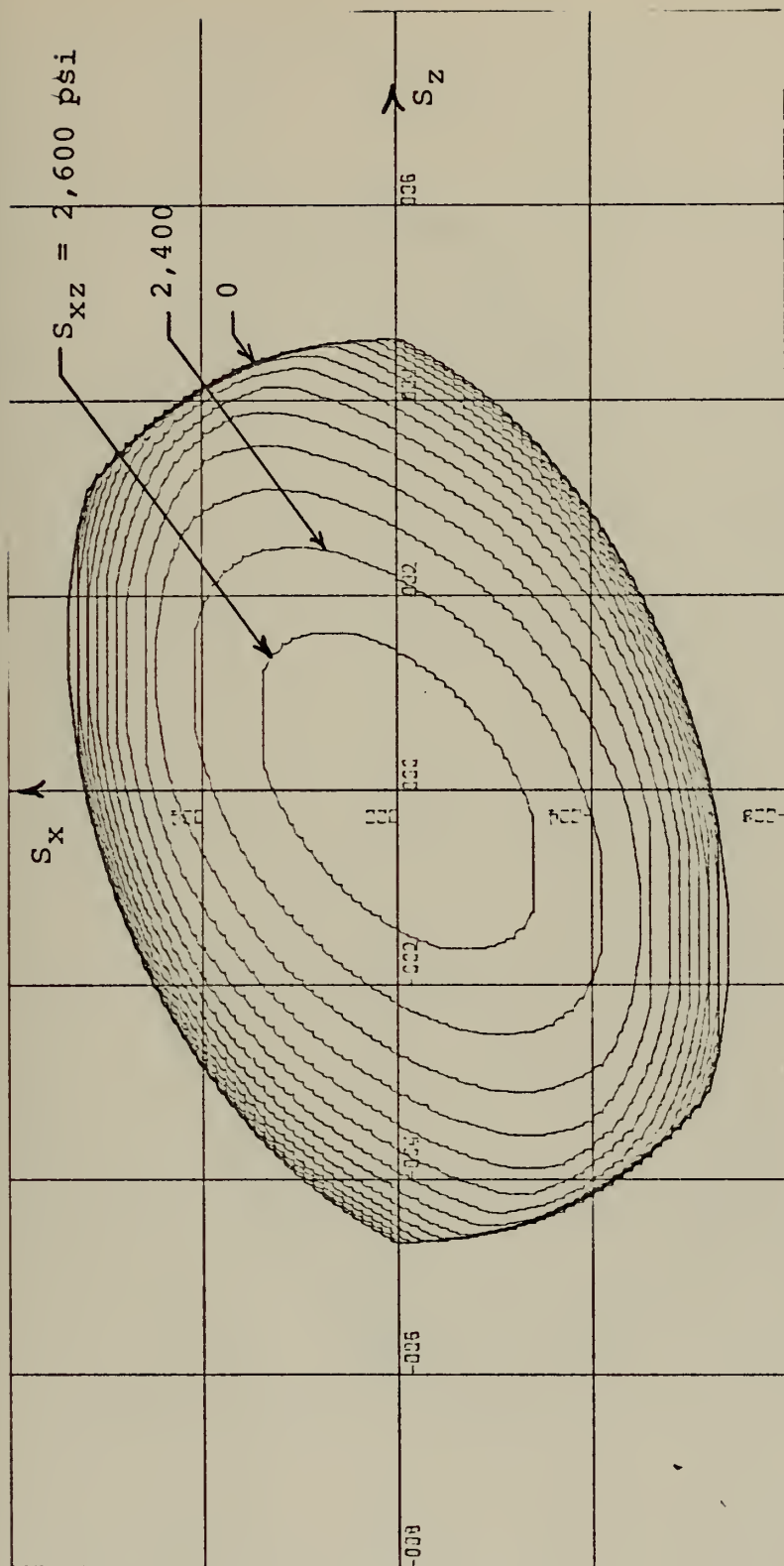


Figure (C-11). Boron/NARMCO Epoxy, $v_f=0.5$



S_x scale = $4 \times 10^3 \text{ psi/in}$ S_{xz} increment = 200 psi

S_z scale = $2 \times 10^4 \text{ psi/in}$

Figure (C-12). E-glass/Epoxy, $v_f = .3$

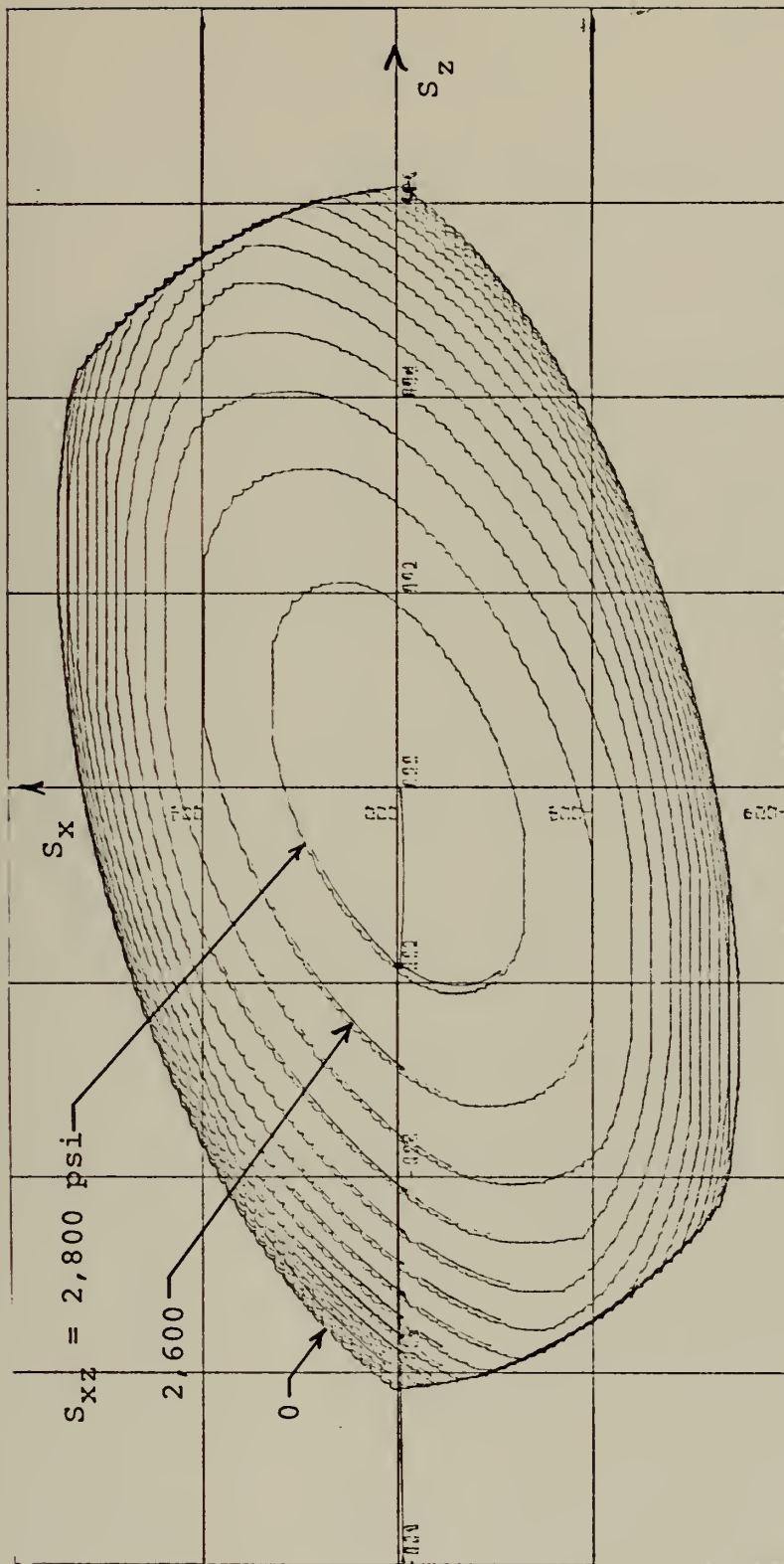


Figure (C-13). E-glass/Epoxy, $v_f = .4$

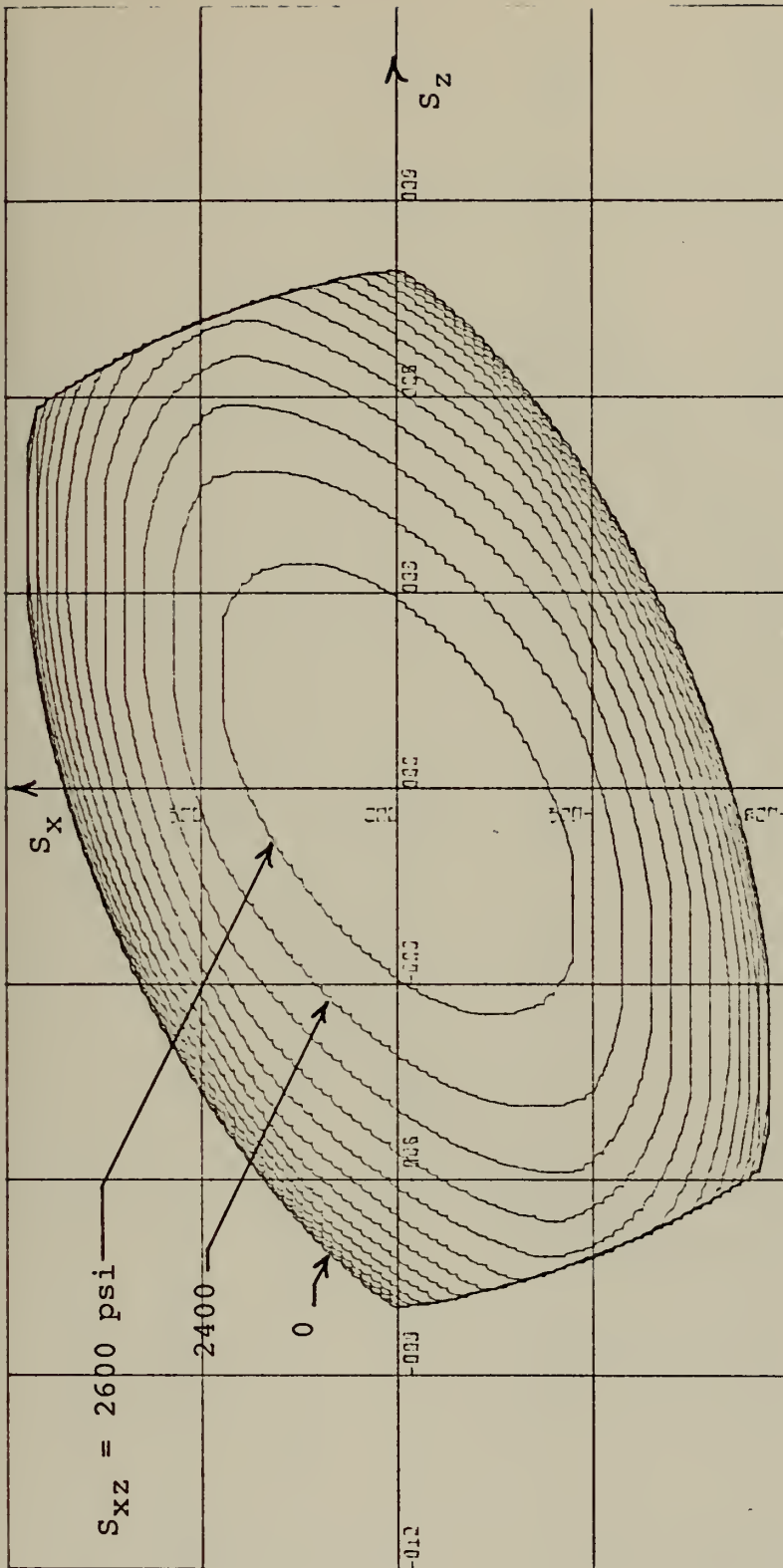
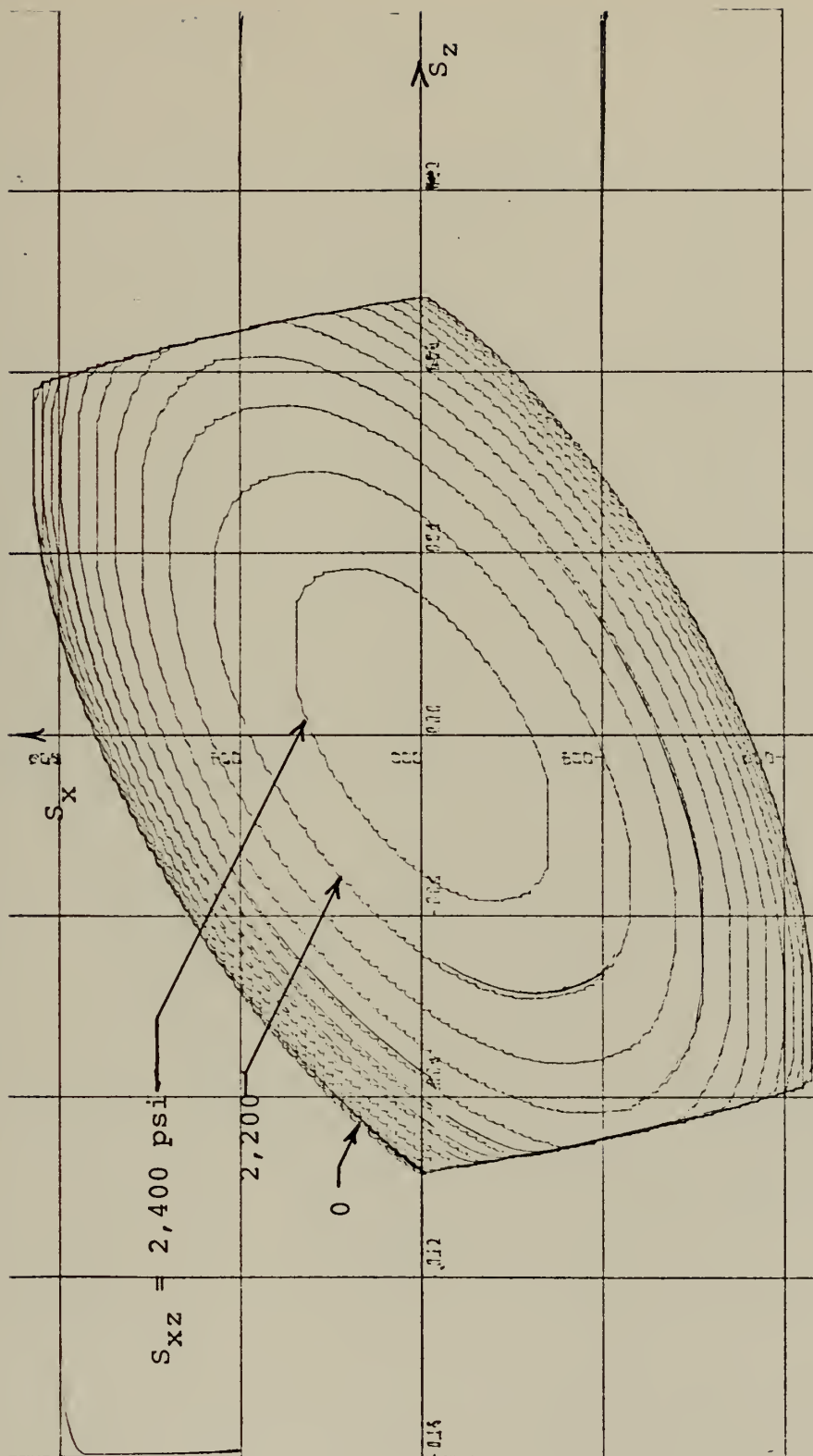
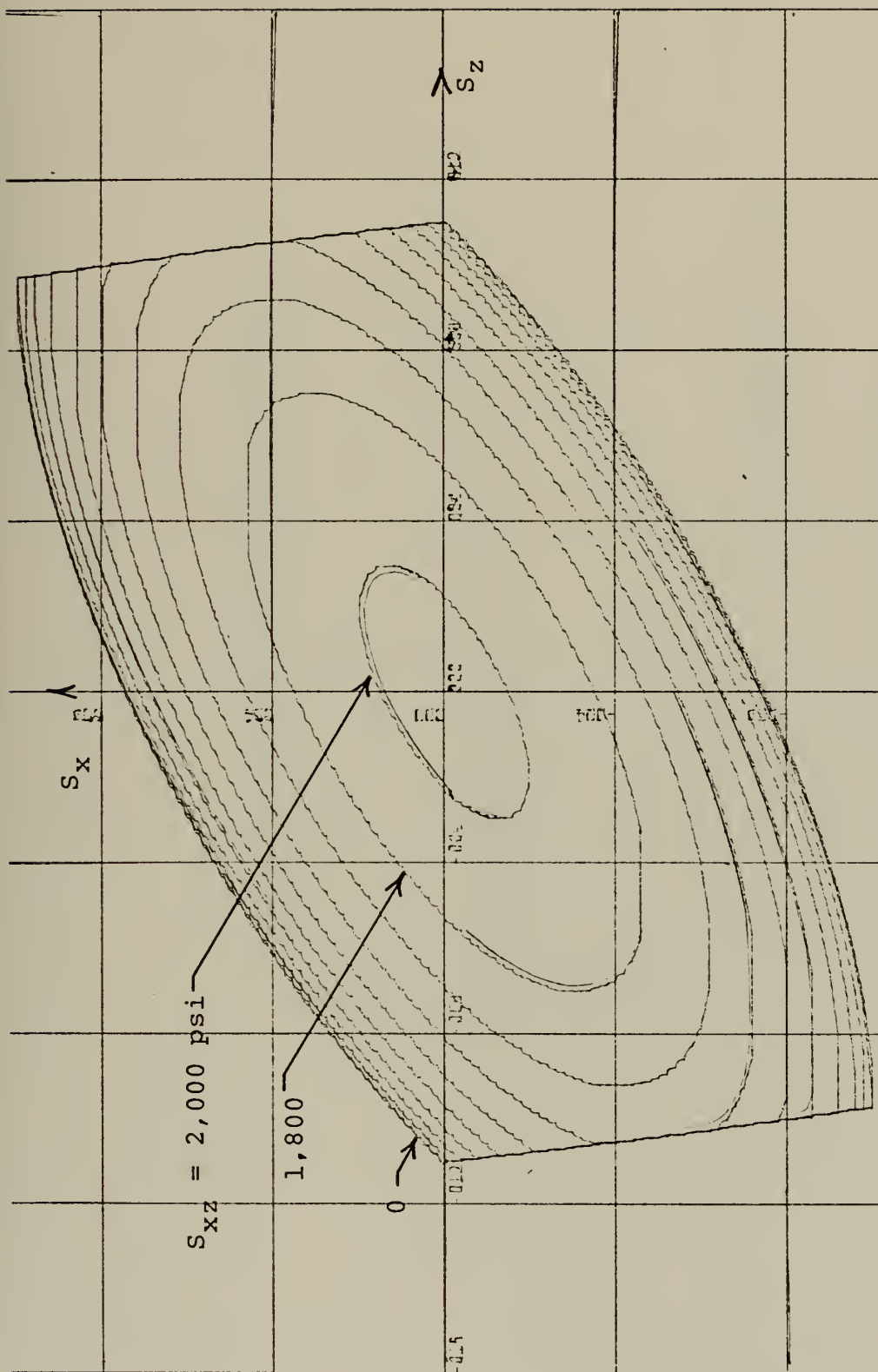


Figure (C-14). E-glass/Epoxy, $v_f = .5$



S_x scale = 4×10^3 psi/in
 S_z scale = 4×10^4 psi/in
 S_{xz} increment = 200 psi

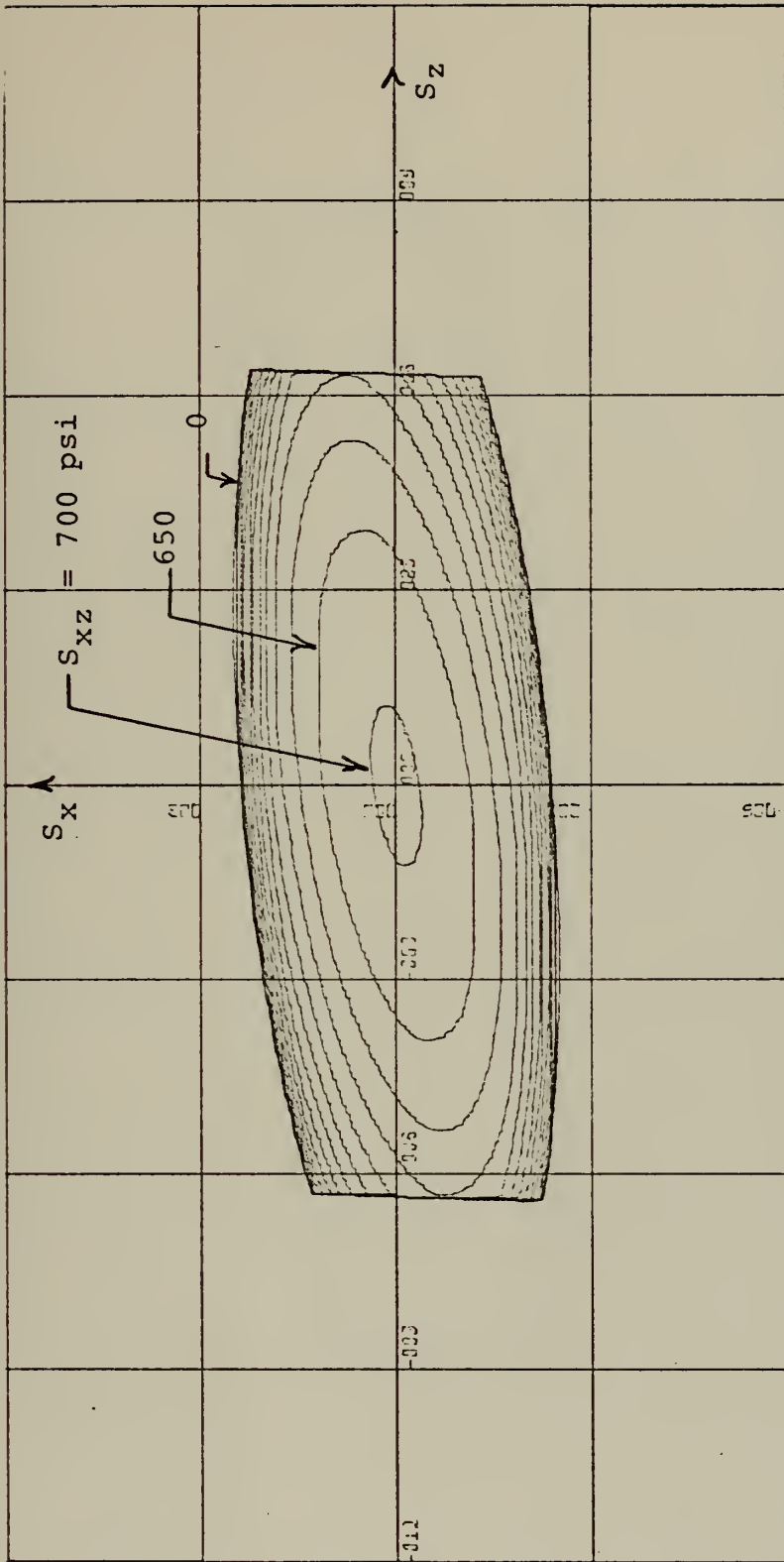
Figure (C-15). E-glass/Epoxy, $v_f = .6$



S_x scale = 4×10^3 psi/in S_{xz} increment = 200 psi

S_z scale = 4×10^4 psi/in

Figure (C-16). E-glass/Epoxy, $v_f=.7$

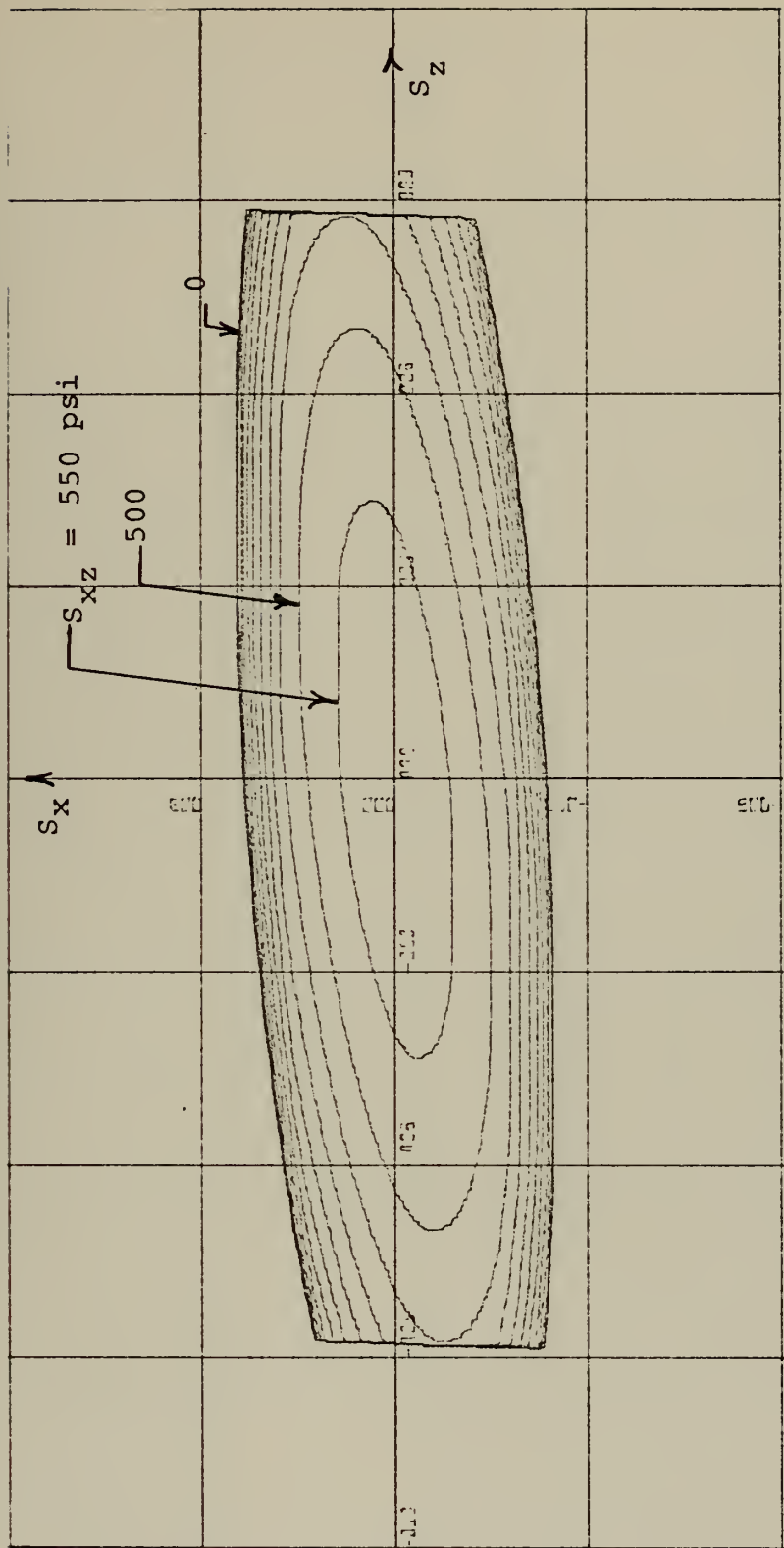


S_{xz} increment = 50 psi

S_x scale = 3×10^3 psi/in

S_z scale = 3×10^4 psi/in

Figure (C-17). MODMOR I(graphite)/NARMCO Epoxy, $\nu_f = 0.3$

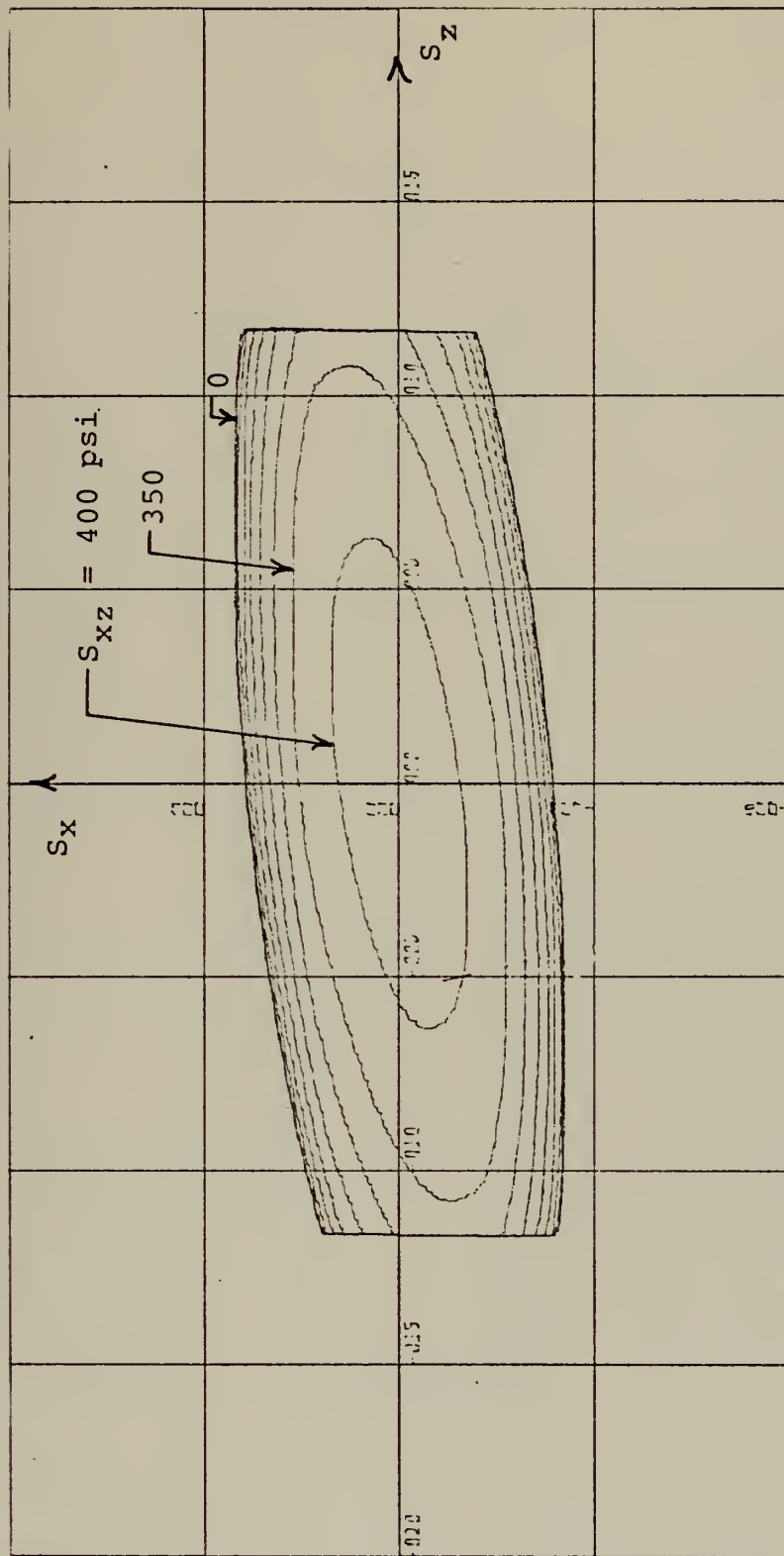


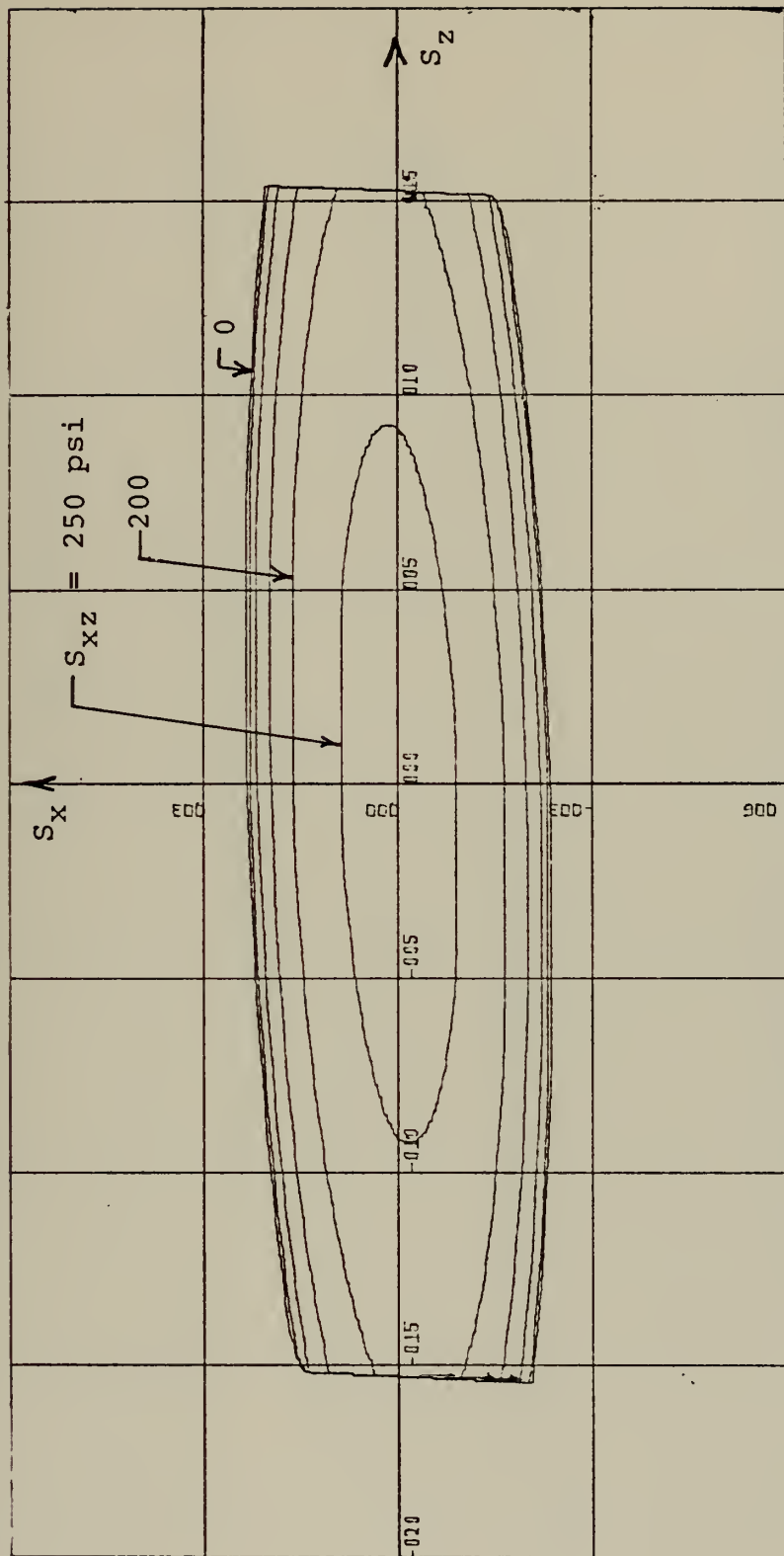
S_{xz} increment = 50 psi

S_x scale = 3×10^3 psi/in

S_z scale = 3×10^4 psi/in

Figure (C-18). MODMOR I (graphite)/NARMCO Epoxy, $v_f = .4$

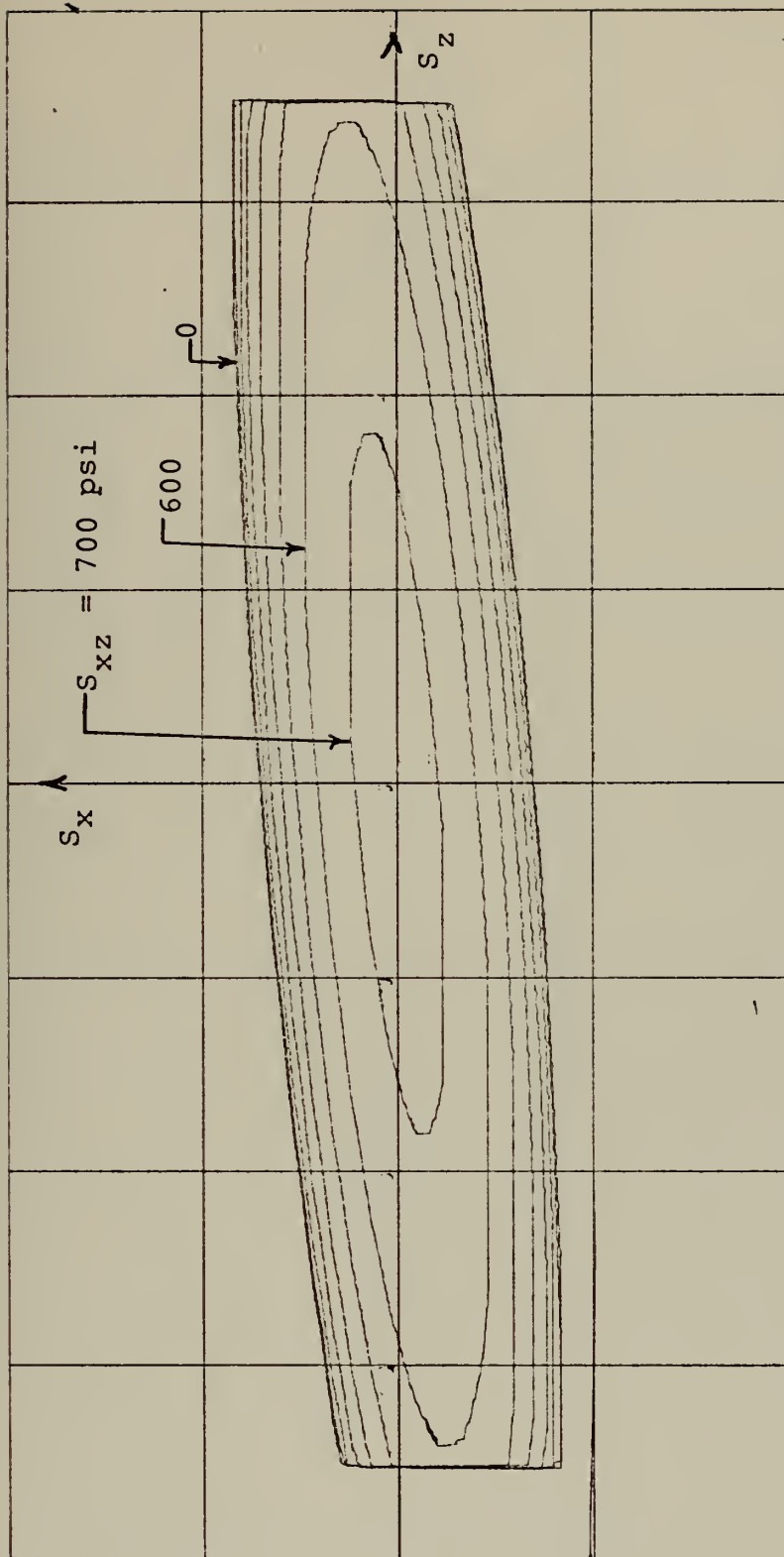




S_x scale = 3×10^3 psi/in S_{xz} increment = 50 psi

S_z scale = 5×10^4 psi/in

Figure (C-20). MODMOR I (graphite)/NARMCO Epoxy, $v_f = 0.6$

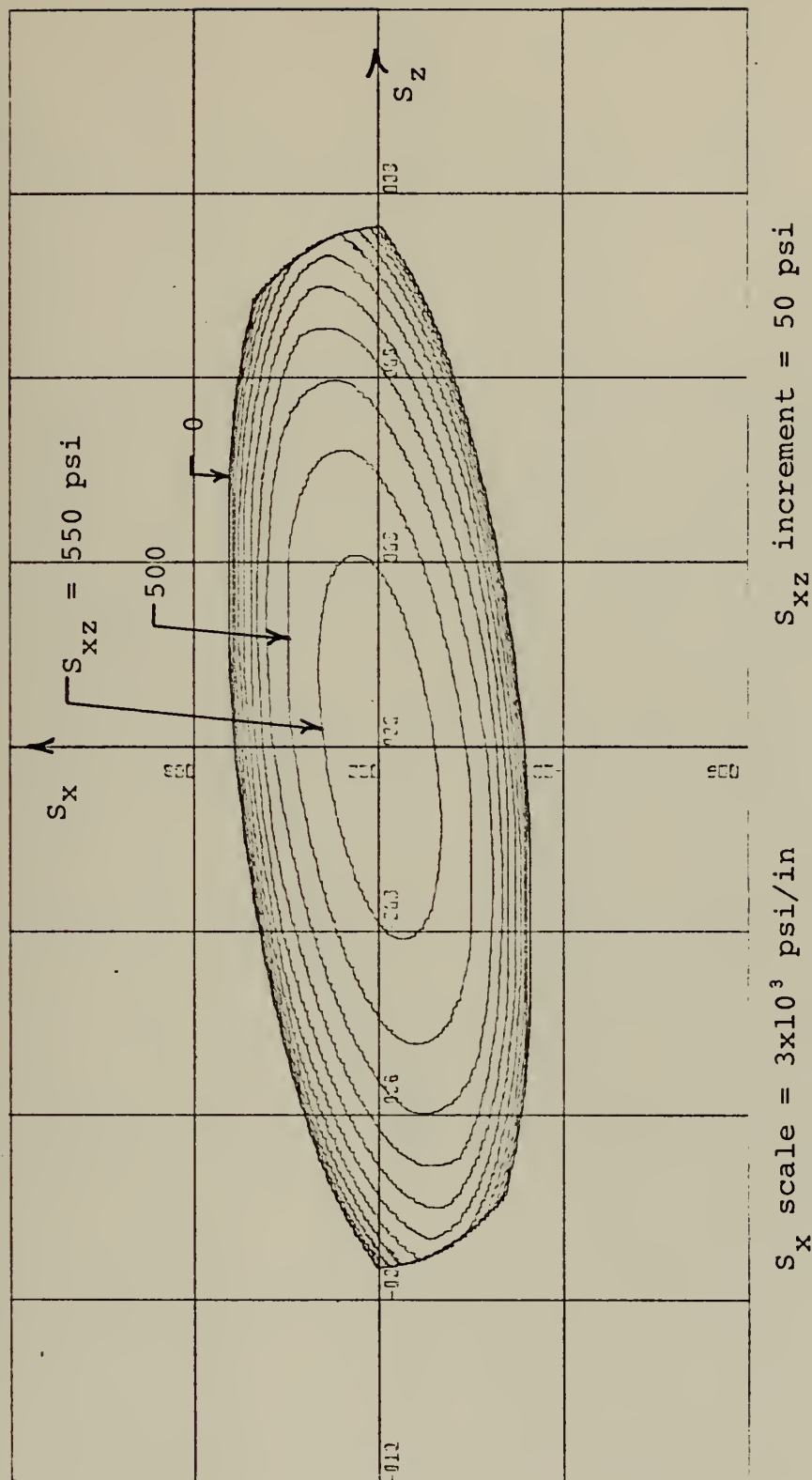


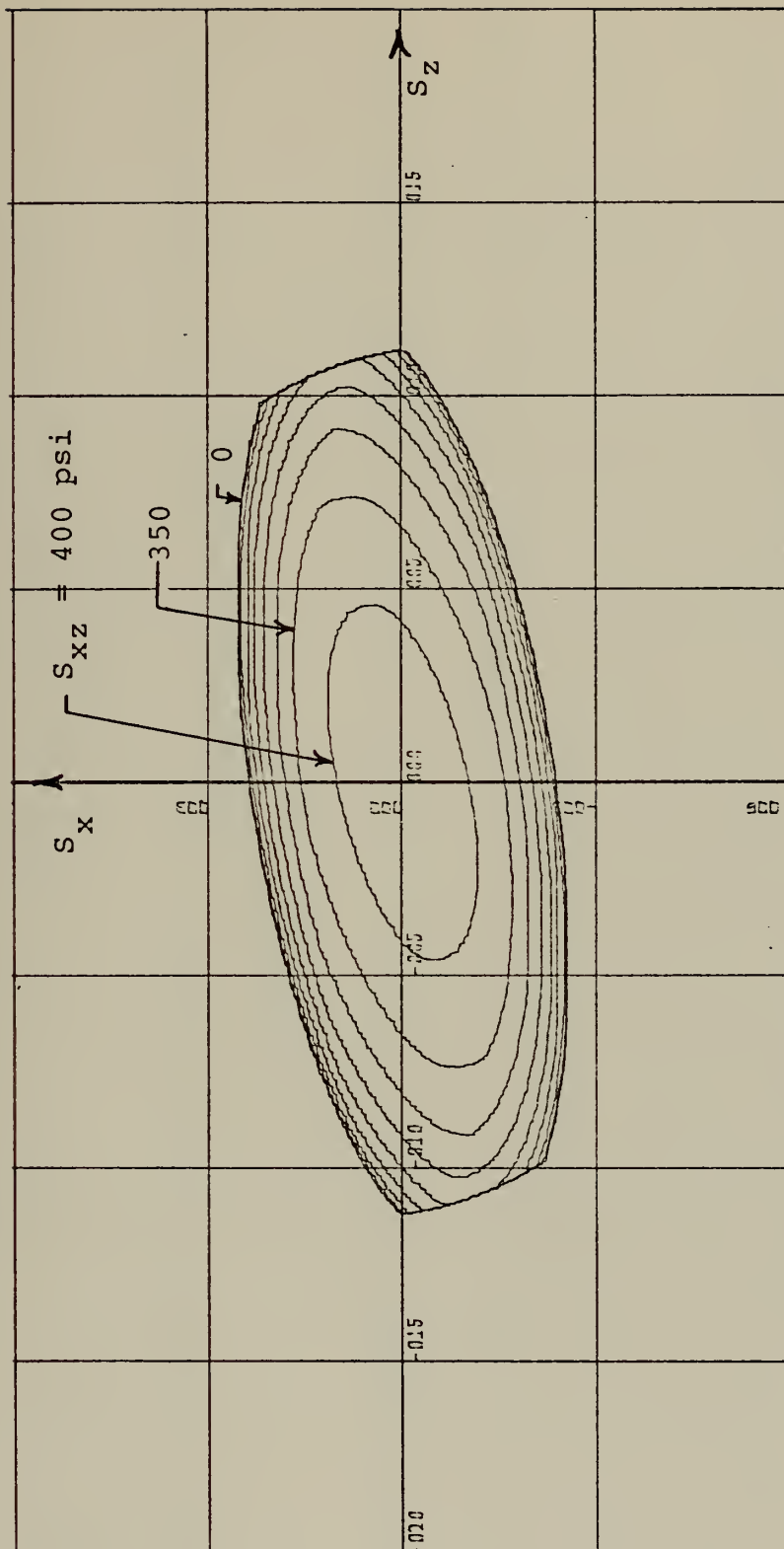
S_x scale = 3×10^3 psi/in

S_z scale = 5×10^4 psi/in

S_{xz} increment = 100 psi

Figure (C-21). MODMOR I (graphite)/NARMCO Epoxy, $\nu_f = .7$



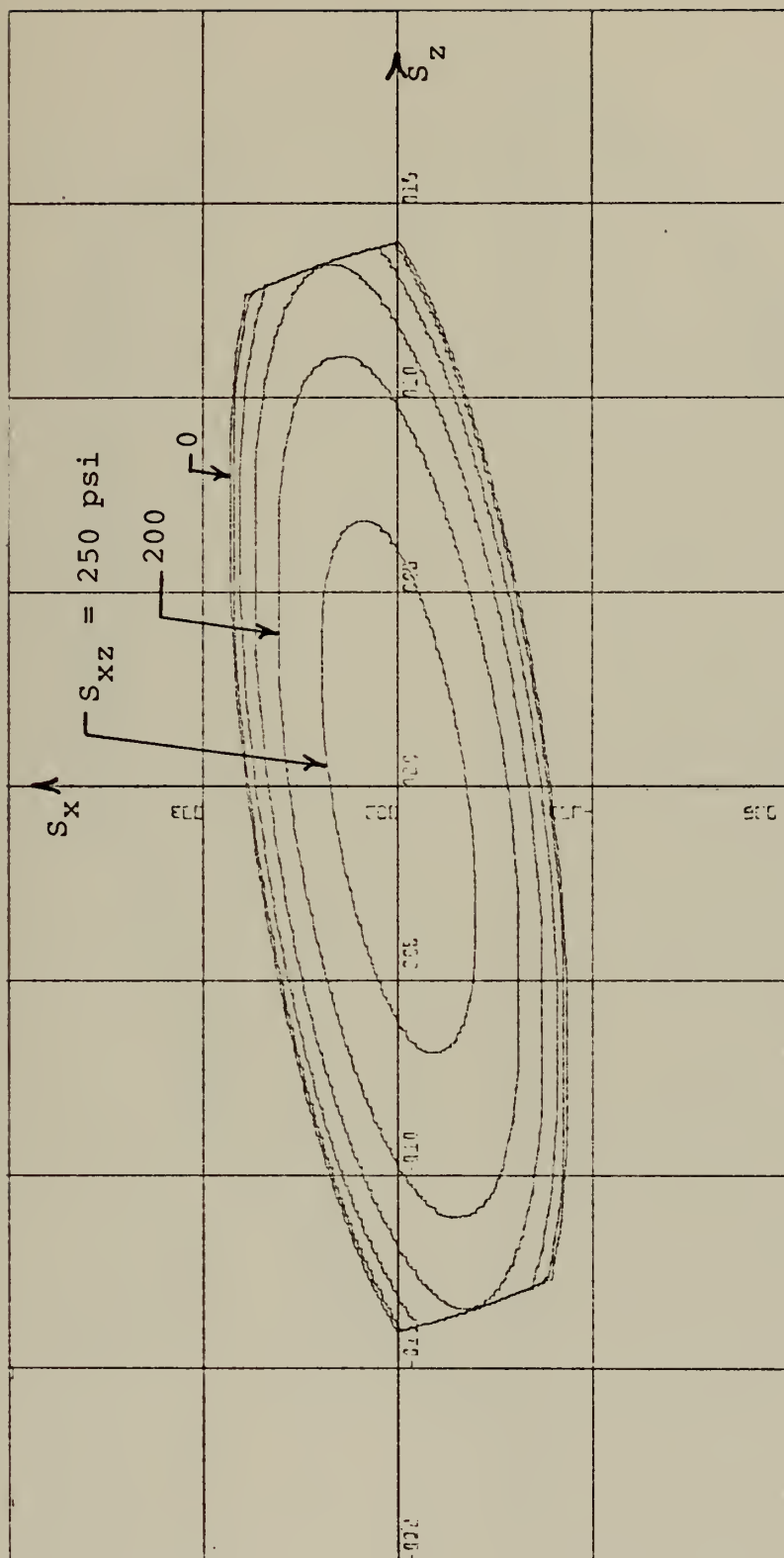


S_{xz} increment = 50 psi

S_x scale = 3×10^3 psi/in

S_z scale = 5×10^4 psi/in

Figure (C-23). MODMOR II (graphite)/NARMCO Epoxy, $v_f = 0.5$

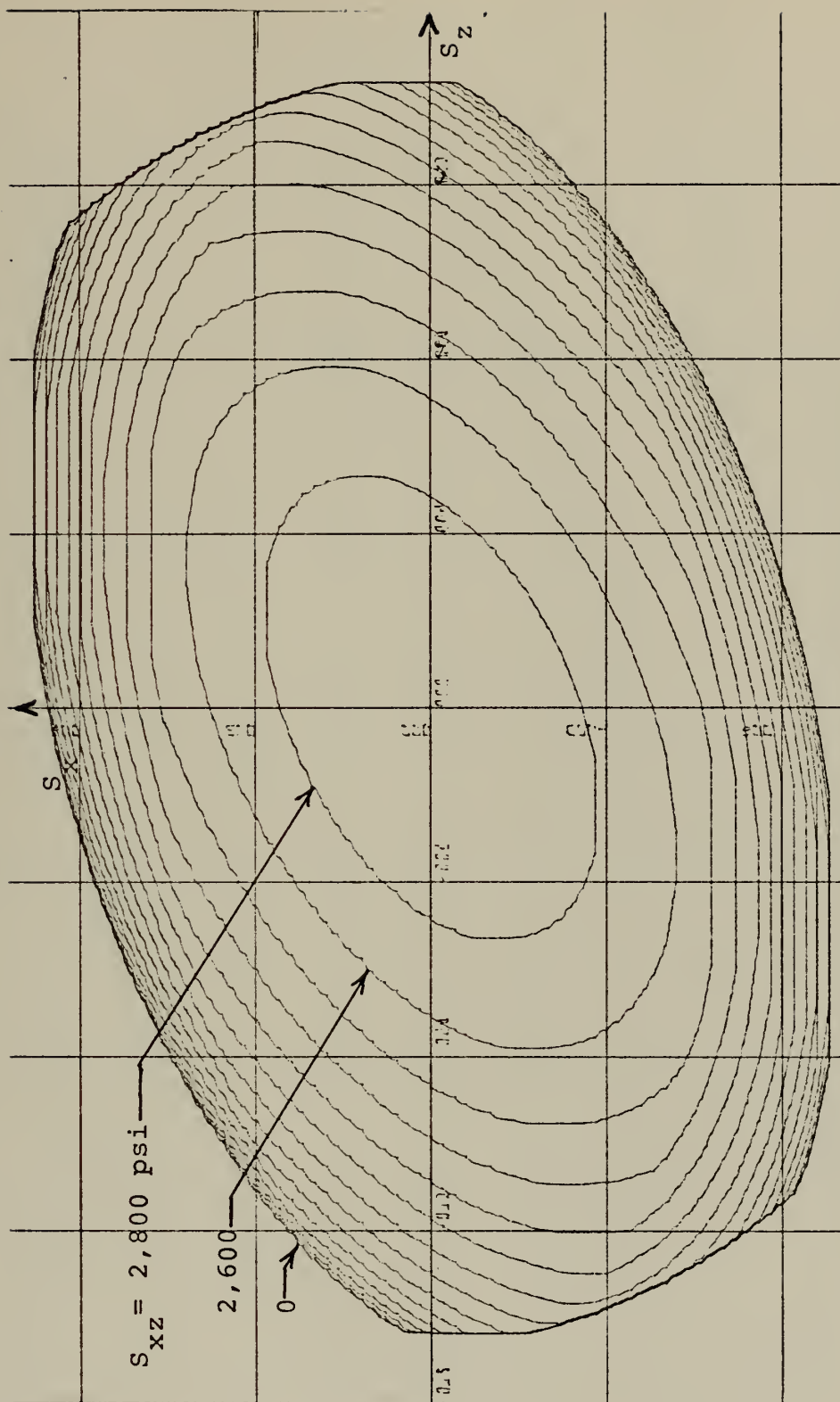


S_x scale = 3×10^3 psi/in

S_{xz} increment = 50 psi

S_z scale = 5×10^4 psi/in

Figure (C-24). MODMOR II (graphite)/NARMCO Epoxy, $\nu_f = .6$



S_x scale = 3×10^3 psi/in S_{xz} increment = 200 psi

S_z scale = 4×10^4 psi/in

Figure (C-25). MODMOR II(graphite)/4617 Epoxy, $v_f = .4$

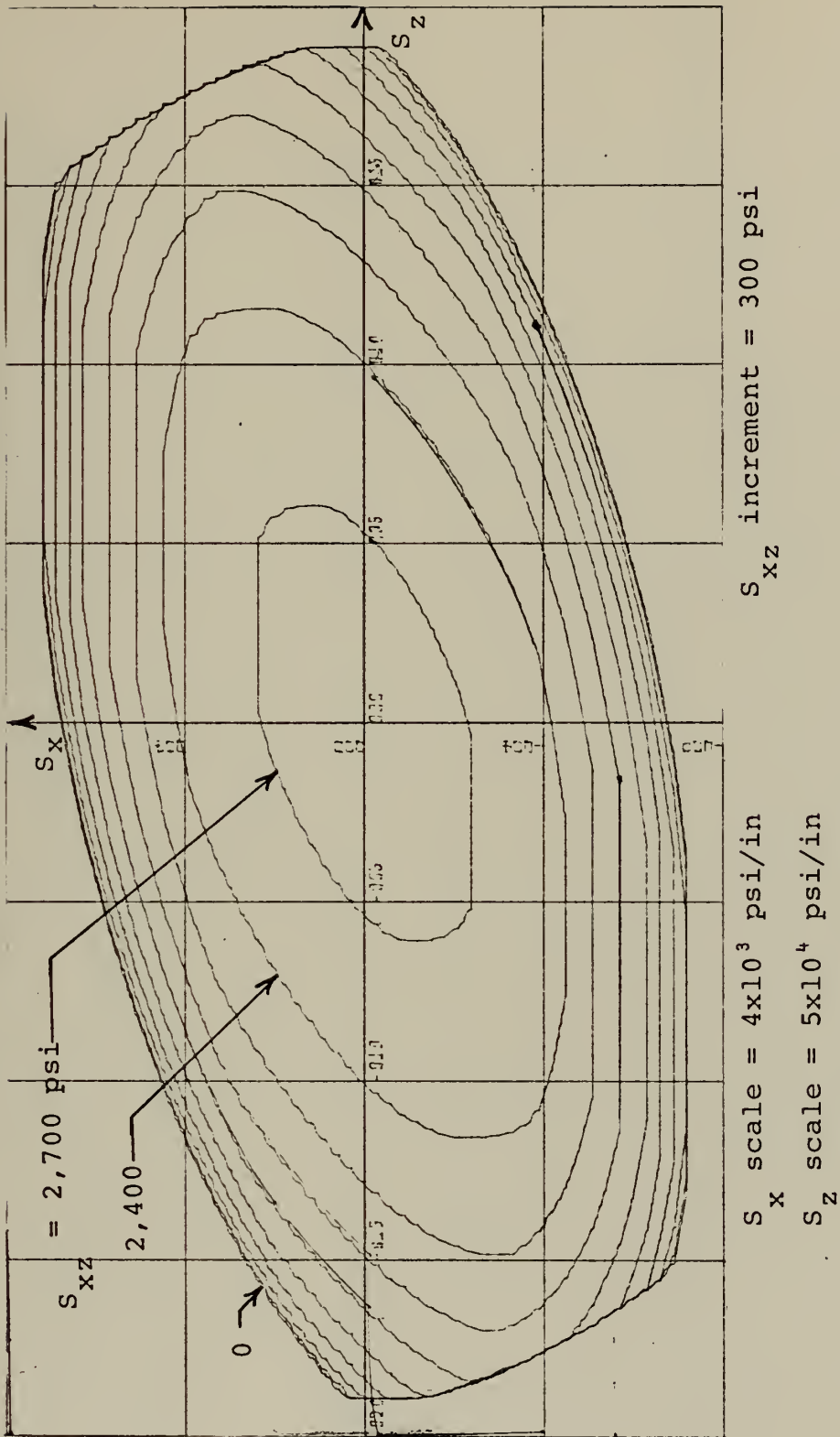
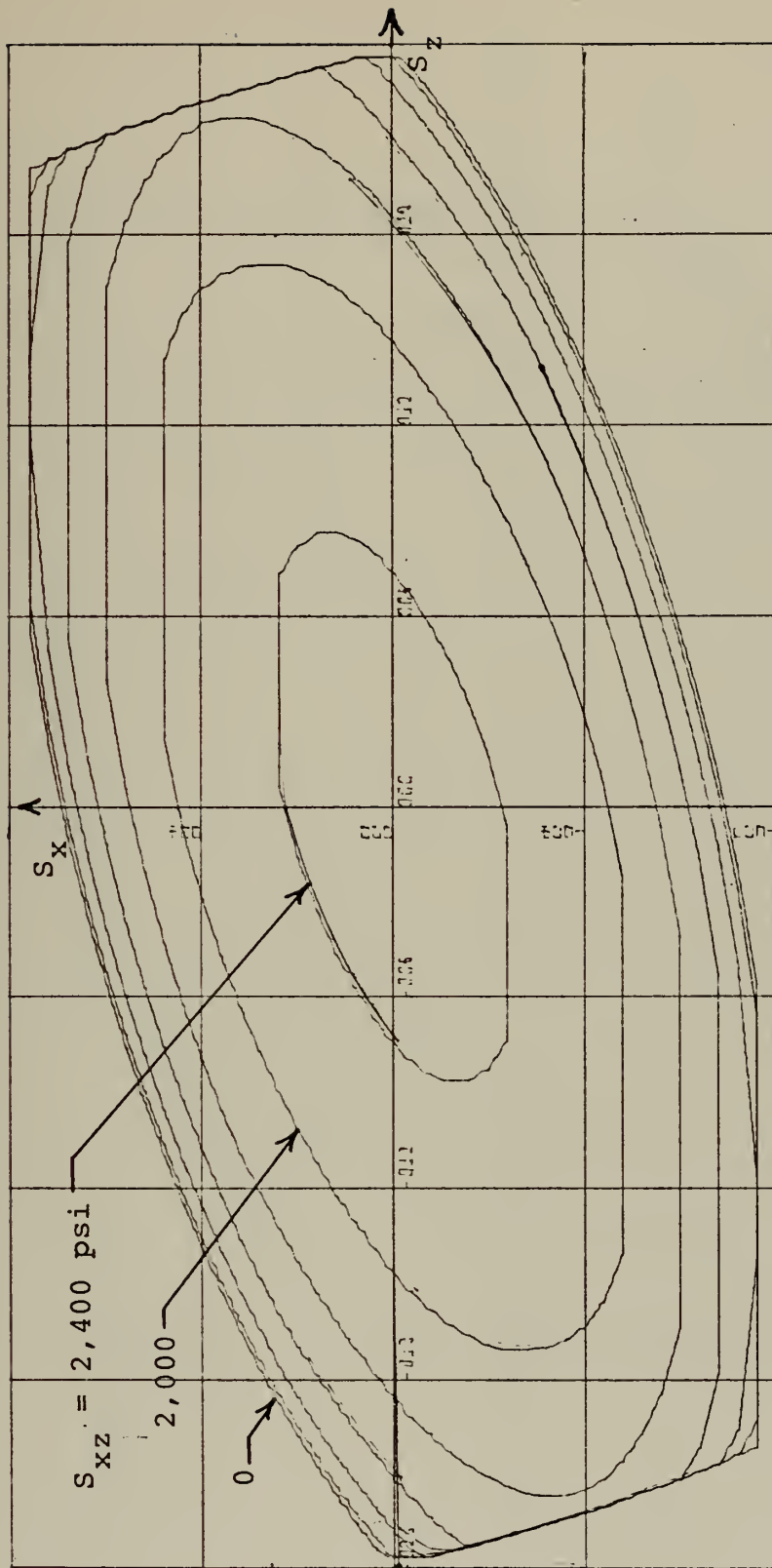


Figure (C-26). MODMOR II (graphite)/4617 Epoxy, $v_f = .5$

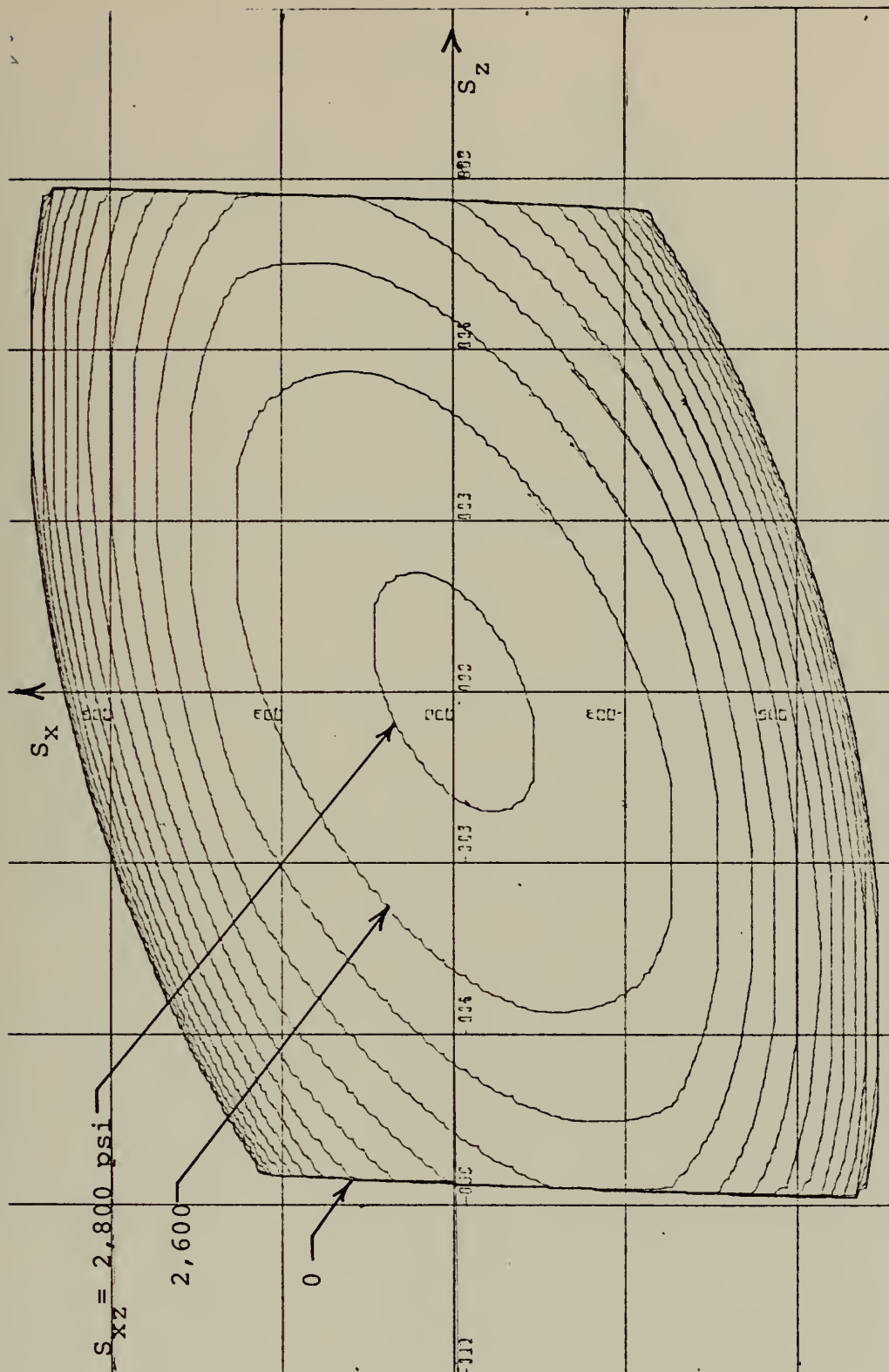


S_{xz} increment = 400 psi

S_x scale = 4×10^3 psi/in

S_z scale = 5×10^4 psi/in

Figure (C-27). MODMOR II (graphite)/4617 Epoxy, $v_f = .6$



S_{xz} increment = 200 psi

S_x scale = 3×10^3 psi/in

S_z scale = 3×10^4 psi/in

Figure (C-28). THORNEL 25(graphite)/Epoxy, $v_f=.5$

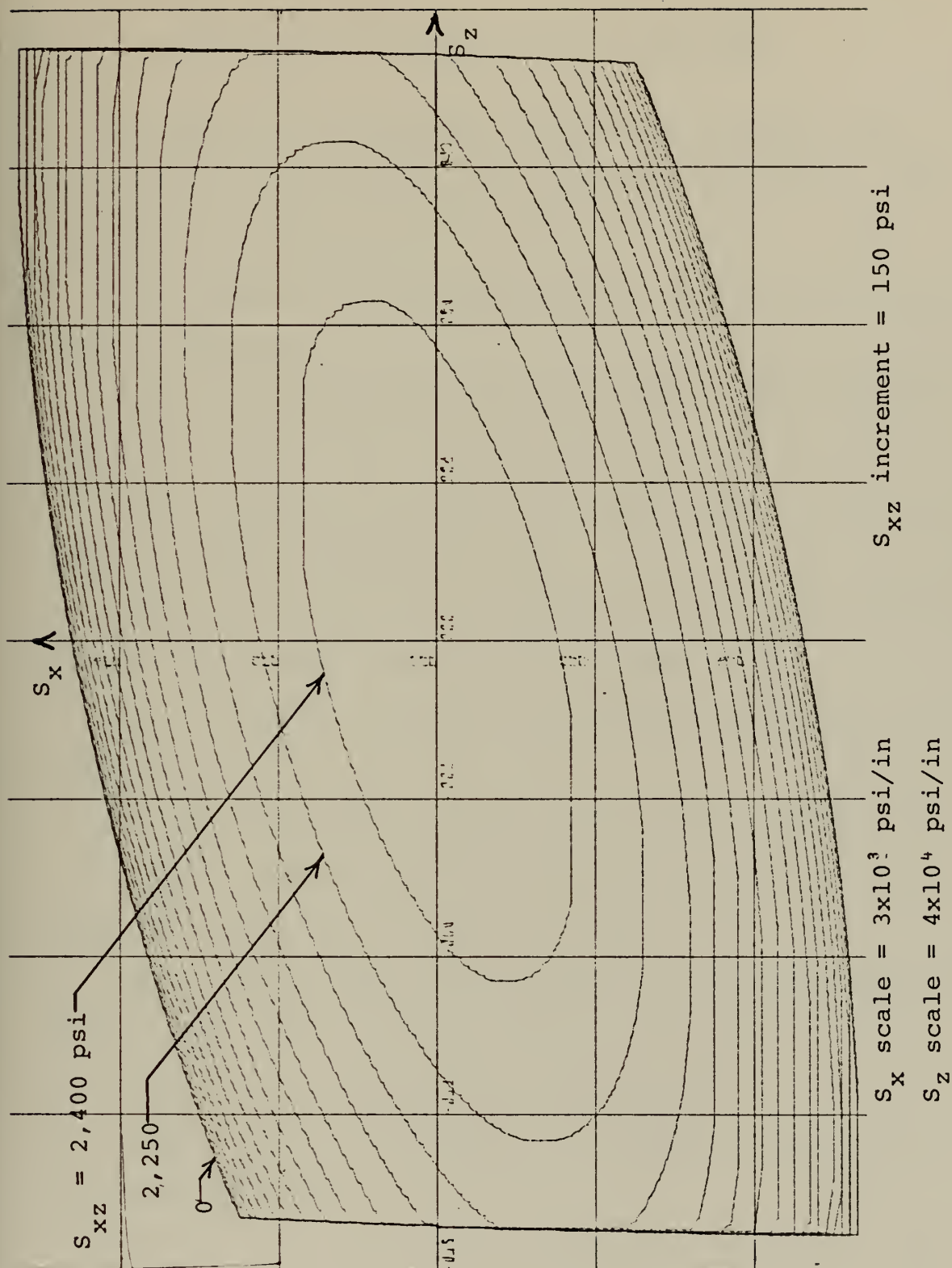


Figure (C-29). THORNEL 40(graphite)/Epoxy, $v_f = .6$

APPENDIX D: PROGRAM OVERLAY STRUCTURE

The overlay root-segment structure is shown in Fig. (D-1) where each rectangle represents a subroutine. The subroutine functions are:

MAIN -Remains in core and controls calling sequence during execution.

BANDEC -Solves banded matrix problems. Used in MAIN1 and MAIN2.

MULI -Multiplies a symmetric banded matrix with a vector. Used in MAIN1 and MAIN2.

MAIN1 -Calculates microstresses and macrostresses for elastic loading of load cases I, II, and III.

DAVES -Computes element stiffness and assembles system stiffness.

CALTAU -Calculates element stresses and strains.

REVGNK - Revises system stiffness to accommodate boundary conditions and applied loads.

MAIN2 - Calculates microstresses and macrostresses for longitudinal shear elastic loading, load case IV.

MAIN3 - Calculates Initial Yield Locus.

MATINV - Matrix inversion with accompanying solution of linear equations.

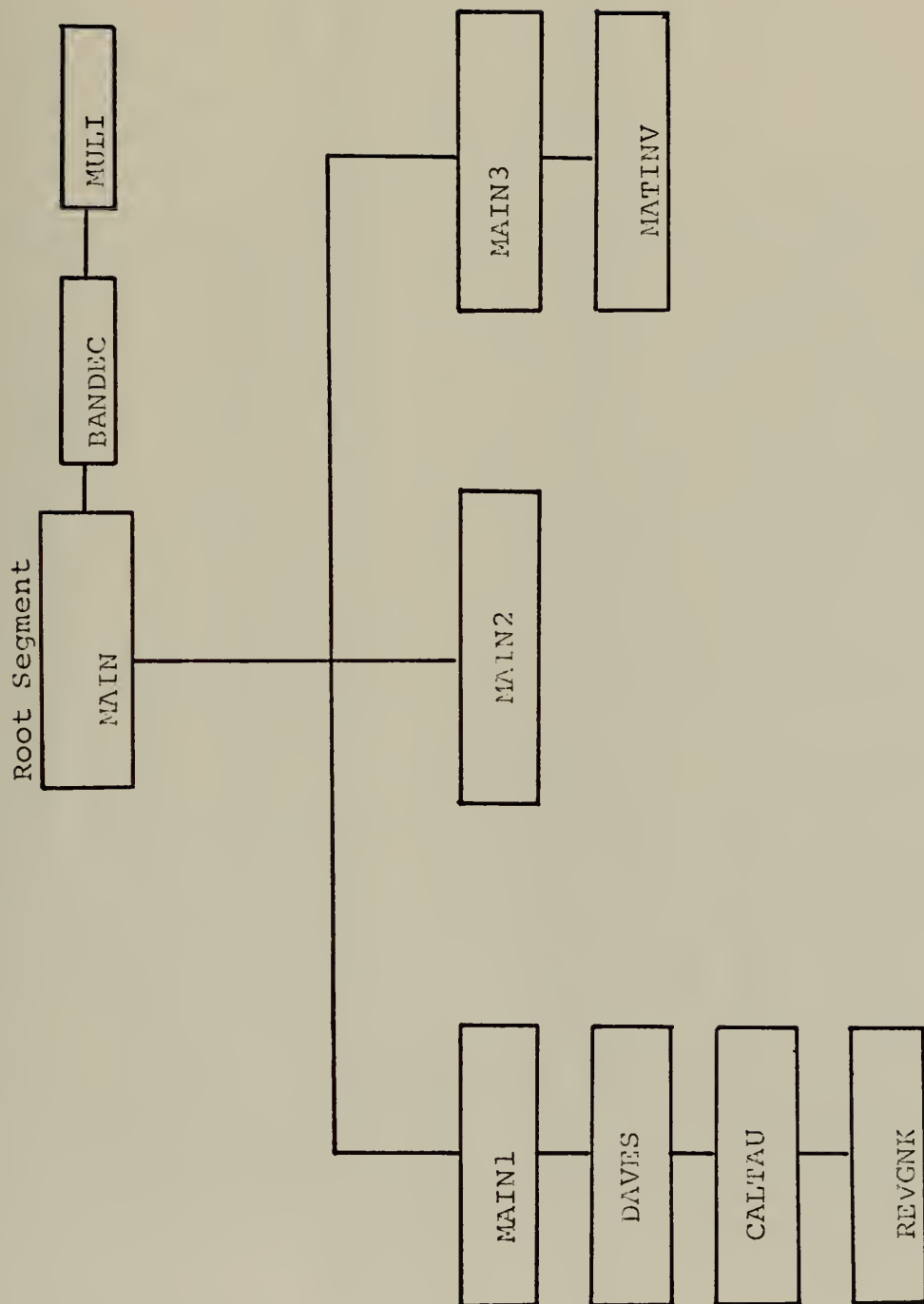


Figure (D-1). Overlay Root-Segment Structure

APPENDIX E: COMPUTER PROGRAM

```

C      ROOT SEGMENT OF OVERLAY
C      ROOT SEGMENT MUST INCLUDE ALL COMMON STATEMENTS
C
COMMON/SPACE/GRANK(498,102)
COMMON/PLACE/P(498),U(498),SXL(498)
COMMON/SLOP/C(4,4,108),POIS(108)
COMMON/LOOP/ZM(9,12,108),A(108)
COMMON/DAV/IR(12)
COMMON/SAL/ZM(9,12),ZK(12,12),ZK(12,12),PH(3,9),XL(12)
COMMON/LINAS/CF(3,3),CM(3,3),CCF(9,9),CCM(9,9),D(9,9)
COMMON/REVP/PV(34),UVC(34),NOLC(34),NUDISP(34),NBDY(64)
COMMON/NEED/TCXX(3,108),TCYY(3,108),TCXY(3,108),TCZZ(3,108),B(3,3)
COMMON/SHEAR/TCXZ(1,108),TCYZ(1,108),AVESXZ(1)
COMMON/DATEA/ITEM(108,6),Y(2,71),X(2,249),T(200),NCP(71)
C
10 CALL MAIN1
CALL MAIN2
CALL MAIN3
GO TO 10
END
C
SUBROUTINE MULI(NUMDF,NBAN,S,F,U)
SUBROUTINE MULI FULL MULTIPLIES A SYMMETRIC BANDED MATRIX WITH A VECTOR
C
DIMENSION S(NUMDF,NBAN),F(NUMDF),U(NUMDF)
DO 120 J=1,NUMDF
F(J)=0
M=MIN0(NBAN,NUMDF+1-J)
DO 105 K=1,M
L=J+K-1
F(J)=F(J)+S(J,K)*U(L)
CONTINUE
IF(J.EQ.1) GO TO 120
L=MIN0(J-1,NBAN-1)+1
DO 110 K=2,L
M=J-K+1
F(J)=F(J)+S(M,K)*U(M)
CONTINUE
110 CONTINUE
120 CONTINUE
RETURN
END
C

```



```

SUBROUTINE BANDEC (NEQ,MAXB,NVEC,A,F,U)
SUBROUTINE BANDEC SOLVES A SYMMETRIC BANDED MATRIX
DIMENSION A(NEQ,MAXB),F(NEQ,1),U(NEQ)
DECOMPOSE-NO PIVOTING.
      LOOP=NEQ-1
      DO 100 I=1,LOOP
CHECK FOR ZERO DIAGONAL ELEMENTS
      IF( ABS(A(I,1))-1.F-30) 1000,1000,10
10      N=I+1
      N=MINO(I+MAXB-1,NEQ)
      DO 100 J=M,N
      L=J+2-M
      D=A(I,L)/A(I,1)
      DO 40 MM=1,NVEC
      F(J,MM)=F(J,MM)-D*A(I,MM)
40      MM=MINO(MAXB-L+1,NEQ-J+1)
      DO 100 K=1,MM
      NN=L+K-1
100      A(J,K)=A(J,K)-D*A(I,NN)
      BACK SUBSTITUTE.
      DO 199 I=1,NVEC
      F(NEQ,I)=F(NEQ,I)/A(NEQ,1)
199      DO 200 I=2,NEQ
      J=NEQ-I+1
      K=MINO(NEQ-J+1,MAXB)
      DO 200 MM=1,NVEC
      DO 190 L=2,K
      M=J+L-1
190      F(J,MM)=F(J,MM)-A(J,L)*F(M,MM)
200      F(J,MM)=F(J,MM)/A(J,1)
      RETURN
1000 WRITE (6,1010) I
      STOP
1010 FORMAT (29H1 ZERO DIAGONAL ELEMENT, ROW I4)
      END

```


SUBROUTINE MAIN1

THIS PROGRAM CALCULATES THE ELEMENT STRESSES DUE TO PROPORTIONAL
LOADING TO THE ELASTIC LIMIT

COMMON/SPACE/GRANK(498,102)
COMMON/PLAC/P(498),UE(498),SXL(498)
COMMON/SLOP/C(4,4,108),POIS(108)
COMMON/LOOP/ZM(9,12,108),A(108)
COMMON/DAVE/IR(12)
COMMON/LINAS/CF(3,3),CM(3,3),CCF(9,9),CCM(9,9),D(9,9)
COMMON/RELIN/PV(34),UVC(34),NUDISP(34),NBDY(64)
COMMON/DATA/ITEM(108,6),Y(2,71),X(2,249),T(200),NCP(71)
COMMON/NEED/TCXX(3,108),TCYY(3,108),TCXY(3,108),TCZZ(3,108),B(3,3)
COMMON/SHEAR/TCXZ(1,108),TCYZ(1,108),AVESXZ(1)

DIMENSION NNX(17),NNY(17)
DIMENSION TAUX(108),TAUY(108),TAUZ(108),TAUXY(108)
DIMENSION SXX(108),SYY(108),SXY(108),SZZ(108)
DIMENSION DELSX(108),DELSY(108),DELSXY(108),DELTZ(108)
DIMENSION DELSX(108),DELSY(108),DELSXY(108),DELSZ(108)
DIMENSION DELX(108),DEY(108),EXY(108)
DIMENSION DELX(108),DELEY(108),DELEY(108),DELSII(108)

LOOP=NUMBER OF LOADING CASES
NUMNP=NUMBER OF NODAL POINTS
NDFNP=NUMBER OF DOF AT EACH NODAL POINT
NUMDF=NUMBER OF DOF
NAL=NUMBER OF APPLIED LOADS
NBOC=NUMBER OF ZERO BOUNDARY CONDITIONS
NUMATE=NUMBER OF NON ZERO BOUNDARY CONDITIONS
NUMATE=NUMBER OF FILAMENT ELEMENTS
UNIFEZ=NUMBER OF LONGITUDINAL STRAIN
NEFPE=NUMBER OF FILAMENT NODAL POINTS
IMNNP=INITIAL MATRIX NODAL POINT
NBPX=NUMBER OF BOUNDARY POINTS ON X FACE
NBPY=NUMBER OF BOUNDARY POINTS ON Y FACE
NTCP=NUMBER OF TRIANGLE CORNERS
NINC=NUMBER OF LOAD INCREMENTS
NPROB=TYPE OF PROBLEM, I, II, III
IPSTP=TYPE OF PLANE PROBLEM, I=LASTIC
POISM=FILAMENT POISSON'S RATIO
NNX(I)=X BOUNDARY POINT (I)

STRAIN AND 2 FOR PLANE STRESS


```

NNY(I) = Y BOUNDARY POINT (I)
NUDISP (I) = NODE NUMBER OF NON ZERO BOUNDARY DISPLACEMENT (I)
NOLQ(I) = NODE NUMBER OF LOAD (I)
UVC(I) = NON ZERO BOUNDARY DISPLACEMENT (I)
PV(I) = LOAD (I)
CONTINUE

```

```

GRANK= SYSTEM STIFFNESS MATRIX
AVETHK= AVERAGE THICKNESS
YF= FILAMENT YIELD STRENGTH
YMC= MATRIX COMPRESSIVE YIELD STRENGTH
YMT= MATRIX TENSILE YIELD STRENGTH
EF= FILAMENT YOUNG'S MODULUS
EM= MATRIX YOUNG'S MODULUS

```

READ IN GRID DATA AND MATERIAL PROPERTIES

```

READ(5,10) NUMEL,NUMNP,NDFNP,NUMDF,NAL,NBC,NUBC,NMATF
WRITE(6,15) NUMEL,NUMNP,NDFNP,NUMDF,NAL,NBC,NUBC,NMATF

```

```

READ(5,10) NFNPN,INMNP,NBPX,NBPY,NTCP,NINC,NPROB,IPS
WRITE(6,10) NFNPN,INMNP,NBPX,NBPY,NTCP,NINC,NPROB,IPS

```

```

READ(5,172) IPR1YP
WRITE(6,172) IPR1YP

```

```

UNIFEZ=1.0

```

```

IF (NPROB.NE.3) UNIFEZ=0.
WRITE(6,73) UNIFEZ

```

```

56 READ(5,20) ((Y(I,J),I=1,2),J=1,NTCP)
WRITE(6,25) (J,Y(1,J),Y(2,J),J=1,NTCP)

```

```

READ(5,30) ((ITEM(I,J),J=1,6),I=1,NUMEL)
WRITE(6,35) (I,T(I),(ITEM(I,J),J=1,6),I=1,NUMEL)

```

```

READ(5,20) POISF,POISM
WRITE(6,20) POISF,POISM

```

```

READ(5,22) AVETHK,YF,YMT,YMC,EF,EM
WRITE(6,23) AVETHK,YF,YMT,YMC,EF,EM

```

CALCULATE COEFFICIENTS FOR STRESS - STRAIN LAW


```

IF (IPS.NE.1) GO TO 2
ZKAPF=1.-POISF
ZKAPM=1.-POISM
ZLAMF=0.5-POISF
ZLAMM=0.5-POISM
ZLRF=EF/(1.+POISF)* (1.-2.*POISF))
ZLRM=EM/(1.+POISM)* (1.-2.*POISM))
2 IF (IPS.NE.2) GO TO 3
ZKAPF=1.
ZKAPM=1.
ZLAMF=(1.-POISF)/2.
ZLAMM=(1.-POISM)/2.
ZLRF=EF/(1.- (POISF**2))
ZLRM=EM/(1.- (POISM**2))
3 CF(1,1)=ZLRF*POISF
CF(1,2)=0.
CF(1,3)=0.
CF(2,1)=CF(1,2)
CF(2,2)=CF(1,1)
CF(2,3)=0.
CF(3,1)=0.
CF(3,2)=0.
CF(3,3)=ZLRF*ZLAMF
CM(1,1)=ZLRM*ZKAPM
CM(1,2)=0.
CM(1,3)=0.
CM(2,1)=CM(1,2)
CM(2,2)=CM(1,1)
CM(2,3)=0.
CM(3,1)=0.
CM(3,2)=0.
CM(3,3)=ZLRM*ZLAMM
C WRITE(6,45) ((CF(I,J),J=1,3),I=1,3)
C WRITE(6,45) ((CM(I,J),J=1,3),I=1,3)
C READ(5,60) (NNX(I),I=1,NBPX)
C READ(5,60) (NNY(I),I=1,NBPY)
C WRITE(6,85) (I,NNX(I),I=1,NBPX)
C WRITE(6,85) (I,NNY(I),I=1,NBPY)
C READ(5,10) (NCP(I),I=1,NTCP)
C WRITE(6,85) (I,NCP(I),I=1,NTCP)

```

FORMAT STATEMENTS

```

10 FORMAT(8I10)
15 FORMAT(1H02X,'NUMBER OF ELEMENTS=',I5//2X,'NUMBER OF NODAL POINTS
1=,I5//2X,'NUMBER OF DOF AT EACH NP=',I5//2X,'NUMBER OF DEGR
2EE3 OF FREEDOM=',I5//2X,'NUMBER OF APPLIED LOADS =',I5//2X,'NUMBER
3 CF BOUNDARY CONDITIONS =',I5//2X,'NUMBER CF NON ZERO DISPLACEMENT
4 BC=',I5//2X,'NUMBER OF FILAMENT ELEMENTS=',I5)
20 FORMAT(2F10.5)
22 FORMAT(8F10.5)
23 FORMAT(5X,F10.5,5E17.8,2F10.5)
25 FORMAT(5X,'CORNER NODAL POINT NO. =',I5,5X,'X(1) COORD. =',F10.5,
15X,'X(2) COORD. =',F10.5)
30 FORMAT(6I10,F10.5)
35 FORMAT(2X,'ELEMENT',I5,2X,'THICKNESS',F10.5,2X,'NP 1 AT',I5,2X,
1'NP 2 AT',I5,2X,'NP 3 AT',I5,2X,'NP 4 AT',I5,2X,'NP 5 AT',I5,2X,
2'NP 6 AT',I5)
45 FORMAT(1H0/(2X,3E20.8))
50 FORMAT(1I10,F10.3)
55 FORMAT(5X,'APPLIED LOAD NO. ',I5,5X,'DEGREE OF FREEDOM ',I5,5X,'L
1OAD =',F10.3)
60 FORMAT(8I10)

```

C

```

65 FORMAT(5X,'BOUNDARY CONDITION NO.',I5,5X,'SUPPRESSED DOF',I5)
70 FORMAT(1I10,F10.5)
75 FORMAT(2I10,F10.5)
73 FORMAT(10X,'THE LONGITUDINAL STRAIN IS ',F10.5)
85 FORMAT(2I10)
172 FORMAT(1I10)
1262 FORMAT(1I10,3E20.8)
11007 FORMAT('1',10X,'THIS IS PROBLEM ',I5)
1282 FORMAT(1H1/(I20,E20.8))
2302 FORMAT(1H05X,'AVESX=',E17.8,10X,'AVESY=',E17.8)
2312 FORMAT('0')
2342 FORMAT(10X,'AVESZ=',E17.8)
3007 FORMAT(10X,'TAUX=',E17.8,8X,'TAUY=',E17.8,8X,
1,'TAUZ=',E17.8,8X,'TALXY=',E17.8)

```

CCCC

CALCULATION OF NBAN

```

NB=1
DO 105 IX=1,NUMEL
J=ITEM(IX,1)
K=ITEM(IX,2)
L=ITEM(IX,3)
JK=IABS(J-K)
KL=IABS(K-L)
LJ=IABS(L-J)
MB=MAXC(JK,KL,LJ)

```



```

C PRINT OUTPUT
C DO 1290 I=1,NUMDF
  UE(I)=P(I)
  CONTINUE
1290 C
      REWIND 1
      READ(1) ((GRANK(I,J),J=1,NBAN),I=1,NUMDF)
      CALL MULI (NUMDF,NBAN,GRANK,P,UE)
C DO 700 I=1,NUMDF
  P(I)=P(I)+$XL(I)*UNIFEZ
  CONTINUE
700 C
      CALCULATE AVERAGE TRACTIONS ON THE SIDES AND FACE OF THE ELEMENTAL BLOCK
C
      NX=NBPX-1
      TOTPX=0.
      DO 2200 I=2,NX
        JJ=NNX(I)
        J=2*(JJ-1)+1
        TOTPX=TOTPX+P(J)
        CONTINUE
      KK=NNX(1)
      K=2*(KK-1)+1
      LL=NNX(NBPX)
      L=2*(LL-1)+1
      TOTPX=(P(L)+P(K))+TOTPX
C
      YLGTH=ABS(X(2,LL)-X(2,KK))
      AVESX=TOTPX/(YLGTH*AVE$THK)
      B(1,INUM)=AVESX
C
      NY=NBPY-1
      TOTPY=0.
      DO 2300 I=2,NY
        JJ=NNY(I)
        J=2*(JJ-1)+2
        TOTPY=TOTPY+P(J)
        CONTINUE
      KK=NNY(1)
      K=2*(KK-1)+2
      LL=NNY(NBPY)
      L=2*(LL-1)+2
      TOTPY=(P(L)+P(K))+TOTPY
      XLGTH=ABS(X(1,LL)-X(1,KK))
      AVESY=TOTPY/(XLGTH*AVE$THK)
2300 C

```



```

C
C
C
B(2, INUM)=AVESY
WRITE(6,2302) AVESX, AVESY
CALCULATE ELEMENT STRESSES AND STRAINS
CALL CALTAU(TAUX, TAU, TAUZ, TAUXY, SXX, SYY, SZZ, SXY, SII, EX, EY, EXY,
1 UNIFEZ, AVTAUZ, NUMEL, NMATF, NUMDF, NL)
WRITE(6,3007) (TAUX(IX), TAU(IX), TAUXY(IX), TAUZ(IX), IX=1, NUMEL)
DO 2311 IX=1, NUMEL
TCXX(INUM, IX)=TAUX(IX)
TCYY(INUM, IX)=TAUY(IX)
TCXY(INUM, IX)=TAUXY(IX)
TCZZ(INUM, IX)=TAUZ(IX)
CONTINUE
2311 WRITE(6,2312)
AA=0.
SUMFZ=0.
DO 2340 IX=1, NUMEL
ZFORCE=TAUZ(IX)*A(IX)
SUMFZ=SUMFZ+ZFORCE
AA=AA+A(IX)
CONTINUE
2340 AVESZ=SUMFZ/AA
B(3, INUM)=AVESZ
WRITE(6,2342) AVESZ
CONTINUE
2350
C
C
RETURN
END
SUBROUTINE DAVES( POISF, POISM, NUMDF, NBAN, NTCP, NUMEL, NMATF )
C THIS SUBROUTINE CALCULATES ELEMENT STIFFNESS MATRICES AND LOAD VECTORS
C AND ASSEMBLES THEM INTO THE SYSTEM STIFFNESS MATRIX AND LOAD VECTOR
C
COMMON/SPACE/GRANK(498,102)
COMMON/PLAC/P(498),UE(498),SXL(498)
COMMON/SLOP/C(4,4,108),POIS(108)
COMMON/LOOP/ZM(9,12,108),A(108)
COMMON/DAV/IR(12)
COMMON/SAL/ZN(9,12),ZZK(12,12),ZK(12,12),PH(3,9),XL(12)
COMMON/LINAS/CF(3,3),CM(3,3),CCF(9,9),CCM(9,9),D(9,9)
COMMON/DATA/ITM(108,6),Y(2,71),X(2,249),T(200),NCP(71)
C

```



```

150 CCF(II,III)=2.*CCF(II,III)
    C CONTINUE
    WRITE(6,152) ((CCF(I,J),J=1,9),I=1,9)
    WRITE(6,152) ((CCM(I,J),J=1,9),I=1,9)
    C C C C C C C C C C
    GRANK IS THE SYSTEM STIFFNESS MATRIX
    ZERO OUT THE GRANK MATRIX
    ZERO OUT SXL MATRIX
160 DO 170 I=1,NUMDF
    SXL(I)=0.
    DO 170 J=1,NBAN
    GRANK(I,J)=0.
170 CONTINUE

```

TABLE FOR REARRANGEMENT OF ELEMENT STIFFNESS MATRIX

```

IR(1)=1
IR(2)=7
IR(3)=2
IR(4)=8
IR(5)=3
IR(6)=9
IR(7)=4
IR(8)=10
IR(9)=5
IR(10)=11
IR(11)=6
IP(12)=12

```

OBTAIN COORDINATES OF TRIANGLE CORNER POINTS

```

DO 180 I=1,NTCP
  J=NCP(I)
  X(1,J)=Y(1,I)
  X(2,J)=Y(2,I)
  WRITE(6,90) J,X(1,J),X(2,J)
180 CONTINUE

```

```

  NBAN=0

```

DO LOOP FOR ELASTIC ELEMENT STIFFNESS MATRICES

```

C TRIANGLE DO LOOP FOR ELASTIC ELEMENT STIFFNESS MATRICES
C C C C C C C C C C

```



```

C
C
C
DO 1000 IX=1,NUMEL
  FORM C AND POIS MATRICES
  IF(IX.GT.NMATF) GO TO 1550
  POIS(IX)=POISF
  DO 1540 II=1,3
  DO 1540 JJ=1,3
  C(II,JJ,IX)=CF(II,JJ)
  1540 CONTINUE
  GO TO 1570
  1550 POIS(IX)=POISM
  DO 1560 II=1,3
  DO 1560 JJ=1,3
  C(II,JJ,IX)=CM(II,JJ)
  1560 CONTINUE
  1570 CONTINUE
  C(1,4,IX)=C(1,2,IX)
  C(2,4,IX)=C(1,2,IX)
  C(3,4,IX)=C(2,3,IX)
  C(4,4,IX)=C(1,1,IX)
C
C
C
  FORM 9X9 D MATRIX
  IF(IX.GT.NMATF) GO TO 250
  DO 240 I=1,9
  DO 240 J=1,9
  D(I,J)=CCF(I,J)
  D(J,I)=CCF(I,J)
  240 CONTINUE
  GO TO 270
  250 DO 260 I=1,9
  DO 260 J=1,9
  D(I,J)=CCM(I,J)
  D(J,I)=CCM(I,J)
  260 CONTINUE
  270 CONTINUE
C
C
C
  COMPUTE GEOMETRIC QUANTITIES
  JJ=ITEM(IX,1)
  KK=ITEM(IX,2)
  LL=ITEM(IX,3)
  A1=X(1,LL)-X(1,KK)
  A2=X(1,JJ)-X(1,LL)
  A3=X(1,KK)-X(1,JJ)
C

```



```

B1=X(2, KK)-X(2, LL)
B2=X(2, LL)-X(2, JJ)
B3=X(2, JJ)-X(2, KK)

```

```

A(IX)=(A3*B2-A2*B3)/2.

```

```

FORM THE 12X12 ELEMENT STIFFNESS MATRIX, SAY ZK

```

```

FORM THE 9X12 ZN MATRIX

```

```

DO 350 I=1,9
DO 350 J=1,12
ZN(I,J)=0.
CONTINUE
ZN(1,1)=3.*B1
ZN(1,2)=-B2
ZN(1,3)=-B3
ZN(1,4)=4.*B2
ZN(1,6)=4.*B3
ZN(2,1)=-B1
ZN(2,2)=3.*B2
ZN(2,3)=-B3
ZN(2,4)=4.*B1
ZN(2,5)=4.*B3
ZN(3,1)=-B1
ZN(3,2)=-B2
ZN(3,3)=3.*B2
ZN(3,5)=4.*B2
ZN(3,6)=4.*B1
ZN(4,7)=3.*A1
ZN(4,8)=-A2
ZN(4,9)=-A3
ZN(4,10)=4.*A2
ZN(4,12)=4.*A3
ZN(5,7)=-A1
ZN(5,8)=3.*A2
ZN(5,9)=-A3
ZN(5,10)=4.*A1
ZN(5,11)=4.*A3
ZN(6,7)=-A1
ZN(6,8)=-A2
ZN(6,9)=3.*A3
ZN(6,11)=4.*A2
ZN(6,12)=4.*A1
DO 360 I=1,3
II=I+3

```

```

350

```

```

C
C
C
C
C
C
C

```



```

III=I+6
DO 360 J=1,6
JJ=J+6
ZN(III,J)=ZN(II,JJ)
ZN(III,JJ)=ZN(I,J)
360 CONTINUE
CC

DO 380 I=1,9
DO 380 J=1,12
ZM(I,J,IX)=ZN(I,J)
380 CONTINUE
CC

DO 400 I=1,12
DO 400 J=1,12
ZZK(I,J)=0.
DO 390 K=1,9
DO 390 L=1,9
ZZK(I,J)=ZZK(I,J)+ZN(K,I)*D(K,L)*ZN(L,J)
390 CONTINUE
ZZK(I,J)=T(IX)*ZZK(I,J)/(48.*A(IX))
400 CONTINUE
CC

REARRANGE THE ELEMENT STIFFNESS MATRIX
CC

DO 500 I=1,12
II=IR(I)
DO 500 J=1,12
JJ=IR(J)
ZZK(I,J)=ZZK(II,JJ)
500 CONTINUE
CC

FORM XL MATRIX
ZN NOW DUMMY
CC

DO 650 J=1,12
JJ=IR(J)
DO 600 I=1,3
ZN(I,J)=0.0
DO 600 K=1,9
ZN(I,J)=PH(I,K)*ZM(K,JJ,IX)+ZN(I,J)
600 CONTINUE
XL(J)=C(1,4,IX)*ZN(1,J)+C(2,4,IX)*ZN(2,J)+C(3,4,IX)*ZN(3,J)
1 XL(J)=T(IX)*XL(J)/6.0
650 CONTINUE

```


ASSEMBLY OF SYSTEM SXL MATRIX

$$\begin{aligned} DC &= 900 & J &= 1,6 \\ JJ &= 2 \cdot (J-1) + 1 \\ JJJ &= JJ + 1 \\ KKK &= I \cdot M(I, J) \\ LKK &= 2 \cdot (K-1) + 1 \\ LLL &= KKK + 1 \\ SXL(KKK) &= XL(JJ) \\ SXL(LLL) &= XL(JJJ) \end{aligned}$$

900 CONTENTS

ASSEMBLY OF THE SYSTEM GRANK MATRIX

```

DO 895 J=1,6
  II=2*(I-1)/M+(I-X,J)-1
DO 890 K=1,6
  II=2*(I-1)/M+(I-X,K)-1
  IF(II.GT.II) GO TO 890
  II=II-I
DO 800 L=1,2
  JJ=II+L
  LL=2*(J-1)+L
  MM=1
  IF(II.EQ.O) M=L
DO 800 N=M,2
  MM=2*(K-1)+N
  KK=II+N-L+1
  IF(KK.GT.NBAN) NBAN=KK
  GRANK(JJ,KK)=ZK(LL,MM)

```

CONTINUED

CONTINUE

```

WRITE(6,55) (I,XL(I),I=1,NUMDF)
FORMAT(5X,'SYSTEM NODAL POINT NO. =',I5,5X,'X(1) COORD. =',F10.5,
15X,'X(2) COORD. =',F10.5)
152 FORMAT(9E13.5)
RETURN
END

```



```

U(I)=UE(JB)
V(I)=VE(JC)
1300 CONTINUE
C
C CALCULATE STRAINS AT TRIANGLE CORNERS
C
DO 1320 I=1,3
  II=I+3
  III=I+6
  EXC(I)=0.
  EYC(I)=0.
  DO 1310 J=1,6
    JJ=J+6
    EXC(I)=EXC(I)+ZM(II,J,IX)*U(J)
    EYC(I)=EYC(I)+ZM(III,J,IX)*V(J)
1310 CONTINUE
  EXC(I)=EXC(I)/(2.*A(IX))
  EYC(I)=EYC(I)/(2.*A(IX))
1320 CONTINUE
C
C CALCULATE CENTROIDAL STRAINS
C
EX(IX)=(EXC(1)+EYC(2)+EXC(3))/3.
EY(IX)=(EYC(1)+EYC(2)+EYC(3))/3.
EXY(IX)=(EXYC(1)+EXYC(2)+EXYC(3))/3.
WRITE(6,1322) (EXC(I),I=1,3),EX(IX)
WRITE(6,1323) (EYC(I),I=1,3),EY(IX)
WRITE(6,1324) (EXYC(I),I=1,3),EXY(IX)
1330 CONTINUE
C
C CALCULATE CENTROIDAL STRESSES
C
C
C
TAUX(IX)=C(1,1,IX)*EX(IX)+C(1,2,IX)*EY(IX)
1 +C(1,3,IX)*EXY(IX)+C(1,4,IX)*UNIFZ
1 TAUZ(IX)=C(1,2,IX)*EX(IX)+C(2,2,IX)*EY(IX)
1 +C(2,3,IX)*EXY(IX)+C(2,4,IX)*UNIFZ
1 TAUZY(IX)=C(1,3,IX)*EX(IX)+C(2,3,IX)*EY(IX)
1 +C(3,3,IX)*EXY(IX)+C(3,4,IX)*UNIFZ
1 TAUZ(IX)=C(1,4,IX)*EX(IX)+C(2,4,IX)*EY(IX)
1 +C(3,4,IX)*EXY(IX)+C(4,4,IX)*UNIFZ
1 TAUZ=TAUZ(IX)*A(IX)
TOTFZ=TOTFZ+FZ
C

```



```

1180 CONTINUE
    GRANK(JJ,1)=1.
    P(JJ)=0.
1190 CONTINUE
    C REVERSE GRANK TO ACCOMMODATE NON ZERO DISPLACEMENT B.C.'S
    C
    IF (NUBC.EQ.0) GO TO 1280
    DO 1260 I=1,NUBC
    JJ=NUDISP(I)
    JJ=JJ-NBAN+1
    IF (JJ.GT.1) GO TO 1200
    JJ=1
    DO 1210 J=JJ,JJ
    K=JJ-J+1
    P(J)=P(J)-GRANK(J,K)*UVC(I)
    CONTINUE
    KK=JJ+1
    KKK=JJ+NBAN-1
    IF (KKK.GE.NUMDF) KKK=NUMDF
    IF (KK.GT.KKK) GO TO 1235
    DO 1230 J=KK,KKK
    JJ=J-JJ+1
    P(J)=P(J)-GRANK(JJ,JJ)*UVC(I)
    CONTINUE
    C
    DO 1240 M=1,NBAN
    KK=JJ-M+1
    GRANK(JJ,M)=0.
    IF (KK.LT.1) GO TO 1240
    GRANK(KK,M)=0.
    CONTINUE
    C
    GRANK(JJ,1)=1.
    P(JJ)=UVC(I)
    CONTINUE
    C
    1280 CONTINUE
    RETURN
    C
    END
    C

```


SUBROUTINE MAIN2

THIS PROGRAM DOES THE SHEAR PROBLEMS IV AND V

```
COMMON/ SHEAR/ ICXZ(1,108),TCYZ(1,108),AVESXZ(1)
COMMON/ DATA/ ITEM(108,6),Y(2,71),X(2,249),T(200),NCP(71)
COMMON/ SPAC/ GRANK(498,102)
DIMENSION ZETA(3,3),G(200),ZX(108,3,6),WK(6,6),UBC(34),
1 UVC(34),PV(34),P(249),UF(249),A(108),SRANK(249,51),STRN31(3),
2 STRN32(3),ZY(108,3,6),TAU31(108),NDO(64),NBDY(64),NUDISP(64),
3 IELBX(20),IELBY(20),TAU32(108),ZETA(1,1),GRANK(10,1),G(1),
EQUIVALENCE IELBX(1,1),ZETA(1,1),GRANK(162,5),WK(1),GRANK(168,5),
1 GRANK(210,1),ZX(1,1),GRANK(162,5),WK(1),GRANK(168,5),
2 ZK(1,1),GRANK(204,5),UBC(1),GRANK(238,5),UVC(1),
3 GRANK(272,5),UF(1),GRANK(306,6),A(1),GRANK(414,6),
4 GRANK(1,1),GRANK(165,32),STRN31(1),GRANK(168,32),
5 STRN32(1),GRANK(171,32),ZY(1,1,1),GRANK(123,36),TAU31(1),
6 GRANK(231,36),NCLC(1),GRANK(265,36),NBDY(1),GRANK(329,36),
7 NUDISP(1),GRANK(393,36),IELBX(1),GRANK(413,36),IELBY(1),
8 GRANK(433,36),TAU32(1)
```

```
NELBX= NUMBER OF ELEMENTS ON X BOUNDARY
NELBY= NUMBER OF ELEMENTS ON Y BOUNDARY
IELRX(I)= X BOUNDARY ELEMENT (I)
IELBY(I)= Y BOUNDARY ELEMENT (I)
```

```
1 READ(5,10) NUMEL,NUMNP,NBAN,NUMDF,NAL,NBC,NUBC,NMATF
WRITE(6,15) NUMEL,NUMNP,NBAN,NUMDF,NAL,NBC,NUBC,NMATF
```

```
READ(5,40) NFNP,INMNP,NDFNP,NTCP,NELBX,NELBY
WRITE(6,40) NFNP,INMNP,NDFNP,NTCP,NELBX,NELBY
READ(5,60) IELBX(1),I=1,NELBX)
READ(5,60) IELBY(1),I=1,NELBY)
WRITE(6,55) (I,IELBX(I),I=1,NELBX)
WRITE(6,95) (I,IELBY(I),I=1,NELBY)
```

```
READ(5,80) GF,GM
WRITE(6,82) GF,GM
```



```

C
      IF(NAL.EQ.0) GO TO 5
      READ (5,50) (NOLO(I),PV(I),I=1,NAL)
      WRITE (6,55) (I,NOLO(I),PV(I),I=1,NAL)

      5 READ (5,60) (NRDY(I),I=1,NBC)
      WRITE (6,65) (I,NRDY(I),I=1,NBC)
      IF(NUBC.EQ.0) GO TO 100
      READ(5,70) (NUDISP(I),UVC(I),I=1,NUBC)
      WRITE(6,75) (I,NUDISP(I),UVC(I),I=1,NUBC)

      100 CONTINUE

C
C
C
C
      FORMAT STATEMENTS
C
      10 FORMAT(8I10)
      15 FORMAT(2X,'NUMBER OF ELEMENTS =',I5//2X,'NUMBER OF NODAL POINTS =',
        1,I5//2X,'NUMBER OF DOF AT EACH NP =',I5//2X,'NUMBER OF DEGR
        2EES OF FREEDOM =',I5//2X,'NUMBER OF APPLIED LCADS =',I5//2X,'NUMBER
        3 OF BOUNDARY CONDITIONS =',I5//2X,'NUMBER OF NON ZERO DISPLACEMENT
        4 BC =',I5//2X,'NUMBER OF FILAMENT ELEMENTS =',I5)
      40 FORMAT(6I10)
      50 FORMAT(1I10,F10.1)
      55 FORMAT(5X,'APPLIED LOAD NO. ',I5,5X,'DEGREE OF FREEDOM ',I5,5X,'L
        1OAD =',F10.1)
      60 FORMAT(8I10)
      65 FORMAT(5X,'BOUNDARY CONDITION NO. ',I5,5X,'SUPPRESSED DOF',I5)
      70 FORMAT(1I10,F10.5)
      75 FORMAT(2E10.4)
      80 FORMAT(2E20.8)
      82 FORMAT(5X,'SYSTEM NODAL POINT NO. =',I5,5X,'X(1) COORD. =',F10.5,
        15X,'X(2) COORD. =',F10.5)
      95 FORMAT(2I10)
      172 FORMAT(1I10)
      1262 FORMAT(1I10,D20.8)
      1282 FORMAT(1H1/(I20,D20.8))
      1352 FORMAT(5X,'ENERGY =',F20.8)
      1602 FORMAT(1I10,4E20.8)
      3002 FORMAT(5X,'AVERAGE SXZ =',E20.8)

      CALCULATION OF NBAN

      NB=1
      DO 105 IX=1,NUMEL
      J=ITEM(IX,1)
      K=ITEM(IX,2)
      L=ITEM(IX,3)

```



```

JK=IABS(J-K)
KL=IABS(K-L)
LJ=IABS(L-J)
MB=MAXO(JK,KL,LJ)
IF(MB.GT.NB) NB=MB
CONTINUE
105 NBAN=NDFNP(NB+1)
WRITE(6,172) NBAN

```

CCCC

ZERO OUT THE GRANK MATRIX

```

160 DO 170 I=1,NUMDF
DO 170 J=1,NBAN
SRANK(I,J)=0.
170 CONTINUE

```

CCCCC

OBTAIN COORDINATES CF TRIANGLE CORNER POINTS

```

DO 180 I=1,NTCP
J=NCP(I)
X(1,J)=Y(1,I)
X(2,J)=Y(2,I)
WRITE(6,90) J,X(1,J),X(2,J)
180 CONTINUE

```

C

NBAN=0

C

TR IANGLE DO LOOP FOR ELASTIC ELEMENT STIFFNESS MATRICES

```

ZETA(1,1)=2.
ZETA(1,2)=1.
ZETA(1,3)=1.
ZETA(2,1)=1.
ZETA(2,2)=2.
ZETA(2,3)=1.
ZETA(3,1)=1.
ZETA(3,2)=1.
ZETA(3,3)=2.

```

CC

```

DO 1000 IX=1,NUMEL
WRITE(6,172) IX

```



```

C      G(IX)=GF
C      IF(IX.GT.NMATF) G(IX)=GM
C      COMPUTE GEOMETRIC QUANTITIES
C
C      JJ=ITEM(IX,1)
C      KK=ITEM(IX,2)
C      LL=ITEM(IX,3)
C
C      A1=X(1,LL)-X(1,KK)
C      A2=X(1,JJ)-X(1,LL)
C      A3=X(1,KK)-X(1,JJ)
C      B1=X(2,KK)-X(2,LL)
C      B2=X(2,LL)-X(2,JJ)
C      B3=X(2,JJ)-X(2,KK)
C
C      A(IX)=(A3*B2-A2*B3)/2.
C
C      FORM THE 6X6 ELEMENT STIFFNESS MATRIX, SAY ZK

```

```

350      DO 350 I=1,3
350      DO 350 J=1,6
350      ZY(IX,I,J)=0.
350      CCNT=NUM
350      ZX(IX,1,1)=3.*B1
350      ZX(IX,1,2)=-B2
350      ZX(IX,1,3)=-B3
350      ZX(IX,1,4)=4.*B2
350      ZX(IX,1,6)=4.*B3
350      ZX(IX,2,1)=-B1
350      ZX(IX,2,2)=3.*B2
350      ZX(IX,2,3)=-B3
350      ZX(IX,2,4)=4.*B1
350      ZX(IX,2,5)=4.*B3
350      ZX(IX,3,1)=-B2
350      ZX(IX,3,2)=-B1
350      ZX(IX,3,3)=3.*B3
350      ZX(IX,3,5)=4.*B2
350      ZX(IX,3,6)=4.*B1
350      ZY(IX,1,1)=3.*A1
350      ZY(IX,1,2)=-A2
350      ZY(IX,1,3)=-A3

```


1202 FORMAT(2I10,F10.5)

C

C INPUT THE APPLIED LOAD VECTOR

C

1050 DO 1100 I=1,NUMDF

1100 P(I)=0.

IF(NAL.EQ.0) GO TO 1160

DO 1150 I=1,NAL

JJ=NOLQ(I)

P(JJ)=PV(I)

1150 CONTINUE

C REVISE GRANK TO ACCOMODATE BOUNDARY CONDITIONS

C

1160 DO 1190 I=1,NBC

JJ=NBDY(I)

DO 1180 J=2,NBAN

KK=JJ-J+1

SRANK(JJ,J)=0.

IF(KK.LT.1) GO TO 1180

SRANK(KK,J)=0.

1180 CONTINUE

SRANK(JJ,1)=1.

P(JJ)=0.

1150 CONTINUE

C REVISE GRANK TO ACCOMODATE NON ZERO DISPLACEMENT B.C.'S

C

IF(NUBC.EQ.0) GO TO 1280

DO 1260 I=1,NUBC

UBC(I)=UVC(I)

JJ=NUDISP(I)

JJJ=JJ-NBAN+1

IF(JJJ.GT.1) GO TO 1200

JJJ=1

DO 1210 J=JJJ,JJ

K=JJ-J+1

P(JJ)=P(JJ)-SRANK(J,K)*UBC(I)

CONTINUE

KK=JJ+1

KKK=JJ+NBAN-1

IF(KKK.LT.NUMDF) GO TO 1220

KKK=NUMDF

1220 IF(KK.GT.KKK) GO TO 1235

DO 1230 J=KK,KKK

JJJ=J-JJ+1

P(JJ)=P(JJ)-SRANK(JJ,JJJ)*UBC(I)


```

1230 CONTINUE
1235 CONTINUE
C
DO 1240 M=1,NBAN
KK=JJ-M+1
SRANK(JJ,M)=C.
IF(KK.LT.1) GO TO 1240
SRANK(KK,M)=0.
CONTINUE
1240
C
SRANK(JJ,1)=1.
P(JJ)=UBC(I)
CONTINUE
1260
1280 CONTINUE
C
C *****
C SOLUTION OF THE DISPLACEMENT-FORCE EQUATION FOR DISPLACEMENT
C *****
CALL BANDEC (NUMDF,NBAN,1,SRANK,P,UE)
C *****
C PRINT OUTPUT
WRITE (6,1282) (I,P(I), I=1,NUMDF)
DO 1290 I=1,NUMDF
UE(I)=P(I)
CONTINUE
1290
C
DO 1295 I=1,NUMDF
P(I)=0.
CONTINUE
1295
C
CALL MULI (NUMDF,NBAN,SRANK,P,UE)
WRITE(6,1282) (I,P(I),I=1,NUMDF)
C
C CALCULATE THE ENERGY E= F*U
E=0.
DO 1350 I=1,NUMDF
E=E+P(I)*UE(I)
CONTINUE
1350
WRITE(6,1352) E
C
C CALCULATION OF CENTROIDAL SHEAR STRAINS AND STRESSES
C

```



```

C
DO 1600 IX=1, NUMEL
  II=ITEM(IX,1)
  JJ=ITEM(IX,2)
  KK=ITEM(IX,3)
  LL=ITEM(IX,4)
  MM=ITEM(IX,5)
  NN=ITEM(IX,6)

  W(1)=U(II)
  W(2)=U(JJ)
  W(3)=U(KK)
  W(4)=U(LL)
  W(5)=U(MM)
  W(6)=U(NN)

C
DO 1450 I=1,3
  STRN31(I)=0.
  STRN32(I)=0.
DO 1400 J=1,6
  STRN31(I)=STRN31(I)+ZX(IX,I,J)*W(J)
  STRN32(I)=STRN32(I)+ZY(IX,I,J)*W(J)
CONTINUE
1400
  STRN31(I)=STRN31(I)/(4.*A(IX))
  STRN32(I)=STRN32(I)/(4.*A(IX))
CONTINUE
1450
  STN31C=(STRN31(1)+STRN31(2)+STRN31(3))/3.
  STN32C=(STRN32(1)+STRN32(2)+STRN32(3))/3.
  TAU31(IX)=2.*G(IX)*STN31C
  TAU32(IX)=2.*G(IX)*STN32C
  TCXZ(1,IX)=TAU31(IX)
  TCYZ(1,IX)=TAU32(IX)

C
  WRITE(6,1602) IX,STN31C,STN32C,TAU31(IX),TAU32(IX)

C
1600 CONTINUE
C
  CALCULATE THE AVERAGE SXZ
C
  SXZ=0.
DO 3000 I=1,NELBX
  II=IELBX(I)
  SXZ=SXZ+TAU31(II)
CONTINUE
3000
  AVESXZ(1)=SXZ/NELBX
  WRITE(6,3002) AVESXZ(1)
C
END

```



```

SUBROUTINE MAIN3
      CALCULATION OF YIELD LOCUS
      COMMON/NEED/TCXX(3,108),TCYY(3,108),TCZZ(3,108),B(3,3)
      COMMON/SPACE/GRANK(498,102)
      DIMENSION IPIVOT(3),INDEX(3,2),NNX(20),PIVOT(3),IDYL(100)
      DIMENSION S(3,3),A(4,3),AZ(108,6.4),SZPC(108),SZMC(108),SZ(20)
      DIMENSION X(250),Y(250),XA(99),YA(99),SZCMAX(108),SZCMIN(108)
      DIMENSION TXX(108),TTY(108),TZX(108),TZY(108),TYZ(108)
      EQUIVALENCE (GRANK(1,1),IPIVOT(1)),(GRANK(4,1),INDEX(1,1)),
      1(GRANK(10,1),NNX(1)),(GRANK(30,1),PIVOT(1)),(GRANK(33,1),
      2IDYL(1)),(GRANK(133,1),S(1,1)),(GRANK(142,1),A(1,1)),
      3(GRANK(154,1),
      4AE(1,1,1)),(GRANK(256,6),SZPC(1)),(GRANK(364,6),SZMC(1)),
      5(GRANK(472,6),SZ(1)),
      6(GRANK(394,7),
      7SZCMAX(1)),(GRANK(4,8),SZCMIN(1)),(GRANK(112,8),TXX(1)),
      8(GRANK(220,8),TTY(1)),(GRANK(328,8),TZX(1)),(GRANK(436,8),
      9TZY(1)),(GRANK(46,9),TZY(1)),(GRANK(154,9),TYZ(1)),(GRANK(263,9),
      10IX(1)),(GRANK(15,10),Y(1)),(GRANK(265,10),XA(1)),(GRANK(364,10),
      2YA(1))
      REAL LABEL,'',//
      REAL*8 TITLE(12),'W.A. ERICSON, BOX E, THESIS',//
      1 INITIAL YIELD SURFACE
      FORMAT STATEMENTS
      108 FORMAT (3X,14.5X,'T11C=',E17.8,5X,'T22C=',E17.8,5X,'T12C=',E17.8,
      110 15X,'T33C=',E17.8)
      115 FORMAT (3E20.8)
      125 FORMAT (2E20.8)
      126 FORMAT (2E10.2)
      130 FORMAT (4E10)
      135 FORMAT (2E20.8)
      140 FORMAT (2X,'SZMAX=',E17.8,5X,'SZMIN=',E17.8)
      145 FORMAT (6E10)
      150 FORMAT (5X,3E20.8)
      157 FORMAT (5X,14.5X,'T13C=',E17.8,5X,'T23C=',E17.8)
      165 FORMAT (8E10)
      175 FORMAT (5X,6E17.8)

```



```

180 FORMAT(2I20)
185 FORMAT(6F10.5)
190 FORMAT(//2X,'SX=',E17.8,5X,'SXZ=',E17.8)
195 FORMAT(1H1///5X,'THIS IS LOOP ',I5)
1842 FORMAT(10X,I10,2E20.8)
2010 FORMAT(5X,'END OF INITIAL YIELD')
      LOOP=NUMBER OF PROBLEMS
      YCM= FILAMENT YIELD STRENGTH
      XSC= X SCALING
      YSI= Y SCALING
      YS2= MAX VALUE OF SX
      SXI= INITIAL VALUE OF SX
      SXZI= INITIAL VALUE OF SXZ
      DELSX= NUMBER OF SX INCREMENTS
      DELSXZ= NUMBER OF SXZ INCREMENTS

```

```

1 READ(5,130) LOOP
  WRITE(6,130) LOOP

```

```

  READ(5,125) YOF,YOM
  WRITE(6,135) YOF,YOM
  ZJ2F=(YOF**2)/3.
  ZJ2M=(YOM**2)/3.

```

```

  READ(5,126) XSC,YSC
  WRITE(6,126) XSC,YSC
  READ(5,145) NFNP,INMNP,NUMNP,NBPX,NUMEL,NMATF
  WRITE(6,145) NFNP,INMNP,NUMNP,NBPX,NUMEL,NMATF

```

```

  READ(5,165) (NNX(I),I=1,NBPX)
  WRITE(6,165) (NNX(I),I=1,NBPX)

```

PROBLEM I RESULTS

```

  WRITE(6,108) (IX,TCXX(1,IX),TCYY(1,IX),TCXY(1,IX),TCZZ(1,IX),
    1 IX=1,NUMEL)
  WRITE(6,110) B(1,1),B(2,1),B(3,1)

```

PROBLEM II RESULTS


```

WRITE(6,108) (IX,TCXX(2,IX),TCYY(2,IX),TCXY(2,IX),TCZZ(2,IX),
1IX=1,NUMEL)
B(1,2)=B(2,1)
B(2,2)=B(1,1)
B(3,2)=B(3,1)
WRITE(6,110) B(1,2),B(2,2),B(3,2)

```

PROBLEM III RESULTS

```

WRITE(6,108) (IX,TCXX(3,IX),TCYY(3,IX),TCXY(3,IX),TCZZ(3,IX),
1IX=1,NUMEL)
55 WRITE(6,110) B(1,3),B(2,3),B(3,3)

```

XZ SHEAR PROBLEM RESULTS

XZ SHEAR PROBLEM RESULTS

```

WRITE(6,157) (IX,TCXZ(1,IX),TCYZ(1,IX),IX=1,NUMEL)

```

CALCULATE AVERAGE SXZ

```

75 WRITE(6,120) AVESXZ(1)

```

SOLUTION FOR SUPERPCSION OF PROBLEMS I, II, AND III

```

DO 690 I=1,3
DO 690 J=1,3
S(I,J)=0.
690 CONTINUE
DO 700 I=1,3
S(I,I)=1.
700 CCNTINUE

```

OBTAIN THE B INVERSE MATRIX

```

CALL MATINV(B,3,S,3,3,IPIVOT,INDEX,PIVOT,DETERM)
WRITE(6,150) ((B(I,J),J=1,3),I=1,3)

```



```

C
C
C
C
C      CALCULATION OF YIELD LOCUS
      DO 2000 NL=1,LOOP
      WRITE(6,195) NL
      READ(5,185) YS1,YS2,SXI,SXZI,DELSX,DELSXZ
      WRITE(6,175) YS1,YS2,SXI,SXZI,DELSX,DELSXZ
      INCR2=YS2/DELSXZ
      INCR1=YS1/DELSX
      WRITE(6,130) INCR1
      WRITE(6,130) INCR2
C
C      CALCULATE YIELD LOCUS FOR CENTROIDAL POINTS
      MC=1
      DO 1990 NK=1,INCR2
      DK=NK-1
      SXZ=SXZI+DELSXZ*DK
      L=0
      DO 1980 NJ=1,INCR1
      DJ=NJ-1
      SX=SXI+DELSX*DJ
      WRITE(6,190) SX,SXZ
C
      DO 1740 IX=1,NUMEL
      TXZ(IX)=0.
      TYZ(IX)=0.
C
C      CALCULATION OF INFLUENCE COEFFICIENTS A(I,J)
C
C
C      ZJ2=ZJ2F
      IF(IX.GT.NMATF) ZJ2=ZJ2M
C
      DO 1710 I=1,4
      DO 1710 J=1,3
      A(I,J)=0.
      1710 CONTINUE
      DO 1720 J=1,3
      DO 1720 K=1,3
      A(1,J)=A(1,J)+TCXX(K,IX)*B(K,J)
      A(2,J)=A(2,J)+TCYY(K,IX)*B(K,J)
      A(3,J)=A(3,J)+TCXY(K,IX)*B(K,J)
      A(4,J)=A(4,J)+TCZZ(K,IX)*B(K,J)
      1720 CONTINUE
      DO 1730 IA=1,4

```



```

DC 1730 JA=1,3
AE(IX,IA,JA)=A(IA,JA)
CONTINUE
1730 AE(IX,5,4)=TCXZ(1,IX)/AVESXZ(1)
    AE(IX,6,4)=TCYZ(1,IX)/AVESXZ(1)
    WRITE(6,822) ((A(N,M),N=1,4),M=1,3)
C
C
C    CALCULATION OF SCRIPO COEFFICIENTS ( ASSUMES SY=SYZ=0)
    DC1=0.3333*((A(1,1)**2)+(A(2,1)**2)+
    1A(1,1)*A(2,1)-A(4,1)*A(1,1)*A(1,1)+A(3,1)**2)-
    DC2=0.3333*(2.*A(1,1)*A(1,3)+2.*A(2,1)*A(2,3)+
    12.*A(4,1)*A(4,3)-A(1,1)*A(2,3)-A(1,3)*A(2,1)-A(2,1)*A(4,3)-
    2A(2,3)*A(4,1)-A(4,1)*A(1,3)-A(4,3)*A(1,1)+2.*A(3,1)*A(3,3)-
    DC3=0.3333*((A(1,3)**2)+(A(2,3)**2)+
    1A(1,3)*A(2,3)-A(4,3)*A(1,3)*A(1,3)+(A(3,3)**2)-
    DC4=((TCXZ(1,IX)**2)+(TCYZ(1,IX)**2))/(AVESXZ(1)**2)
C
C    CALCULATES SZ FOR GIVEN SX AND SXZ
    AWIGC=DC3
    BWIGC=DC2*SX
    CWIGC=DC4*(SXZ**2)+DC1*(SX**2)-ZJ2
    BACC=(BWIGC**2)-4.*AWIGC*CWIGC
    IF(BACC.LE.0) GO TO 1985
C
C    SZPC(IX)=(-BWIGC+ SQRT(BACC))/(2.*AWIGC)
    SZMC(IX)=(-BWIGC- SQRT(BACC))/(2.*AWIGC)
C
C    SZCMAX(IX)=AMAX1(SZPC(IX),SZMC(IX))
    SZCMIN(IX)=AMIN1(SZPC(IX),SZMC(IX))
    IF(IX.LE.NMATF) GO TO 1740
1740 CONTINUE
    MINMAX=1
    MAXMIN=1
    DO 1760 I=2,NUMEL
    IF(SZCMAX(I).LT.SZCMAX(MINMAX)) MINMAX=I
    IF(SZCMIN(I).GT.SZCMIN(MAXMIN)) MAXMIN=I
1760 CONTINUE
    WRITE(6,140) SZCMAX(MINMAX),SZCMIN(MAXMIN)
    WRITE(6,180) MINMAX,MAXMIN
    IF(SZCMAX(MINMAX).LT.SZCMIN(MAXMIN)) GO TO 1985
    L=L+1
    Y(L)=SX
    X(L)=SZCMIN(MAXMIN)
    YA(L)=SX
    XA(L)=SZCMAX(MINMAX)

```



```

C
C
10 UNO=0.0
15 NO=0
20 DETERM=1.0
30 DO 20 J=1,N
    IPIVOT(J)=NO
    DO 550 I=1,N
        SEARCH FOR PIVOT ELEMENT
        AMAX=UNO
        DO 105 JJ=1,N
            IF (IPIVOT(JJ).EQ.1) GO TO 105
        DO 100 K=1,N
            IF (IPIVOT(K).EQ.1) GO TO 100
            IF (IPIVOT(K).GT.1) GO TO 740
            IF (ABS(AMAX).GE.ABS(A(JJ,K))) GO TO 100
            IROW=JJ
            ICOLUM=K
            AMAX=A(JJ,K)
        CONTINUE
        IPIVOT(ICOLUM)=IPIVOT(ICOLUM)+1
        INTERCHANGE ROWS TO PUT PIVOT ELEMENT ON DIAGONAL
        IF (IROW.EQ.ICOLUM) GO TO 260
        DETERM=-DETERM
        DO 200 L=1,N
            SWAP=A(IROW,L)
            A(IROW,L)=A(ICOLUM,L)
            A(ICOLUM,L)=SWAP
        IF (M.LE.NO) GO TO 260
        DO 250 LL=1,M
            SWAP=B(IROW,LL)
            B(IROW,LL)=B(ICOLUM,LL)
            B(ICOLUM,LL)=SWAP
        INDEX(I,1)=IROW
        INDEX(I,2)=ICOLUM
        PIVOT(I)=A(ICOLUM,ICOLUM)
        DETERM=DETERM*PIVOT(I)
        DIVIDE PIVOT ROW BY PIVOT ELEMENT
        DO 350 L2=1,N
            A(ICOLUM,ICOLUM)=1.0
            DO 380 IF (M.LE.NO) GO TO 380
            DO 370 L3=1,M
                B(ICOLUM,L3)=B(ICOLUM,L3)/PIVOT(I)

```



```

CC
CC      REDUCE NON-PIVOT ROWS
380      DO 550 LI=1,N
390      IF (LI.EQ.ICOLUM) GO TO 550
400      T=A(LI,ICOLUM)
420      A(LI,ICOLUM)=0.0
430      DO 450 IL=1,N
450      A(LI,IL)=A(LI,IL)-A(ICOLUM,IL)*T
460      DO 500 JL=1,M
500      B(LI,JL)=B(LI,JL)-B(ICOLUM,JL)*T
550      CONTINUE

CC
CC      INTERCHANGE COLUMNS
600      DO 710 II=1,N
610      KL=N+1-II
620      IF (INDEX(KL,1).EQ.INDEX(KL,2)) GO TO 710
630      JROW=INDEX(KL,1)
640      JCOLUM=INDEX(KL,2)
650      DO 705 KK=1,N
660      SWAP=A(KK,JROW)
670      A(KK,JROW)=A(KK,JCOLUM)
700      A(KK,JCOLUM)=SWAP
705      CONTINUE
710      RETURN
740      END

```


BIBLIOGRAPHY

1. Lin, T. H., Theory of Inelastic Structures, Wiley, 1968.
2. Chamis, C. C., and G. P. Sendekj, "Critique on Theories Predicting Thermoelastic Properties of Fibrous Composites," Journal of Composite Materials, Vol. 2, No. 3, July 1968.
3. Adams, D. F., and D. R. Doner, "Longitudinal Shear Loading of a Unidirectional Composite," Journal of Composite Materials, Vol. I, No. 1, Jan. 1967.
4. Tsai, S. W., D. F. Adams, and D. R. Doner, Analysis of Composite Structures, NASA Contractor Report CR-620, Nov. 1966.
5. Bloom, J. M. and H. B. Wilson, Jr., "Axial Loading of a Unidirectional Composite," Journal of Composite Materials, Vol. 1, No. 3, 1967.
6. Adams, D. R. and D. R. Doner, "Transverse Normal Loading of a Unidirectional Composite," Journal of Composite Materials, Vol. 1, No. 2, April 1967.
7. Foye, R. L., An Evaluation of Various Engineering Estimates of the Transverse Properties of a Unidirectional Composite, presented at the 10th Annual SAMPE Symposium, Advanced Fibrous Reinforced Composites, Nov. 1966.
8. Lin, T. H., D. Salinas, and Y. M. Ito, "Initial Yield Surface of a Unidirectionally Reinforced Composite," Journal of Applied Mechanics, Paper No. 71-APMN-21.
9. Lin, T. H., D. Salinas, and Y. M. Ito, Elastic-Plastic Microstress Analysis of a Unidirectional Composite Under Longitudinal Loading," Journal of Composite Materials, Vol. 6, No. 1, Jan. 1972.
10. Salinas, D., T. H. Lin, and Y. M. Ito, "Post-Yield Surface of a Unidirectional Reinforced Composite," to be published.
11. Adams, D. F., "Inelastic Analysis of a Unidirectional Composite Subjected to Transverse Normal Loading," Rand Corporation Memorandum RM.-6245-PR, May 1970.
12. Felippa, C. A., Refined Finite Element Analysis of Linear and Nonlinear Two-Dimensional Structures, University of California, Berkeley, Dept. of Civil Engineering, Report 66-22.

13. Wilson, H. B., Jr., "Stress and Displacements in an Infinite Elastic Plate Containing a Doubly Periodic Array of Holes or Rigid Inclusions," Mathematical Studies of Composite Materials II, Rohm and Haas Special Report No. S-50, 1965.
14. Pickett, G., "Analytical Procedures for Predicting the Mechanical Properties of Fiber Reinforced Composites," Quarterly Program Report No. 5, Air Force Materials Laboratory Contract No. AF 33 (615)-2030, Jan. 1966.
15. Dow, N. F., B. W. Rosen, and Z. Hashin, Studies of Mechanics of Filamentary Composites, NASA Contractor Report CR-492, June 1966.
16. Ekvall, J. C., Structural Behavior of Monofilament Composites, AIAA 6th Structures and Materials Conference, April 1965.
17. Whitney, J. M., and M. B. Riley, "Elastic Properties of Fiber Reinforced Materials," AIAA Journal, Sept. 1966.
18. Blakslee, O. L., and others, "Fabrication, Testing and Design Studies with 'Thornel' Graphite-Fiber, Epoxy-Resin Composites, SAMPE, Vol. 12, 1967, AC-6.
19. Riedinger, L. A., M. H. Kural, and G. W. Reed, "Evaluation of the Potential Structural Performance," Mechanics of Composite Materials, Edited by F. W. Wendt, H. Lieberwite, and N. Perrone, Pergamon, 1970.
20. Tsai, S. W., Structural Behavior of Composite Materials, NASA Contractor Report CR-71, July 1964.
21. Hashin, Z., and B. W. Rosen, "The Elastic Moduli of Fiber Reinforced Materials," Journal of Applied Mechanics, June 1964.
22. Holister, G. S., and C. Thomas, Fiber Reinforced Materials, Elsevier, 1966.
23. Rosen, B. W., N. F. Dow and Z. Hashin, Mechanical Properties of Fibrous Composites, NASA Contractor Report CR-31, April 1964.
24. Timoshenko, S., Strength of Materials, Part I, Van Nostrand, 1955.
25. Smith, E. A., Editor, Carbon Fibres, Morgan-Grampian, 1970.
26. Hanby, K. R., Fiber-Reinforced Metal-Matrix Composites 1968, Defense Metals Information Center Report S-27, July 1969.

27. Sokolnikoff, I. S., Mathematical Theory of Elasticity, McGraw-Hill, 1956.
28. Sines, G., Elasticity and Strength, Allyn and Bacon, 1969.
29. Dow, N. F., and B. W. Rosen, Evaluation of Filament-Reinforced Composites for Aerospace and Structural Applications, NASA Contractor Report CR-207, April 1965.

INITIAL DISTRIBUTION LIST

	No. Copies
1. Defense Documentation Center Cameron Station Alexandria, Virginia 22314	2
2. Library, Code 0212 Naval Postgraduate School Monterey, California 93940	2
3. Asst. Professor D. Salinas, Code 59Zc Department of Mechanical Engineering Naval Postgraduate School Monterey, California 93940	1
4. Professor G. Cantin, Code 59Ci Department of Mechanical Engineering Naval Postgraduate School Monterey, California 93940	1
5. Department of Mechanical Engineering Naval Postgraduate School Monterey, California 93940	1
6. Lieutenant Walter A. Ericson, USN 49 Reservoir Road San Rafael, California 94903	1

DOCUMENT CONTROL DATA - R & D

(Security classification of title, body of abstract and indexing annotation must be entered when the overall report is classified)

1. ORIGINATING ACTIVITY (Corporate author) Naval Postgraduate School Monterey, California 93940		2a. REPORT SECURITY CLASSIFICATION Unclassified	
		2b. GROUP	
3. REPORT TITLE An Investigation of Initial Yield Surfaces for Unidirectional Reinforced Composites			
4. DESCRIPTIVE NOTES (Type of report and inclusive dates) Mechanical Engineer Thesis, March 1972			
5. AUTHOR(S) (First name, middle initial, last name) Walter A. Ericson			
6. REPORT DATE March 1972		7a. TOTAL NO. OF PAGES 203	7b. NO. OF REFS 29
8a. CONTRACT OR GRANT NO.		9a. ORIGINATOR'S REPORT NUMBER(S)	
b. PROJECT NO.			
c.		9b. OTHER REPORT NO(S) (Any other numbers that may be assigned this report)	
d.			
10. DISTRIBUTION STATEMENT Approved for public release; distribution unlimited.			
11. SUPPLEMENTARY NOTES		12. SPONSORING MILITARY ACTIVITY Naval Postgraduate School Monterey, California 93940	
13. ABSTRACT <p>Initial yield surfaces of unidirectional fiber reinforced composites subjected to combined longitudinal, transverse normal, and longitudinal shear loads are calculated. The composite is composed of filaments arranged in a periodic square array embedded in a matrix material. The constituent materials are assumed to be homogeneous and isotropic, while the composite is assumed to be macroscopically homogeneous and transversely isotropic. The finite element method, using linear strain triangles, is employed to calculate the stresses throughout the composite. Von Mises yield criterion is used to calculate the elastic limit of the local microscopic combined stresses in the composite. A parametric evaluation is carried out by changing individual constituent properties and evaluating the effect of this variation on the composite properties. Yield surfaces for several functional composites are included, as well as a computer program, in FORTRAN IV language, for the calculation of a yield surface.</p>			

134460

Thesis

E575 Ericson

c.1

An investigation of
initial yield surfaces
for unidirectional re-
inforced composites.

134460

Thesis

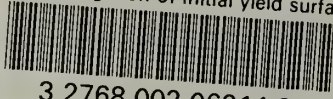
E575 Ericson

c.1

An investigation of
initial yield surfaces
for unidirectional re-
inforced composites.

thesE575

An investigation of initial yield surfac



3 2768 002 06214 3

DUDLEY KNOX LIBRARY